Design of a Tissue Ring Contractile Force Measurement Device

A Major Qualifying Project Report:

Submitted to the Faculty

of

WORCESTER POLYTECHNIC INSTITUTE

In partial fulfillment of the

requirements for the

Degree of Bachelor of Science

By

Matthew Cyr

Colleen Heckley

Alison Su

Mohamed Yatim

Date: April 26, 2012

Marsha W. Rolle, PhD, Major Advisor

Authorship Page

Section	Primary Author	Editor
Chapter 1	**All**	**All**
Chapter 2	**All**	**All**
Chapter 3	**All**	**All**
Chapter 4	**All**	**All**
Chapter 5	**All**	**All**
Chapter 6	**All**	**All**
Chapter 7	**All**	**All**
Chapter 8	**All**	**All**
Appendices	**All**	**All**

Acknowledgements

The team would like to thank some very important people that provided tremendous help and assistance throughout our entire project.

We would like to thank Dr. Marsha Rolle, Lisa Wall and Dr. Sakthikumar Ambady for their continued guidance and assistance throughout the entire design process.

We would also like to thank Dr. Siobhan Craige, Dr. Adriana Hera, Dr. Domhnull Granquist-Fraser, Amanda Zoe Reidinger, Dr. Tracy Hookway and Harry Hovagimian for helping us with their expertise in specific areas of our project.

We would also like to thank the MQP project group of Mary Clare McCorry, Carolynn Ohlson, Samuel Gunnel and Sydney Higginbottom for letting us test some of their C2C12 tissue ring constructs.

Abstract

The field of tissue engineering is one of rapid expansion and newly forming possibilities. One major area of potential still very much unexplored is using *in vitro* three-dimensional (3D) tissue constructs for drug testing and development. These constructs may provide a relatively inexpensive and convenient segue to animal testing as the effects of various chemical compounds can be tested on 3D tissues to study their structure and function. For this project, we developed a device to measure the contractile force of tissue rings comprised of smooth muscle cells (SMCs) in response to chemical stimuli. Our device is made of poly(dimethylsiloxane) (PDMS), a silicone-based elastomer, which is molded into a well consisting of a center base post along with four small microposts extending from the base. SMCs are seeded into separate agarose wells with center posts where they aggregate around the post to form a ring. When the cultured ring is ready to be tested, it is gently removed from the agarose mold and mounted on the tips of the microposts of our PDMS device where the rings are induced to contract with agonists. The amount of deflection of the microposts in response to ring contraction is used to calculate the force of ring contraction. We developed a software model to predict deflection in response to a known input force. We also conducted validation testing to determine the mechanical properties of the PDMS posts and the feasibility of creating tissue constructs in a PDMS mold. We observed an average contractile force of 32.00 ± 5.71 μN for rat aortic smooth muscle cell (rASMC) rings induced to contract by the addition of potassium physiological saline solution (KPSS). This was a statistically ($p \leq 0.05$) greater amount of contraction than that of rASMC rings induced by the addition of physiological saline solution (PSS) without potassium (10.28 ± 5.72 μN). The maximum contraction found was consistent with values from reported literature. In addition to rASMCs, we were able to test contraction in C2C12 mouse skeletal myoblast cell rings. Ultimately, we created a device that measures the contractile force of tissue rings of different muscle cell types that is both inexpensive and easy to manufacture. It also has the potential to be made high throughput and allow for cell culture and testing on the same device.

Table of Contents

Table of Figures

Table of Tables

Chapter 1: Introduction

Tissue engineered blood vessels (TEBVs) have become a subject of great interest in the field of tissue engineering in recent years due to the continual demise of cardiovascular health and the need for new vascular tissue constructs (Harris, 2009; Rhim, 2006; Thomas, 2003). Although many TEBVs have been successfully constructed and implanted into animal models for various tests and analyses, the need for *in vitro* models of human tissues is still very much existent. Additionally, a frequently overlooked application for 3D tissue engineered constructs is *in vitro* toxicity testing of known and unknown chemical compounds (Hansen, 2010; Hecker, 2008). All tissue properties and physiological responses must be tested to characterize how tissues react to various drugs. *In vitro* vascular ring models derived from human cells allow for an important and informative step in drug discovery. Furthermore, a high throughput method for testing several important properties of vascular constructs allows for a greater amount of data to be collected in a shorter amount of time than expensive *in vivo* animal models provide (Truskey, 2010; Piersma, 2004).

Currently, many tests that analyze the mechanical properties of 3D tissue rings, such as tensile strength and burst pressure, are commonly conducted. However, minimal testing has been done to measure and analyze the contractile properties of TEBV constructs (Hecker, 2008). Contractility is an essential property of functional blood vessels, and contractile properties of TEBVs must be made to mimic those of native vessels. The most common types of devices currently used to measure contractile force of various microscale tissue constructs are force transducers, wire myographs, and micropost arrays (Legant et al., 2009; Vandenburgh, 2008; Zheng, 2010; Kim, 2011; Danish Myotechnology, 2011). Force transducers are extremely accurate and allow for measurements of extremely small forces, but are very expensive and often require technical expertise or training to use (Kim, 2011; Desai, 2007). The wire myograph has a force transducer that allows for the measurement of various forces, ranging from ±200 to ±1600 milliNewtons (mN) with a force resolution of 0.01 mN (Danish MyoTechnology, 2011). In 2010, a three-axis micro-force transducer was created to allow for the determination of force ranges from 20 to 200 microNewtons (μN) (Muntwyler, 2010). Micropost arrays, on the other hand, are much less expensive and can be applied to several different cell types, but have never been used to measure contractile forces of ring shaped vascular smooth muscle cell (SMC) tissue constructs (Cheng, 2010; Legant, 2009; Vandenburgh, 2008).

Our client statement, as given to us by our project advisor, instructed the team to design a high throughput device to accurately measure the contractile force of TEBV rings induced to contract by chemical agonists. Based on extensive research and interviews with lab technicians, we devised a list of objectives that our device must successfully meet and then brainstormed a variety of different design alternatives to achieve these objectives. We then conducted several experiments and functional tests to determine which aspects of each design were most useful and effective in achieving our objectives. While testing, we also continued to conduct research and gain more information about the field of *in vitro* tissue testing, in order to generate more ideas and brainstorm more effective designs. After several rounds of testing, we were able to evaluate our design alternatives and narrow our ideas down to one final modified design that led us to the best results in measuring tissue ring contraction on a high throughput scale. We then completed extensive testing to validate the success of our final design and created a working prototype.

We chose a multifunctional four-post poly(dimethylsiloxane) (PDMS) design as our final device. PDMS is a silicone elastomer that is relatively inexpensive and easy to fabricate. It has measurable mechanical properties and can be molded to any desired shape (Sasoglu, 2007). Our final design allows for tissue rings to be cultured and tested within the same device. Smooth muscle cells (SMCs) can be seeded into the wells of the device and allowed to aggregate into rings, where they can then be induced to contract in response to a known chemical stimulus around four microposts. Knowing the mechanical and dimensional properties of the posts, the contraction force of the rings can be measured based on overall post deflection. To validate our final design, we conducted mechanical tests to determine a value for PDMS modulus and develop a working finite element model to determine contraction force from any known deflection.

Through our testing, we found an average contraction force of 32.00 ± 5.71 μN on our device from rat aortic smooth muscle cell (rASMC) rings soaked in potassium physiological saline (KPSS) solution. In the control group, when the rings were only soaked in physiological saline solution (PSS), the average contraction force was 10.28 ± 5.72 μN, which was a significantly lower contraction force ($P \leq 0.05$). This allowed us to conclude that the KPSS caused rASMC ring contraction. In order to ensure that the contraction was based on the action of the cells and not the extracellular matrix structure of the tissue rings, we lysed the cells by soaking them in deionized water and then tested them by soaking them in KPSS. For this testing, we found the average contraction force to be 6.19 ± 2.16 μN, showing that the action of the smooth muscle cells caused contraction. Additionally, we were able to test some C2C12 mouse skeletal myoblast rings on our

PDMS device. Although they did not exhibit contraction, this testing showed that we were able to test rings from different cell types on our device.

Our final design is both versatile and easy to use. It is also reproducible and easy to manufacture. Most importantly, our device provides a means to calculate the contractile force of 4 mm diameter vascular tissue rings. The final device is also inexpensive and reusable, giving it a positive impact on sustainability and environmental concerns. Due to time and money constraints, there are certainly some advancements and improvements that can be made to this device. The device can be made high throughput in the future, with the ability to culture and test tissue ring constructs from multiple cell types and of various diameters and thicknesses.

Our current device presents the potential of a high throughput and inexpensive *in vitro* testing method of chemical compounds. Toxicological and pharmaceutical testing of 3D tissue constructs will help to provide new drugs and therapies to combat cardiovascular ailments and diseases that are rapidly increasing across the globe. Our device provides an example of a relatively simple yet effective means of assessing tissue function and response to various external stimuli.

In the following report, we outline the current state of contractility testing on tissue constructs and our project design process. We present our design criteria, detailed descriptions of alternative designs and the testing procedures conducted on these designs. A discussion of testing and results with respect to our final design validation is also presented. We conclude with a detailed analysis of the system, its context in the field of toxicity testing, and our recommendations for future work and research.

Chapter 2: Literature Review

2.1 Tissue Engineered Blood Vessels and Vessel Constructs

Over the past two decades, tissue engineering technologies have allowed for advancements in the fields of wound healing and regenerative medicine. In particular, tissue engineered blood vessels (TEBVs) have shown potential in generating blood vessel substitutes to be used for a wide variety of medical and pharmaceutical applications. To date, research has been heavily based on developing functional TEBVs used for implantation for patients with arterial diseases (Harris, 2009; Rhim, 2006; Thomas, 2003). However, the pharmacological potential for *in vitro* TEBV testing has been largely neglected. Before TEBVs can be implemented and become extensively used in medical research, effectively analyzing the properties of vascular tissue constructs and modeling them to closely mimic native vessels is necessary.

2.1.1 In Vitro Testing

The emergence of TEBVs has led to remarkable breakthroughs with regards to *in vivo* testing and grafting methods (Dahl, 2011; Neff, 2011; Rhim, 2006). Pharmaceutical effects have most commonly been tested on TEBVs that are used as *in vivo* grafting materials on animals such as pigs, rabbits, and baboons (Dahl, 2011; Byrom, 2010). However, it appears that the *in vitro* testing of vascular tissue constructs still requires increased attention and research (Hecker, 2008).

The need for a high throughput model for pharmacological drug screening applications on engineered vascular constructs is still very much necessary and desired (Hansen, 2010). Additionally, although animal testing has provided a plethora of information to the medical world, the testing of constructs derived from human cell lines may lead to more accurate and revealing results to be used in pharmaceutical applications. Additionally, *in vitro* testing of engineered vascular constructs requires an entirely different set of standards and regulations than *in vivo* testing and experimentation (Hansen, 2010).

According to the National Toxicology Program (2010), *in vitro* testing is both high throughput and inexpensive when compared to *in vivo* testing. Additionally, *in vivo* testing procedures are often very complex, requiring much more time to perform than *in vitro* testing (Piersma, 2004). *In vitro* studies can help advance the field of pharmaceutical and toxicity testing on blood vessels and can provide a means to initially observe the reaction of human tissues to specific dosages of drugs with much less effort, money and time than an *in vivo* test. Toxicological testing of

human cells on an *in vitro* scale is a necessary scientific step for the research and development of new chemical compounds to protect cardiovascular health (Purchase, 1999).

2.1.2 Animal Testing

Several animal models have been used for toxicity and pharmaceutical testing throughout the last decade. Animal cells are generally easy to obtain and readily available for *in vitro* toxicology screening and drug discovery purposes (Tawqeer-Rashid, 2004). One of the main problems is that different animal models provide various results for different testing categories. For example, sheep and pigs have the closest hematology and clotting results when compared to human tissue. However, when looking at tensile testing and burst pressure results, rabbit arteries come closest to human values, but are considerably smaller in physical size (Byrom, 2010). In addition, *in vivo* testing using animal models can be time consuming and very expensive, and animal specimens are limited in number (Piersma, 2004). Animal models are also limited by increasing regulatory restrictions, driven by ethical concerns (Knight, 2008).

In vivo animal testing is a very controversial issue, as many people consider it unethical to test drugs on animal subjects. Unfortunately, any drug must successfully pass animal testing before it can continue on to human clinical trials and then be approved for commercial sales ("Advancing Tissue Engineering", 2007). Some companies are now using tissues from donated human organs that are not deemed suitable for implantation for *in vitro* testing and research (Moss, 2010). This provides a means for using viable human tissues that would otherwise be discarded.

There currently exists a gap in the process of drug testing and discovery, which can be filled by three dimensional tissue constructs, allowing for *in vitro* testing of collections of cells in specific morphologies. Rather than just assessing tissue response, 3D vascular tissue construct testing also allows for studies of tissue function. Pharmacological and toxicity *in vitro* testing with human cells provides a method to "bridge the gap" between 2D tissue culture and *in vivo* animal testing.

2.1.3 Toxicology Testing

Toxicological testing has been based mostly on the use of laboratory animals (National Toxicology Program, 2010). However, this approach is low throughput and expensive, resulting in limitations in evaluating large amounts of chemicals. For example, testing a new drug to combat hypertension on animals would take a length amount of time (several days or even weeks) to set up experimentation and obtain results. Additionally, in order to obtain statistically significant results, a large number of animal samples would be needed. Due to this, models in toxicity testing that offer

an alternative or a testing step prior to the use of animals and are high throughput in nature have gained attention.

It has been recognized that technological advances in molecular biology and computer science have made possible the use of *in vitro* biochemical and cell-based assays and non-animal models for testing (Bhogal et al., 2005; Knight, 2008; National Toxicology Program, 2010). However, the application of the new biotechnology to the assessment of chemicals has been a slow process (Bhogal et al., 2005). On the other hand, these assays do provide a much higher throughput (often the ability to test tens or hundreds of samples at a time) at a reduced cost.

One example of high throughput technology can be seen in human hepatocyte toxicity testing. The liver is responsible for drug metabolism and toxicity within the human body (Khetani, 2008). Preclinical animal studies are inadequate to evaluate toxicity because of species-specific variation between human and animal cellular functions (L'Heureux, 2001; Knight, 2008). Therefore, implementations of assays to evaluate human responses are needed. The need for such *in vitro* testing models is often overlooked because pharmaceutical companies as well as the Food and Drug Administration and other regulatory agencies deem *in vivo* results more important in an effort to market their drugs (Khetani, 2008). However, *in vitro* testing of cell constructs can reveal results that help improve and/or advance *in vivo* testing. Salman Khetani and his colleagues implemented a new approach involving the use of human liver tissue constructs on a high throughput scale. It is a micro-based technique using elastomeric stencils and soft lithography to culture human hepatocytes in multi-well format. The multi-well culture system allows for extensive testing of several different drugs to be conducted simultaneously (Khetani, 2008).

Testing on TEBV constructs can be conducted in a similar way. Usually cardiovascular pharmacology is heavily dependent on the contractile responses of blood vessels tested in an organ bath. In addition, animal models are the only samples being used for pharmacology tests; these models do not correctly model human responses (L'Heureux, 2001). It is vital to evaluate the effect of pharmaceuticals on the human cardiovascular system before the drugs can be administered to the body. High throughput toxicological testing on TEBV constructs can allow for a variety of drugs to be tested all at the same time. Also, this type of testing allows for human, rather than animal, tissue samples and much less money and time spent than conducting a full-scale animal model study for toxicity.

2.2 Tissue Engineered Blood Vessel Construct Sources

TEBVs can be constructed in several different ways. Smooth muscle cells (SMCs) are very commonly used to construct TEBVs. Generally, SMCs in culture can be formed into strips that display many similar properties to SMCs in a ring shape (L'Heureux, 1998; Auger, 2004). Additionally, SMCs can be obtained from various animal specimens that show minimal functional and physiological variation when compared to human cells (Auger, 2004). SMCs comprise the thickest layer of human arteries and are the primary source of vasoconstriction and vasodilation; TEBV constructs composed solely of SMCs still provide most of the same mechanical functions as native blood vessels (Clark, 2005; Auger, 2004). An example of a vascular ring composed of rat aortic smooth muscle cells (rASMCs) can be seen in Figure 1.

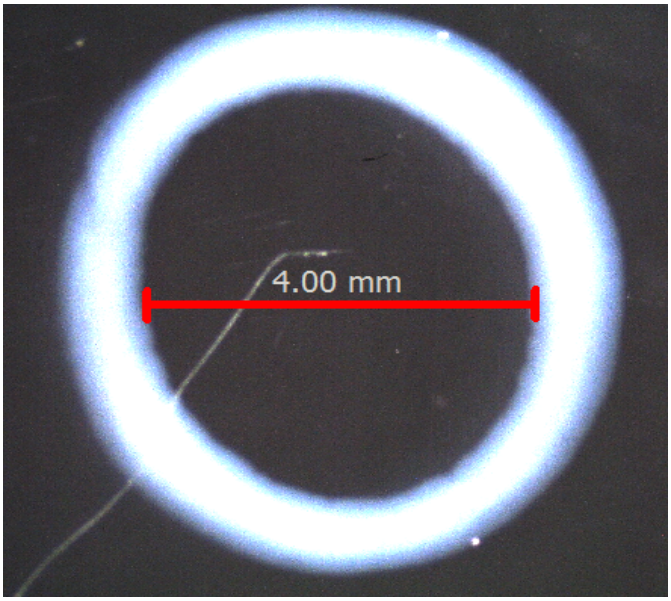

Figure 1: Vascular tissue construct derived from rat aortic smooth muscle cells (rASMCs). Constructed in the process described by Gwyther, 2011. Scale bar= 4 mm

The aforementioned tissue ring was developed using the method formulated in Dr. Marsha Rolle's laboratory at Worcester Polytechnic Institute. Round-bottomed agarose wells with 4 mm diameter center posts were cast from poly(dimethylsiloxane) (PDMS) negative templates. Cells were seeded into the wells and allowed to aggregate to form a viable tissue ring. These tissue rings are observed to aggregate within 24 hours (Gwyther, 2011). Figure 2, below, depicts the agarose wells allowing the formation of viable tissue rings. Many tests have been conducted on these ring constructs, including burst pressure analyses and tensile strength measurements (Gwyther, 2011). However, there is still a need to develop a method to assess and quantify the contractility of the ring constructs.

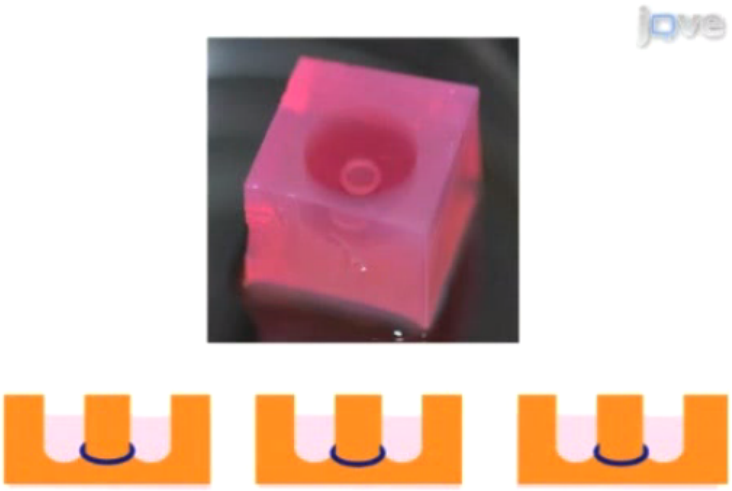

Figure 2: The vascular ring system constructed at Worcester Polytechnic Institute in Dr. Marsha Rolle's laboratory (Gwyther, 2011).

In order to work with cells of human origin, many laboratories are now utilizing human mesenchymal stem cells (hMSCs) for the purpose of making tissue rings (Harris, 2011; Sanz, 2008). These stem cells can be differentiated into SMCs, creating a SMC ring that is of human origin. Testing human cells allows for the possibility of observing chemical reactions and side effects of drugs that may not occur in animal cells. Proponents of this method of TEBV construction stress the importance of testing human cells in order to better understand possible *in vivo* tissue responses (Harris, 2011; Sanz, 2008). Additionally, hMSCs do not incur nearly as strong of an ethical dilemma as using embryonic stem cells for testing purposes because they are harvested from adult tissue.

Native blood vessels consist of an inner lining (intima layer) of endothelial cells (EC) and a medial layer of SMCs (Clark, 2005; Gentile, 2008). Most arteries consist of three distinct layers: the intima, the media and the adventitia. The native vessel functions by means of communication between the endothelium and the smooth muscle layer. For example, acetylcholine (ACh) treatment to a SMC tissue ring will cause the ring to contract, but ACh treatment to a native blood vessel will lead to vasodilation (Furchgott, 1984). For these reasons, many recent studies have aimed at co-culturing endothelial and smooth muscle cells (EC-SMC) in order to form rings comprised of both cell types (Clark, 2005; Ziegler, 1994). Many laboratories have made spheres of EC-SMC co-culture successfully, but a 3 dimensional co-culture ring construct has not been made. Additionally, EC-SMC co-cultures do not communicate as well *in vitro* as in native vessels (Rouwkema, 2008). Researchers now must better understand the mechanisms of cell signaling

between the endothelium and the smooth muscle layer in order to create co-culture rings that better mimic native blood vessels (Truskey, 2010; Ziegler, 1994).

2.3 Need for Contractility Testing in TEBVs

Since the emergence of TEBVs in the field of tissue engineering, several forms of testing have been conducted in an attempt to mimic the native tissue as close as possible. A plethora of research to date has been done on the tensile properties and burst pressure properties of TEBVs (Konig, 2009). However, very little testing has been done to characterize the physiological function, such as contractile forces, of TEBVs and other vascular tissue constructs (Hecker, 2008). In the human body, vessels undergo both vasoconstriction and vasodilation in response to several different hormones and chemicals. For example, SMCs contract in response to acetylcholine, potassium chloride, and phenylephrine while vessels contract *in vivo* due to hormones such as epinephrine and norepinephrine (Gentile, 2008; Hecker, 2008; Zheng, 2000; L'Heureux, 1998). The method of vasoconstriction occurs primarily by the action of the SMCs. The primary means by which vasoconstriction takes place is similar to the action of skeletal muscle fiber contraction. Calcium influxes into the SMCs cause myosin cross bridges to pull on actin fibers and contract the cells, causing an overall decrease in vessel diameter (Hecker, 2008; Yagi, 1988). Vasoconstriction is a means by which mammals keep warm in cold environments, as blood flow is lowered in peripheral vessels to allow warm blood to stay as close as possible to the core of the body and heat the vital organs (Clark, 2005). By understanding the physiological function of native blood vessels, more in-depth tests can be done to analyze and optimize the development of TEBVs to better mimic native vessels.

TEBVs must be made to contract in response to given chemicals with similar forces that are experienced in native vessels, which is between 9-30 microNewtons per square centimeter ($\mu N/cm^2$) (Murphy, 1974). Additionally, it has been found in studies that human airway SMCs contract with a force of around 29.4 $\mu N/cm^2$ (Bramley, 1994). In order to assess contractility of TEBVs, extensive *in vitro* testing of vascular constructs must be conducted.

2.4 Need for High Throughput Screening Methods

When testing TEBV rings in culture, an ideal method would provide a large amount of data in a relatively short amount of time. High throughput screening (HTS) is a method used for scientific experimentation that allows a researcher to quickly perform numerous amounts of chemical tests (Bevan, 2000). Ideally, these systems provide a greater amount of results with

relatively little error, making data collection more efficient (Truskey, 2010). High throughput systems are also very useful for toxicity testing, as a variety of chemical compounds can be tested for their effects on living tissues simultaneously (National Toxicology Program, 2010). Outputs should be quantifiable and relative to cell function. Due to the cost of reagents and cell culture systems, small volumes are preferable for these testing systems. These methods are needed to test the vasoactivity and toxicity of chemical compounds, and have revolutionized the process of drug discovery.

Endothelial and smooth muscle cell co-culture systems make promising candidates for high throughput applications (Truskey, 2010). Microplates and microfluidic flow systems are feasible for cell culture and high throughput screening. Microplate systems are widely used for many diagnostic applications, while microfluidics is an area of research that deals with the microscale level of the behavior of various biological tissues (Truskey, 2010). Both of these high throughput screening applications allow for several tissue samples to be grown in the same culture and then be tested all at the same time. In terms of toxicological testing, various drugs can be tested on different samples in order to compare the tissue reactions and draw conclusions about which drugs are most effective (National Toxicology Program, 2010; Truskey, 2010).

Common cell culture uses single cells of whole tissues (Khetani, 2008). This is a problem as it neglects higher-order cellular processes, meaning the way a single cell acts may not reflect how the entire tissue (a collection of cells) reacts. Two-dimensional cell culture provides few options for studying contractile force production as a cellular function (Bitar, 2006). Also, cells that are tested in this manner are not allowed to establish normal physiological function. In order to measure the mechanical properties and processes of the cell, including contractility, microfabrication techniques have been attempted (Moraes, 2010). These approaches have been used to create an efficient and effective environment for testing, and will to be used more frequently in the future for successful studies of tissue and cellular processes.

2.5 Contractility Testing Methods

Over the past decade, the focus on developing functional TEBVs that exhibit substantial contractile properties has led to the development of several methods to test contractile forces *in vitro*. Force transducers, microposts, and cantilever beams are some of the most commonly used methods of testing contractility of tissue samples. Contraction on a microscale level has been made much easier to observe with the aid of high-speed photography, ever improving microscopy, and imaging enhancement techniques, such as fluorescent labeling (Desai, 2007; Kim, 2011; Li, 2007;

Zheng, 2010). These tools allow the mechanisms of contraction to be studied, even if not visible to the naked eye.

2.5.1 Force Transducers

Perhaps the most common method of measuring contractile force is by the use of a force transducer. Although expensive, transducers allow for real time, continuous readings and can often be combined with software packages to create plots and advanced data analyses (Danish MyoTechnology, 2011). Also, force transducers allow for easy calibration and very precise readings with minimal error. Force transducers were previously only used to measure larger scale forces, but advancements in technology now allow for even microscale forces to be measured accurately. Some methods for contractile testing that include the use of force transducers are two-pin fixation methods and wire myographs.

The DMT wire myograph implements a force transducer that allows for the measurement of contractile forces of tissue ring constructs, ranging from 200 to 1600 milliNewtons(mN) with a force resolution of 0.01mN (Danish MyoTechnology, 2011). In 2010, an even more sensitive three-axis micro-force transducer was created to allow for the determination of force ranges from 20 to 200 microNewtons (μN) (Muntwyler, 2010).

Additionally, fully submersible force transducers have been custom built in order to limit frequency response and sensitivity (Gisela, 2001; Lin, 1995). These low-mass transducers are only a few cubic millimeters in size and are of higher fidelity (100 nN and 13.3 kHz in solution) (Gisela, 2001). This system can be coupled with a video microscope, allowing for contractile measurement of heart cell forces in the 100nN to 50N range. This transducer was successfully operated with cardiac myocytes in a saline bath surviving multiple solution exchanges under steady state and oscillatory conditions (Gisela, 2001). Moreover, there is potential for the use of this device with other cell types and even tissue constructs at higher fidelities.

2.5.1.1 Two-Pin Fixation Methods

The use of two-pin fixation methods to measure the force generated by a tissue construct has been thoroughly investigated in recent years. This concept often involves anchoring one end of a tissue to a poly(dimethylsiloxane) (PDMS) coated tissue culture plate with a stainless steel pin and hooking the other end to another stainless steel pin that is attached to an optical force transducer (Bitar, Hecker, Baar, & Somara, 2006; Sato, Ito, Kawabe, Nagamori, & Kamihira 2011). The general set up of this method can be seen in Figure 3. Cardiac myocyte strips and skeletal

muscle rings have been tested using this set up. Other studies have used cardiac myocyte tissue rings anchored and attached to a force transducer and a micromanipulator with stainless steel pins and electrically stimulated to contract (Akiyama, Ito, Sato, Kawabe, & Kamihira, 2010). From these findings, it is shown that with the use of the two-pin fixation, a variety of cellular constructs and types can be tested.

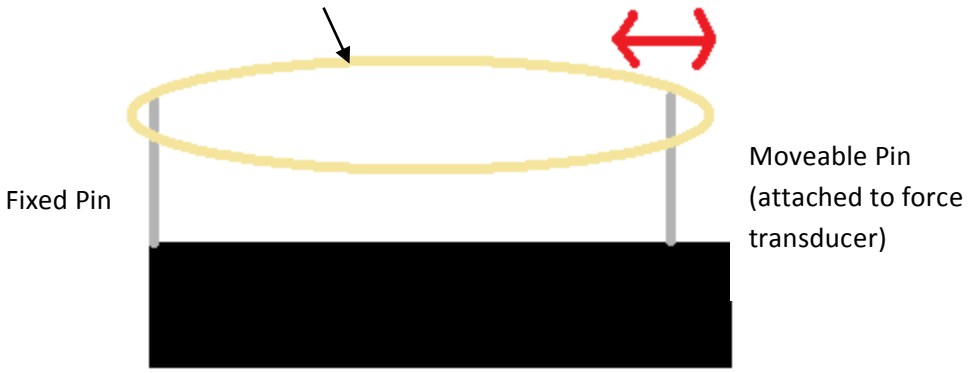

Figure 3: Representation of a two-pin fixation system. One pin (left) is fixed in place, while the other (right) is allowed to move freely, in response to tissue contraction or expansion

Birla, Borschel, & Dennis (2005) studied the contractile performance of rat cardiac myocytes developed in a cardioid construct by the use of electrical stimuli to induce contraction. Findings in Birla's work showed that the tissue engineered cardioids had an output of 1050 μN of contractile force whereas native rat papillary muscle exhibited 8130 μN of contractile force. As seen in the large difference of these numbers, contractility of tissue-engineered constructs is generally significantly lower than that of native tissues (Birla et al., 2005). The exact reason why is still uncertain to researchers, but this is a factor that must be taken into account when dealing with contraction studies of TEBV constructs.

Patent# US 7,368,279

Khalil Bitar et al. (2006) at the University of Michigan filed for patent# US 7,368,279 in November 2005. This patent was for tissue engineering a 3D tissue ring that resembled an internal anal sphincter (IAS) that responded to appropriate agents that induced contraction and relaxation in SMCs. For this patent, SMCs were extracted from rabbit colon and cultured on fibrin in a 5 mm PDMS mold for a time frame between five to ten days. After the period of culture time, the tissue-engineered sphincter was removed from its mold and the cross-sectional area was measured and calculated (Bitar et al., 2006). The IAS was put in a petri dish that was on top of a heated aluminum plate maintained at 37°C, to mimic *in vivo* body temperature. The culture media (15% FBS DMEM)

was replaced with 37°C Krebs Solution. A piece of stainless steel pin (10 mm × 0.1 mm diameter) was used to fix one end of the sphincter in place. Another stainless steel pin was attached to a custom-made force transducer with a resolution range of 1.4 μN-2.0 mN.

LabVIEW software was used to record all the data. Contraction in the tissue was induced by addition of 10^{-10} and 10^{-6} M of acetylcholine (ACh) to the Krebs Solution. The variables measured for this procedure included the cross sectional area, passive baseline force and the peak change in isometric force. Results of these tests showed that at maximum contraction, about 12 μN, were seen between 30 and 60 seconds after addition of the agonist, ACh (Bitar et al., 2006). Figure 4 depicts the data recorded for inducing the engineered sphincter rings with different concentrations of ACh. It can be observed that increasing the agonist concentration induces a higher force production from the cells (Bitar et al., 2006).

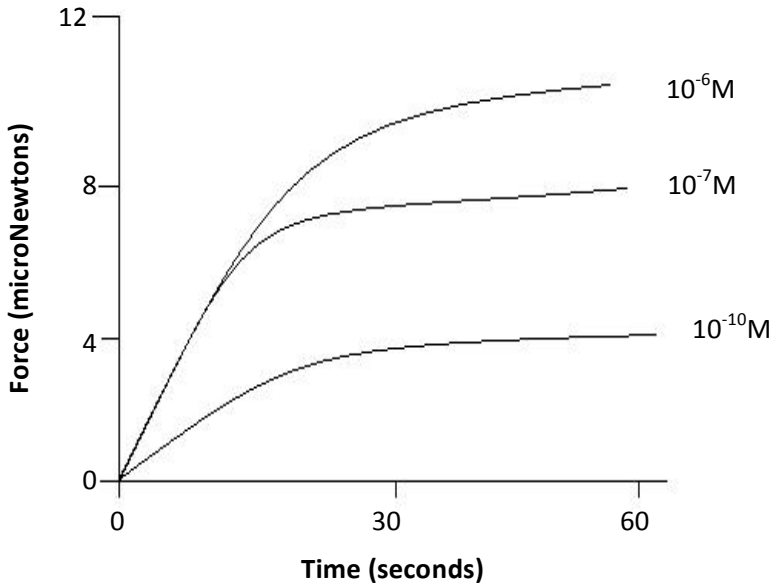

Figure 4: Graphical representation of the contractile force generated by the rIAS ring when induced by various concentrations of acetylcholine with respect to time. (derived from Bitar et al., 2006)

By the use of the two-pin fixation method, precise force measurements of various cell types, shapes and sizes can be collected by using LabVIEW software. However, the use of chemicals to induce contractile responses requires various equilibrating, stabilizing, relaxing and conditioning procedures before and after adding the appropriate agonist to induce contractile responses from the tissue (Hecker et al., 2008). In addition, the use of the two-pin fixation method coupled with data acquisition from a single force transducer is very low throughput. Only one sample can be

tested at a time and it is time consuming to test each sample. The acquisition of multiple force transducers (in order to create a high throughput device) is impractical due to the high-cost of transducers that are sensitive enough to measure minute forces (Hecker et al., 2008). Thus, a more time and cost effective, high throughput method to testing contractility of tissue constructs is desired.

2.5.1.2 Myographs

A myograph is a device for quantifying contractile forces generally through a force transducer. Wire myographs are currently the "gold standard" of contractility testing of tissue constructs. They are the most widely used devices for testing contractile forces of small diameter vessel rings with internal diameters between 60 μm and 10 mm (Danish MyoTechonology, 2011). These devices allow for the measurement of various small forces, ranging from 200 to 1600 milliNewtons (mN) with a force resolution of 0.01mN. Danish MyoTechnology (DMT) Inc. currently has a device that can test four vessel rings simultaneously. Each ring is mounted on two stainless steel wire pins in its own chamber (Danish MyoTechnology, 2011). The configuration of one vessel testing chamber on the DMT is represented in Figure 5. One pin is connected to a micrometer that is used to calibrate the tissue and the other is attached to an isometric force transducer (Perry et al., 2003). As the device is operating, the data is collected and shown by using LabChart computer software developed by DMT. *In vivo* conditions, including 37°C temperature and oxygenation, can be mimicked with these devices due to the incorporation of an organ bath chamber that has heating and bubbling features. Toxicity testing can be done with myographs because the chemical agents can be added to the organ baths, which then can induce contractile responses from the tissue and the data is recorded through computerized programs (Perry et al., 2003).

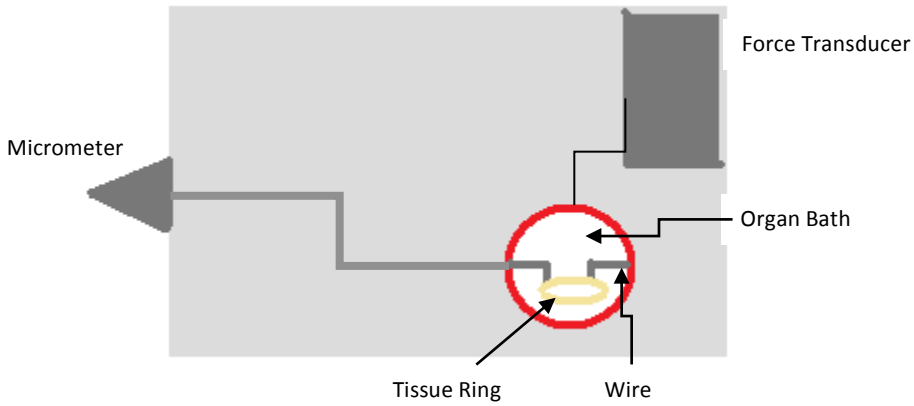

Figure 5: Testing set up for the DMT Myograph. The ring samples are placed on two wires in an organ bath. The wires are attached to a force transducer and the micrometer controls the wire movement and allows for the vessel ring to be stretched to a desired position. (adapted from Danish Myotechnology, 2011).

2.5.2 Multistation Culture Force Monitor (CFM)

A CFM system, containing vertical cantilever beams, semiconductor strain gauges, and a computerized data acquisition set, was created in order to effectively measure the contractility of human skin fibroblasts (Campbell, 2003). Cell-mediated contraction was induced on cell populated collagen gels (CPCG) located in silicone dishes and the force was determined by measuring the change in gel area over time.

The base of the CFM is made of aluminum and allows for up to six CPCG to be tested (Campbell, 2003). A support rod holds the beam clamps and the tension unit fixes one end of the gel and allows for a tare load to be applied. The beams are also made of aluminum and are responsible for detecting the contractile force. Beam strain was measured by four semiconductor strain gages. The force generated from the cells is transferred from the CPCG to the beam via a piece of suture that connects the beam to the CPCG unit (wire frames and vyon bars). CPCG contraction results in the deflection of the beam, which is monitored by the strain gages. A LabVIEW program records the output voltage signals of the strain gages. The CFM apparatus was proven to be accurate by conducted studies (Campbell, 2003).

2.5.3 Micropost Arrays

Micropost arrays have measured the contraction of cardiomyocytes, smooth muscle cells, and fibroblasts using PDMS micropost arrays microfabricated by a replica molding technique (Kim, 2011; Li, 2007; Legant, 2009). The cells were seeded on the tightly packed array and as the cells contracted, the microposts displaced towards each other. This data was obtained by a video post-processing program written in MatLab (Kim, 2011). With calibration and quantitative image analysis, this study demonstrates that micropost systems can provide precise high throughput applications of contractility measurements.

Many tests involve single cell contraction assays but the results do not provide an accurate representation of how cells react in a blood vessel environment. Additionally, many of these micropost arrays measure single cell motility, and little has been done with regards to testing of tissue constructs on PDMS microposts (Kim, 2011). Previous methods for cell force recording may not be as suitable or feasible since they require fixation and dehydration that induce undesirable

external stimulation (chemical, electrical, etc.) that may alter the mechanical properties of the cells (Zheng, 2010).

Cell contractility can be recorded using a transducer utilizing Moiré patterns as a visual and quantitative tool (Zheng, 2010). Light diffracted from two closely placed microfabricated periodic substrates is capable of mapping cell contraction forces via mapping cell displacement on the sample substrate. The force exerted by cell traction can then be conveniently studied through Moiré pattern evolution. However, this technique is extremely precise, expensive, and uses advanced technology. Additionally, the Moiré technique is more useful in measuring the motility properties of aggregating cells, and has not been used to measure ring contraction.

Similar to the micropost arrays and Moiré-based techniques is the method on a vertical array of flexible cantilevers, where individual cells are situated across many cantilevers and are deflected upon contraction (Zheng, 2010; Desai, 2007). These substrates are called microfabricated post-array-detectors, or mPADs. Deflections can be measured under a microscope and magnitude and direction of traction forces can be calculated as the cells contract. This allows for the observation and calculation of single cell traction and motility forces (Desai, 2007).

2.5.4 Cantilever Beams

Cantilever beams have also been developed by various researchers to study cellular contraction. An array of two flexible PDMS posts, with varying distances and diameters, are fabricated in a well, as shown in Figure 6. Distances between the posts can vary between 0.02-0.8 mm (Vandenburgh, 2008; Legant, 2009). Cells are seeded into the wells and have been observed to aggregate around the two posts, Figure 6c. Vandenburgh et al. (2008) used mouse myoblasts to create miniature bioartificial muscle (mBAM) and Legant et al. used a cell line of mouse fibroblasts (Vandenburgh, 2008; Legant, 2009). In one tray of PDMS, about 96 flexible posts could be made, enabling high throughput measurements to be conducted (Vandenburgh, 2008).

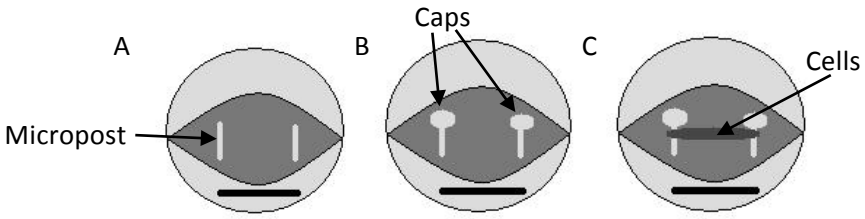

Figure 6: Flexible microposts; Scale bar = 20 µm. (A, B, C) Microposts of varying diameters, (B) Micropost with caps to prevent mBAM from slipping down or off the top of the post during deflections (C) Cells conjugated around the post. (derived from Vandenburgh, 2008).

This method tested the contractile properties of the cells in response to electrical stimulation, recombinant human insulin-like growth hormone, and Atorvastatin (Vandenburgh, 2008). Based on the chemical stimulation on the mBAMs, the degree of flexion of the posts could be observed and the force of contraction could be measured. Equation 1, a force-deflection equation for a cantilever beam, was used to calculate contractile force.

$$F = \frac{3\pi E R^4 \delta}{4L^3} \qquad (1)$$

In Equation 1, E is the elastic modulus (stiffness) of the PDMS posts, R is the micropost radius, δ is the distance of micropost deflection, and L is the length of the micropost. The post deflection angle can be observed using bright field images with an A-plan 10x objective on a Zeiss Axiovert 200 M (Legant, 2009). Angles were calculated with MatLab software after using Adobe Photoshop software to better observe the post images. Using this technique, even microNewton forces could be detected with 2-3% variability (Vandenburgh, 2008). Cheng et al. (2010) from the University of Missouri also used this equation to map cell motility and forces of smooth muscle cells on a micropost array. The deflection of their microposts allowed detection of single cell nanoNewton forces (Cheng, 2010). Other methods have used the spring constants in the posts to measure the post deflection. The above equation would change only slightly to take into consideration the spring constants of the post material but the concepts are still the same (Legant, 2009). Figure 7 shows the use of Equation 1 schematically.

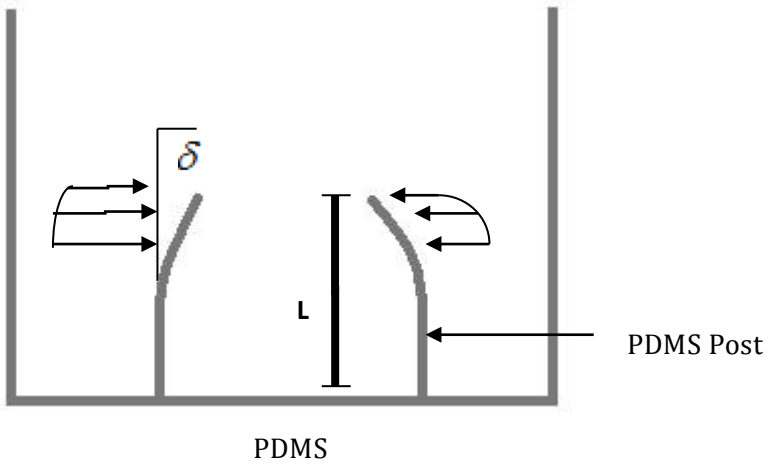

Figure 7: Model of post displacement, allowing for the force/displacement equation to be used to determine the contractile force exerted on the posts. Gamma is the displacement of the tip of the post from its original position (derived from Vandenburgh, 2008).

Cantilever Array Sensory System: U.S. Patent 2002/0092340-A1

Cantilevers were developed for atomic force microscopes as chemical sensing devices (Prater, 2002). In atomic force microscopy (AFM), the cantilever can be used as an extremely sensitive detector of contractile forces. To use a cantilever as a chemical sensor, the cantilever layer is typically coated to be a sensing layer in order to detect the target chemical. As a chemical binds to the cantilever, the physical properties may be altered which can be detected by measuring the resulting change in motion. To date, cantilevers are used for either assessment of mass detection; stress induced bending, or the bimetallic effect to detect heat from induced chemical reactions (Cheng, 2010; Prater, 2002).

Prater et al. (2002) created a cantilever sensor system, which includes an array of cantilevers, and a deflection measuring system. This invention specifically measures static and dynamic properties such as deflection, frequency, and other oscillation properties as a function of time in response to various target substances. Additional components, such as a high frequency clock may be added to the system in order to obtain accurate readings over specific time intervals.

However, there are a few shortcomings in this technique. First, the posts experience creep and hysteresis over a period of time, especially if there are errors in microfabrication of the posts (Cheng, 2010; Legant, 2009). These cantilever arrays are usually manufactured by photolithography, which involves using ultraviolet radiation to destroy the undesired PDMS and leave only the post arrays (Cheng, 2010). This process can occasionally cause weaknesses or defects in the remaining microposts. After several uses, the posts may not return to vertical and thus create readings that do not accurately reflect true contractile force. This can be compensated by measuring the deflection of the post—where the post actually stands—and starting data acquisition at that point instead of assuming the post is perfectly vertical. (Legant, 2009). A wide variety of cell types have not yet been tested in this method thus it is hard to determine how accurately the posts will be able to measure the contractility of cells with higher or lower contraction forces (Vandenburgh, 2008). Using a similar method, it was also found that the stiffness (elastic modulus) of the posts affected the contractile forces of the cells (Legant, 2009). Thus, if the stiffness of the posts is too high, the tissue rings will not be able to freely contract. Stiffness of the cantilever posts can be controlled by adjusting the thickness of the posts and tailoring the manufacturing techniques (Legant, 2009). Additionally, it must be ensured that the tissue rings do not fall off of the posts when the posts are deflected. To combat this, some studies

have constructed posts with a greater thickness at the tops ("heads") of the posts, so that the rings will not slip off (Legant, 2009).

Cantilever micropost arrays are a relatively recent technology that still requires more testing and research. Besides myoblasts and fibroblasts, rat heart cells have also been tested on cantilever microposts (Hansen, 2010). Thus, the cantilever micropost approach provides the potential for a high throughput means of measuring contractile forces, but this method has never been used to measure tissue rings comprised of any cell sources. Although the cantilever system has been successfully applied to a variety of cell types, it has yet to be used for the testing of vascular construct properties.

Imaging Modes to Observe Tissue Contraction

Imaging is a critical part of visualizing the contraction of tissue ring constructs, regardless of the method of contraction measurement. On cantilever microposts arrays, proper imaging is essential due to the need to observe and measure the deflection of the posts. This section addresses some of the optical approaches that may be used to observe and measure post contraction.

Various researchers have analyzed the contractile properties of a variety of cells on micropost array systems. In order to indirectly measure this property it is imperative to obtain high-resolution images of the posts deflecting. This allows for proper dimensions to be determined which can then be used in the appropriate contractile force equation.

Many imaging platforms have been utilized by researchers. They include high resolution cameras, phase contrast microscopy, scanning electron microscopy (SEM), and other relevant microscopes (Kim, 2007; Li, 2007; Sniadecki, 2008). High resolution cameras are usually coupled with a video post-processing program written in Matlab in order to calculate displacement of the posts. Contrastingly, microscopes are coupled with appropriate image analysis programs in order to properly analyze the deflections in the obtained micrographs. Both phase contrast microscopy and SEM provides high contrast micrographs, which have resulted in accurate force measurement (Li, 2007; Sniadecki, 2008). Magnification in a SEM can be controlled over a large range of up to 6 orders of magnitude from about 10 to 500,000 times (Science Learning Hub, 2012). High quality SEM imaging systems can cost from $250,000 to $1,000,000. On the other hand, the magnification of phase contrast microscopes cannot be varied by such a degree, usually ranging from 100x to 1000x. The Leica EZ4D phase contrast stereomicroscope costs about $2000 (LabLife, 2011). This

particular stereomicroscope contains a 3.0 Mega-Pixel CMOS Camera with a maximum resolution of 2048 x 1536 pixels.

Magnification variations due to changes in focus setting pose problems for depth from focus and defocus and thus visualizing data (Watanabe, 1997). This magnification problem can be minimized by using an optical configuration, known as telecentric optics or "constant-magnification imaging." Telecentric optics allows for the magnification of images. Additionally, magnification is kept constant between the images taken at different focus settings (Watanabe, 1997). Telecentricity on the object side implies that the image projection model in three-dimensions is represented in two-dimensions. Contrastingly, telecentricity on the image side leaves the image in perspective but yet the magnification of scene points is constant with respect to the location of the image detector behind the lens. A telecentric lens is a viable option to view either a fixed pin system or a micropost array system in action during tissue contraction.

In image-side telecentricity, magnification remains constant despite focus changes (Watanabe, 1997). A commercially available lens is easily transformed to telecentric ones by just adding an extra aperture as shown in Figure 8. The added lens is the aperture, which controls the amount of light that reaches the film. The quality of focus does change, however this can be minimized by decreasing the aperture (Visual Illusions, 1996). Using this system, if the object is moved nearer or farther from the lens system, its size on the film does not change. There is an optimum location for both object and film for best image sharpness, which can be determined by moving the camera closer or farther away from the object.

In order to accurately and precisely measure this minute distance, it is certainly an advantage to implement this magnifying image system. A telecentric lens is available at WPI by Professor Granquist-Fraser.

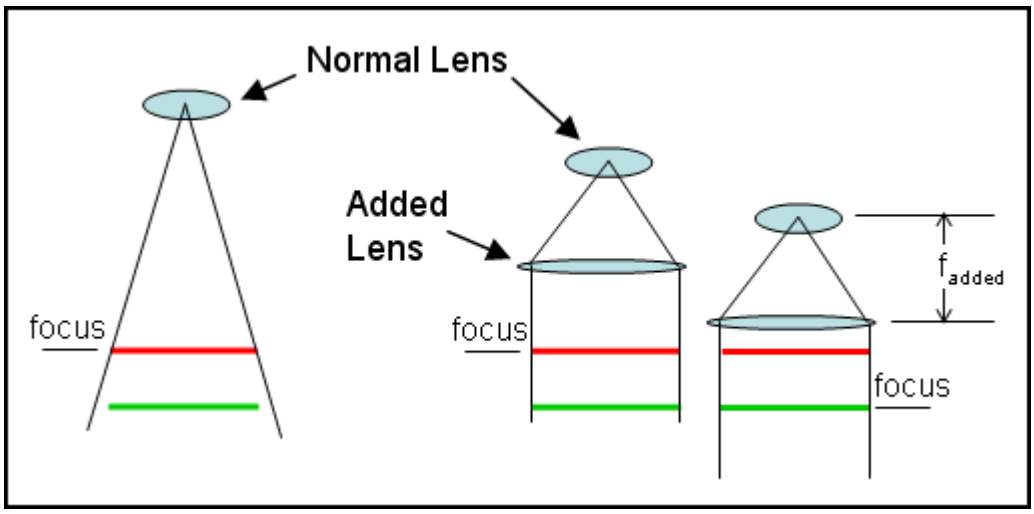

Figure 8: Diagram of a telecentric lens system (derived from Photomacrography, 2005).

For the scope of our project it is necessary to adapt one of these techniques in order to visualize and properly analyze deflection of the microposts. Specifically, we chose to use the LEICA EZ4D stereomicroscope for our imaging system. Although this microscope has not been utilized by any researcher thus far for measuring micropost deflection, it offered all of the imaging capabilities that we were looking for and was available for our use. Additionally, we experienced time and budget constraints; therefore, it was of our best interest to utilize this system.

The Leica EZ4D stereomicroscope, shown in Figure 9 below, offers a high quality imaging technique (Leica, 2012). The numerous light-emitting diodes (LEDs) provide high quality contrast and illumination and provide a 3D image of the sample being viewed. This device offers the ability to capture 3 Mega Pixel color images either directly on an SD card or onto a computer via a USB cord connection (Leica, 2012). Stereomicroscopes generally do not provide high power magnification, but vascular tissue rings used at WPI are generally either 2mm or 4mm in diameter, meaning a large amount of magnification is not necessary. The Leica EZ4D is available for use at WPI in the cell culture lab. Another potential option for imaging is to use the telecentric lens recommended by Professor Granquist-Fraser (outlined in Appendix A).

Figure 9: LEICA EZ4D Stereomicroscope (Leica, 2012).

2.6 Conclusions

As discussed in this literature review, the gap between native blood vessels and functional TEBVs with regards to their contractile properties has still not been extensively studied. Perhaps even more importantly, contractility testing will allow for the possibility to test the effectiveness of various drugs, perhaps leading to new treatments for cardiovascular disease. Many of the current methods of testing for contractility are low-throughput and expensive. There are no contractility methods that are high throughput and successful in testing 3D vascular ring constructs, made of strictly SMCs. Figure 10 displays a schematic of the overall aim that our project addresses in the process of toxicology testing: using engineered 3D tissue constructs for testing of various chemical compounds.

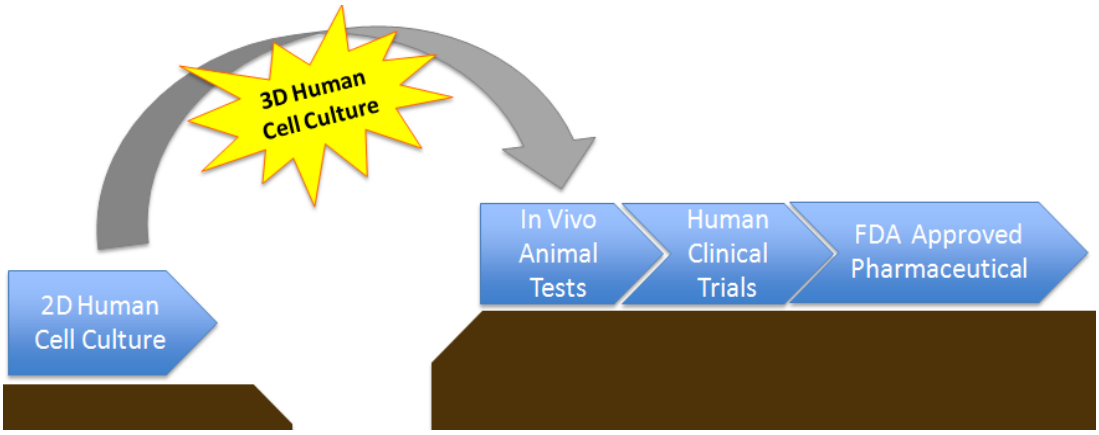

Figure 10: An overview of the current process of drug testing. 3D tissue construct testing in vitro can "bridge the gap" in the current testing process.

After extensively studying the current technologies and patent literature, we proposed to create a high throughput device that measures contractile forces of a tissue engineered ring construct. The device utilizes the effectiveness of testing a high number (at least 24 samples) of vascular tissue samples in an *in vitro* manner to quickly and effectively gathers information about the effects of various chemical compounds on blood vessel contractile properties.

Chapter 3: Project Strategy

The goal of this project is to design a device that can measure the contractile force of vascular tissue rings in a high throughput manner. We conducted an extensive literature review using a variety of journal articles and patent literature to gain a better understanding of the advancements and designs for high throughput contractility testing. Upon gathering the appropriate information from our literature review and interviews with our client and users of current devices, we brainstormed a list of objectives and constraints for our device. With the use of these objectives, we were able to fine-tune our client statement and make it more specific. The objectives were ranked by both the team and the advisor, and metrics were developed by the team to determine how to constitute the success of the device in completing each objective. The objectives and constraints also enabled us to develop a list of functions that the device must perform, and means for achieving these functions, which in turn allowed us to generate alternative designs for our device, all of which we outline in Chapter 4.

3.1 Initial Client Statement

The initial client statement provided to us by our advisor, Marsha Rolle Ph.D., stated: "High throughput screening methods are needed to test the vasoactivity (and/or toxicity) of chemical compounds. Tissue engineering approaches have shown promise for generating microscale living tissues that can be used to screen potential drugs for their effects on tissue function. The goal of this project is to adapt the cell-derived tissue ring system to create a microscale model of vascular tissue contraction which can be used to measure tissue function in response to known and unknown chemical compounds." Developing our objectives, constraints and functions from the use of our background research and client and user interviews allowed us to further refine this client statement and better complete our project goals.

3.2 Objectives and Metrics

Based upon our initial client statement and research on published literature, we developed the following main objectives for our device:

- **Measure contractile force**: It would be ideal to have an actual value output of force reading that is accurate and precise. For accuracy, measurements will follow the "gold standard" as measured on the DMT myograph contractile force measurement device. Values should be ± 10% when compared to DMT readings of the same tissue ring samples.

For precision, the force readings should be within 10% of each other when testing the same size and type tissue rings with the same chemicals. In order to obtain statistical significance, a p-value of ≤ 0.05 is desired. Additionally, the device must properly secure the tissue ring samples in place to prevent slippage or tissue damage and ensure an accurate force reading.

- **Easy to use**: The device should be easy to use. There should be minimal set-up time, ideally under 1 hour, which is the time it takes to set up the mouse aorta ring segments on the DMT myograph, and the device should allow for straightforward calibration, meaning it is not difficult to calibrate and recalibration can be done periodically. Overall, the entire testing procedure including set up, inducing contraction, and obtaining readings, should take under 3 hours in total, which is approximately the time it takes to test up to four total samples on the DMT myograph machine.
- **Versatile**: The device should be able to test more than one cell type, test rings of various diameters ranging from 0.5-6mm, and be able to culture and test rings on the same platform. This large diameter range is because mouse aortas can be as small as 0.5 mm, but smooth muscle rings can be made as large as 6 mm in diameter. Ideally, the device should be able to test the contraction of smooth muscle cells, cardiac myocytes, and even skeletal muscle cells (if they can be made to form rings), as *in vitro* contraction studies may be desirable for all three of these cell types. Additionally, it would reduce set up time and potential for tissue damage if the tissue ring samples could be cultured and tested using the same device (without the need to handle or transfer them to another device).
- **High throughput**: The device should be able to test at least 24 samples at the same time, as this was the ideal number given to us by our project advisor. It also should be able to test different concentrations of chemical agonists on these samples. This would allow for a large amount of force data from a wide variety of chemical agonists to be collected simultaneously in a relatively short amount of time. At WPI, the rings are made on twelve well plates, being able to test 24 samples simultaneously would permit the force measurements of two-twelve well plates at be conducted.
- **Easy to Manufacture**: The device should have minimal number of parts and be inexpensive to manufacture. This will allow for a large number of devices to be produced inexpensively and in a short amount of time, if many devices are desired. Additionally, if our device is reusable, it would reduce the overall number of devices needed for manufacturing.

To better understand and organize all of our objectives, we created an objectives tree complete with main objectives and corresponding sub-objectives (Appendix B). The team also developed a Pairwise Comparison Chart (PCC) in order to rank our main objectives in terms of importance. Five main objectives were analyzed and ranked based on levels of importance. We also had our project advisor, Professor Marsha Rolle, fill out the same PCC in order to better understand her opinions of which objectives were most important. The summary of our PCC can be seen in Table 1. Our PCC as well as Professor Rolle's PCC is included as Appendix C.

After obtaining her results, we averaged the scores of each objective from our chart and our advisor's chart and developed a weighted score based on the average scores of all objectives. The results can be seen in Table 1, below. It appears that we both agreed that the device must be able to successfully measure the contractile force of the rings. This is of the utmost importance due to the fact that if our device is unable to provide a force reading then none of the other objectives would matter. The next most important objective is that the device be easy to use, although we ranked this objective higher than our advisor. Straightforward calibration is important in order to have time-efficient accurate data. If it takes too much time to collect data then our device will not be feasible for the user. Versatility (being able to culture and test on the same device and test multiple cell types) is also important because this aspect sets the uniqueness to our design. The device should be versatile and can limit the experimental set up time by being able to culture and test rings on the same platform. It should be able to test a variety of ring sizes and ring cell types.

Our advisor seemed to think that making the device high throughput was also important, so we must take this into account when designing our device. Making our device high throughput will allow for a large amount of data to be obtained in a much shorter time period. Creating the pairwise chart and weighing the objectives will help us to evaluate our conceptual designs, as the best designs will be the ones that meet the most objectives and especially meet the most important objectives. The property of being easy to manufacture received the least attention because through the design process this aspect will always be considered in hindsight. In other words, the team is not going to go out of its way to make the device expensive or hard to make, but if the device completes all of the other objectives and is not very easy to manufacture, we will still consider the device successful.

Table 1: Pairwise Comparison Chart with Team, Client and Weighted Scores

Objectives	Team's Score	Professor Rolle's Score	Average	Weighted (%)
Successful in Measuring Contractile Force	5	5	5	38%
Easy to Use	4	2	3	22%
High Throughput	1.5	4	2.75	20%
Versatile	2.5	3	2.75	20%
Easy to Manufacture	0	0	0	0%

Once we ranked all of our objectives, it was vital to make sure that each objective had corresponding metrics to determine what constitutes the success of our device in completing each objective. Our metrics were mainly derived from our research of tissue engineering literature and from the standards set by the DMT myograph device. Based on our research and talking with operators of the DMT myograph, we developed the following metrics for each objective:

Objective: Measure contractile force

Metrics:

- All force values (same ring type and agonist) obtained within 10% of each other – 1 point
- All force values (same ring type and agonist) obtained within 50% variation of each other – ½ point
- All force values (same ring and agonist) greater than 50% variation – 0 points

Objective: Easy to use

Metrics:

- Entire set up and procedure completed in less than 3 hours – 1 point
- Entire set up and procedure completed in 4-5 hours – ½ point
- Entire set up and procedure completed in more than 5 hours – 0 points

Objective: High throughput

Metrics:

- Test more than 24 samples at the same time – 1 point
- Test 24 samples at the same time – ½ point
- Test less than 24 samples – 0 points

Objective: Versatile

Metrics:

- Device can measure more than one cell type – 1 point
- Device can only measure one cell type – 0 points
- Device can test various rings with diameters 0.5 – 6 mm – 1 point
- Device can only test one size diameter of rings – 0 points
- Device allows for both culture and measurement - 1 point
- Device allows for only measurement – 0 points

Objective: Easy to manufacture

Metrics:

- Can be manufactured in less than 4 days – 1 point
- Can be manufactured in 1 week – ½ point
- Can be manufactured in more than 1 week – 0 points

The DMT myograph device will serve as the "gold standard" for our accuracy and set up time objectives. Our interview with Dr. Siobhan Craige (post-doctoral fellow, Division of Cardiovascular Medicine, UMass Medical School) allowed us to see that the entire set up and testing time for a mouse aorta with the DMT machine takes 4-5 hours, so we want our device set up and procedure time to be significantly less than this. Based on our initial interview with our advisor, we would like our device to be able to test at least 24 samples at the same time, to allow for high throughput measurements. We want our device to be able to test rings from diameters 0.5 mm to 6 mm because mouse aortas can be as small as 0.5 mm, but smooth muscle rings can be made as large as 6 mm in diameter. Ideally, our device should be created in less than 4 days because we want to be able to manufacture multiple prototypes in order to complete a majority of complete testing in a short period of time and keeping in time with the growing rate of the cells. Additionally, this would allow us to make adjustments to our design and have a new mold design machined within one week. Summaries of the interviews with Dr. Craige and Professor Rolle can be found in Appendix A.

3.3 Constraints

Along with project objectives, we also developed constraints for our project to allow us to better define the client statement. Two of the most limiting constraints in this design process are time and money. Our project must be completed for Project Presentation Day in April 2012 and our report must be submitted by April 19, 2012. The total allotted budget for the project is $524. This is the maximum we can spend to build and test our device. All alternative designs must be safe for the user and nontoxic to the cells. Biocompatibility must be stressed to keep cells alive. We have a

limited number of tissue samples available and must work with the available smooth muscle cells or mouse aortas provided to us by UMASS or the WPI Biomedical Engineering Department. It takes time to create the tissue rings (usually 4-7 days) and each mold currently produces up to 15 tissue rings. This limits the number of tests that can be run to determine the effectiveness of our device. All of these constraints must be taken into account when creating the conceptual designs of our device.

3.4 Revised Client Statement

After carefully conducting research on the current field of vascular tissue engineering and better understanding our objectives, constraints and design metrics, we were able to compose an updated client statement pertaining more specifically to our device design. The revised client statement is as follows:

> "The goal of this project is to design an efficient (taking less than 3 hours of setup and testing time) and low-cost (less than $524 to manufacture and test) microscale high throughput vascular tissue ring contraction measurement device. The device must be both easy to manufacture and to use and may test 24 samples of tissue rings that are less than 6 mm in diameter. It can allow for several types of tissue to be tested and must be safe to the user, accurate, and precise in measuring the contractile force of tissue ring samples. The device must also allow for the uniform distribution of various amounts of chemicals to each sample to induce contraction and not damage tissue samples."

This revised client statement allowed us to better understand the problem and the goals of our overall design. We then were able to enter the design development stage, which is outlined in Chapter 4.

Chapter 4: Design Alternatives

The team facilitated a brainstorming session in order to develop different design alternatives for a potential device based on our objectives, constraints, functions, and means. During design conception, we made an effort to use minimal parts that were inexpensive in order to meet the design constraints. A total of six main design alternatives were devised, some of which have parts that can be altered or modified if necessary, as determined after our testing. Each alternative is described thoroughly in this chapter through illustrations, descriptions, and some brief advantages and disadvantages.

4.1 Functions and Specifications

As part of developing our project strategy (Chapter 3), we defined functions, specifications and means for how we wanted our final device to work. The morphological chart, as seen in Table 2, lists the functions and means we have brainstormed and developed. A function and means tree can be found in Appendix D. We used this morphological chart to develop the various alternative designs outlined in subsequent sections.

Table 2: Morphological Chart

Function/Mean	1	2	3	4
Measure contractile force	Micropost arrays/Cantilever beams	Force transducer	Fixed-moveable post	Liquid/gel displacement
Culture and measure on same device	Molds with solid base post and microposts	Solid cover with micropost attachments	•••	•••
Test variety of cells	Seed and culture rings in wells	Seed cells on micropost	•••	•••
Test different diameter rings	Adjustable spacing of microposts	Fixed microposts of different spacing	Adjustable squeezing posts	Moveable pin system
Measure post deflection	High speed camera, δ measurement, force equation, code in MatLab	Force transducer	Change in volume within tube, tells pressure achieved	•••
Secure rings on posts	Fat heads	Caps	Notches	Solid cover
Promote cell growth/ ring aggregation	Smooth surface	No wires	No sharp edges	•••
Add/remove chemicals	Vacuum	Pipetting	•••	•••
Minimize cross contamination	Wells	Chambers	•••	•••

Induce contraction	Electrical stimuli	Chemical stimuli	•••	•••

As seen in Table 2, several options are available for completing all of the device's main functions. Contractile force can be measured by various micropost arrays, force transducers, moveable pin systems, or liquid/gel displacement mechanisms. Culturing and measuring can be done on the same device by molds that include microposts or by covers for the molds that have attached microposts. There are a variety of methods to secure the rings in place and to measure the deflection of the microposts. Also, there is more than one way to induce contraction and to add and remove the chemicals. To prevent damage to the endothelium if co-culture rings are used, it should be ensured that the device has a smooth surface and no sharp edges, so the measurements can be accurately taken. It must be taken into account that wires or metal features can slough off the endothelium layer or damage smooth muscle rings, so great care must be taken when handling the tissue rings.

In order to get a better idea of the details of each of our conceptual designs, each of our functions had to be assigned certain specifications. All of the details of our designs must have reasoning behind them from the available literature, so that all of our designs can be properly verified during our testing procedures. A list of some of the important design specifications, along with the corresponding functions of our device, can be viewed in Table 3.

Table 3: Functions and Specifications

Functions	Specifications
Measure contractile force	• Expected time of maximum contraction: between 30-60 seconds[1] • Microscopy allowing for at least 4X magnification and 3 megapixel images[2]
Culture and measure on same device	• Size of molds: fit in 6-well plate or 5.75 inches × 4.5 inches • Cell culture time: 1-5 days • 100,000 to 300,000 cells in a 2 mm tissue ring sample
Test variety of cells	• Cardiac myocytes • Skeletal myocytes • Smooth muscle cells • Endothelial/smooth muscle cell co-cultures
Test different diameter rings	• Size of tissue rings grown in the WPI lab: 4 mm and 2 mm diameter[3] • Size of the mouse aorta used at UMASS: 2 mm thickness, 0.7 mm diameter[4]
Measure post deflection	• Micropost: 700-800 μm diameter[1] • Elastic modulus of PDMS with 10% curing agent: 200 kPa – 400 kPa[5]

Secure rings	• Entire ring must remain on post or pin when measurements are beings taken
Promote cell growth/ring aggregation	• Make sure that the well in the device is no thicker than 2.5 mm, so that the SMCs can aggregate[6]
Add/remove chemicals	• Acetylcholine – 10-30 microMolar • Phenylephrine – 30 microMolar • Potassium Chloride – 66 milliMolar or 0.1 %[7]
Minimize cross contamination	• Prevent any splashing, leaking, mixing of fluids and agonists between the wells
Induce contraction	• Expected force readings – 1-30 μN[8] • Using a microscope/high speed camera, visible constriction and shrinking of diameter in rings

[1] Vandenburgh (2008)
[2] Leica (2012)
[3] Gwyther (2011)
[4] Siobhan Craige, personal communication, 3 October 2011
[5] Sasoglu (2007)
[6] Marsha Rolle, personal communication, 13 March 2012
[7] Scholar Chemistry (2008); Spires (2005)
[8] Murphy (1974)

Table 3 displays some of the important specifications that our designs must follow. The design specifications are based on standards found in literature from a variety of tissue contraction studies or from our interviews with Dr. Craige at UMASS Medical School and our project advisor. Further details will be provided in the design descriptions that are presented in the following sections.

4.2 Versatile Culture and Testing Device

To meet the versatility objective, we developed a design which allowed for both tissue ring formation and testing of tissue ring contraction. The outstanding characteristic of this device is that tissue rings can be cultured by self-aggregation and tested in the same device. This design alternative incorporates a portion at the bottom of the well that enables seeding and culturing of ring segments as well as an extension of the center post with four additional smaller microposts. We decided to use four microposts instead of two that was presented in the literature, so the ring can maintain its circular integrity, mimicking a native blood vessel's structure, instead of an ellipsoid structure that will be produced during contraction on two posts. These microposts are used to measure the contractile forces inflicted by stimulated vessel rings. Thus, when the cells are fully aggregated into a ring, they can be slid upward onto the microposts by the use of forceps, or they may potentially slide up the posts on their own, and tested by stimulation with chemical agonists. Small adjustable pipettes can be used to add and remove chemical agonists. Use of a high speed (3-5 frames per second), high-resolution (at least 2 megapixels) camera, or an adequate form of microscopy, can record the process of contraction. This high resolution is necessary to allow for

accurate deflection measurements, as contraction of SMCs may be very small. Frames from the beginning and end of the experiment can be used to measure the deflection on the posts, which then can be used to calculate the contractile force experienced from the ring segments, derived from a force-deflection equation. Our rationale is that four posts will provide increased stability and structural integrity. Ring constructs have never been tested on micropost arrays, so there is no prior literature containing a separate equation for a four-post array of posts. However, contraction force can be calculated based on the deflection of simply one post and all posts will have the same properties. Thus, it does not seem that the equation used for a four post array would be any different than that used by Vandenburgh, 2008 on their two micropost array. Additionally, because the ring will be completely submerged in chemical agonist, it should contract uniformly around the microposts, allowing for deflection of any of the four posts to be used for the force calculation.

The wells and base posts, where the cells are cultured, can be made out of 2% agarose with supplemented media and each base post will be 4 mm in diameter, a diameter commonly produced in Professor Rolle's lab. The four microposts extruding from the center base will be made out of PDMS and have a diameter between 700-800 μm. This material and dimension was decided upon reference to Vandenburgh's findings when he tested the tetanic forces exerted by the mBAM and hysteresis and creep of the PDMS (Vandenburgh, 2008). He found that there was minimal deflection from resting tension to the microposts, hysteresis was 6.5 ± 1.55% and creep was <1% after 100 deflection tests and these microposts provided accurate force measurements (Vandenburgh, 2008). Figure 11 shows the basic structure of a single well.

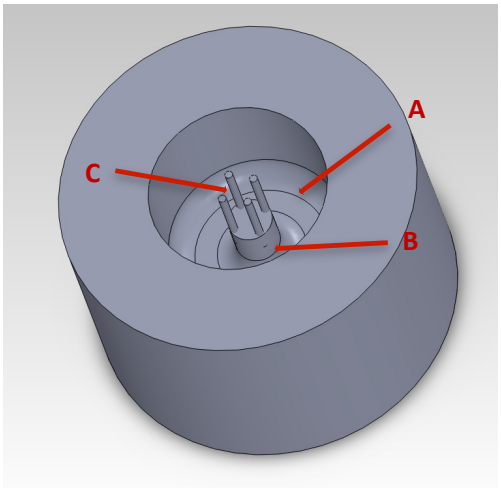

Figure 11: Single multifunctional culture and test design. (A) Seeding well where rings are cultured and tested. (B) Base post where cells aggregate around to form a ring. (C) Microposts where rings are tested.

This design also allows for variations and modifications for each component that can be made after testing, if necessary. A variety of different cell types, including cardiac myocytes, skeletal myocytes, airway smooth muscle cells etc., have the potential to be tested with the four microposts because any cell type that can be aggregated into a ring shaped construct can be placed around the posts. Since most studies have reported only seeding cells onto the tops of micropost arrays and calculating the contractile force from recorded deflections, that same concept can be applied to the microposts we propose to design. However, we plan to guide the tissue rings around the posts, and then measure the contractile force of the rings by the deflection of the tops of the posts. To prevent the cells from slipping off the microposts (by contracting and sliding off the tops of the posts), each micropost can have a bulge ("cap") at the top to prevent the ring from sliding off the posts or they can be embossed inward at the tip to create a notch that will keep the ring in place. A solid cover can be designed to contact flush with the tops of the microposts and prevent tissue rings from slipping off, while still allowing the ability to add and remove solutions and allowing the posts to deflect freely. Figure 12 shows some of our post design ideas for preventing ring slippage.

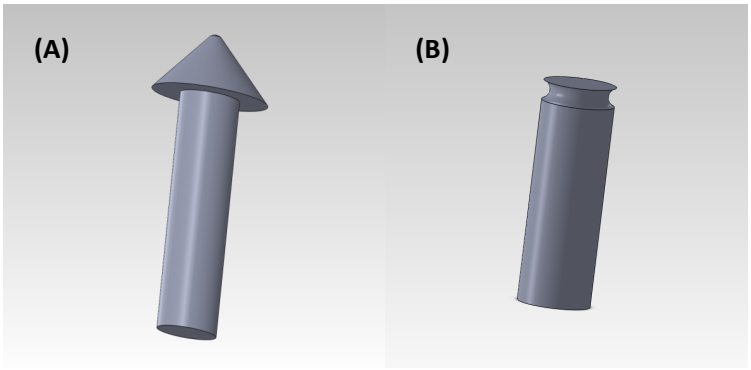

Figure 12: Post designs. (A) Cap on tip of micropost used to prevent tissue ring from sliding off top. (B) The tissue ring rests in the groove/notch that it prevents it from slipping during contraction.

Another variation of this design can be to adjust the depth of the wells to enable the addition of chemicals and the uniformity of chemical interaction with the cells. Also a chamber-well design can be used to ensure the chemicals surround the entire tissue to produce the desired effect on the rings. A last variation of design is to develop a base that can fit in six-well cell culture plates. Thus, the use of this design is very time efficient, allowing for fast and uniform chemical addition or removal.

However, some problems could be associated with this overall design. The securing of the PDMS microposts to the 2mm base post while keeping all the components sterile may be difficult.

Thus, we will look into making the posts potentially out of another material, such as agarose (which is commonly used in cell culture) or polyacrylamide gel. In addition, the PDMS microposts may be damaged from handling procedures.

Overall, there is much potential in this design. It addresses most of our objectives and has many components that can be altered and combined to make it a better and more efficient design. This culture and testing design allows for growing and testing of tissue-engineered rings to be performed all in one device.

4.3 Cap Design

This design alternative is composed of four distinct parts as shown in Figure 13. It involves two main microplates. One plate is used to culture cells; it has a central post that is 2 mm in diameter, so the cells can aggregate into a ring. The second microplate, or the "cap," has four PDMS microposts 700-800 μm in diameter protruding from the cover that aligns with each of the posts on the cell culturing plate. At each corner of the cap component, there is a peg (not shown in Figure 13) that is used to secure the two plates and ensure alignment of the culturing post and the microposts. The device is then able to be flipped allowing the rings to either slide down or be moved onto the four microposts with forceps. The rings are then initiated to contract around each bed of microposts where deflection can be calculated. This method is both high throughput and multifunctional, as a large number of ring samples can be induced to contract at the same time.

However, tissue rings could be damaged when the ring is flipped over. Additionally, it is still an unknown how well the rings will slide down the posts, and whether or not this could be damaging to the inner diameters of the rings.

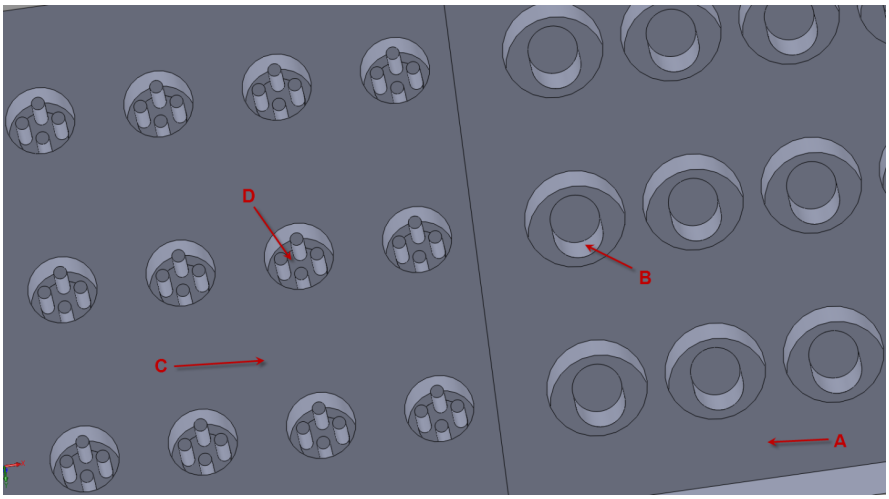

Figure 13: Cap design. (A) microplate where cells are cultured. (B) post where cells aggregate into ring. (C) PDMS microplate. (D) wells containing four microposts. The device would work by growing the tissue rings in (A) and then placing (A) on top of (C) to allow the ring to slide down onto the microposts, where contraction can be induced.

4.4 Prong Design

The prong post design has many similar aspects as the multifunctional culture and testing device listed in Section 4.2 but a different method of obtaining a force reading. Upon adding the chemicals to the rings on the top of the post, the rings would shrink and slide down the prongs while contraction is taking place and stop sliding down once contraction is ended. Through the use of a high-speed camera to track the time it takes for the ring to shrink and the known change in diameter, force calculations could be derived. This design again could be manufactured to culture and test the rings on the same piece. The prongs are no wider than the base at the top, which will allow for the rings to fit tightly around the top. One of the ways of preventing the rings from slipping off that have been listed above can be employed in this design as well. The well of this design may be made to have a larger diameter than those of designs previously mentioned, which would allow for easier use of calipers for measurements. An optical imaging form of measurement may be also be used with this design. This will make the use of pipettes to add and remove chemicals much easier. Figure 14 depicts the prong design.

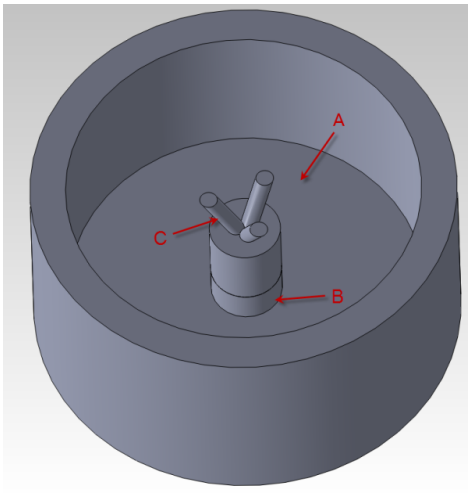

Figure 14: Three-pronged post design. (A) Well where rings are cultured and tested. (B) Base post where cells aggregate around to form a ring. (C) Microposts "prongs" where rings are tested.

This device has some potential advantages and disadvantages. This technique could be used to grow the cells around the base as well, making it another potential multifunctional design. It could also be high throughput as these posts can be placed in the wells of a standard cell culture plate for several rings to be grown and then tested simultaneously. However, it may be difficult to machine and hard to get the rings to stay on the top of the three prongs. It is not known to what extent the rings will slide down the prongs on their own, or if the prongs will damage the interior diameter of the tissue rings. The friction between the prongs and the ring's inner diameter has the potential to limit the sliding of the rings down the prongs, and thus skew the force calculation. An additional force that may need to be taken into account is gravity, as this will be acting on the tissue ring to slide it down the post.

4.5 Fixed Pin System Design

After conducting background research on various contractile measurement devices, the most prevalent devices found were force transducers. Although our budget most likely will not allow us to design a fully functional force transducer, we have decided to take the basic concepts of force transducers in order to design our own device. Most of the force transducers we discovered consisted of a fixed pin placed on one side of the inner diameter of a tissue ring and another movable pin placed on the opposite side of the inner diameter. When the ring contracts, the movable pin will displace with the tissue movement and can measure the force causing the movement of the pin. We plan to design a similar device with two pins, one fixed and one able to move freely. We will also have a small measurement scale (similar to that on a ruler or calipers) on the device in order to measure the displacement of the movable pin, or use an imaging system to

tell how much the pin has moved based on the tissue ring contraction. The tip of such a device can be seen in Figure 15. This device would be hand held, so that it would be moved from one tissue ring sample to the other for contraction measurements.

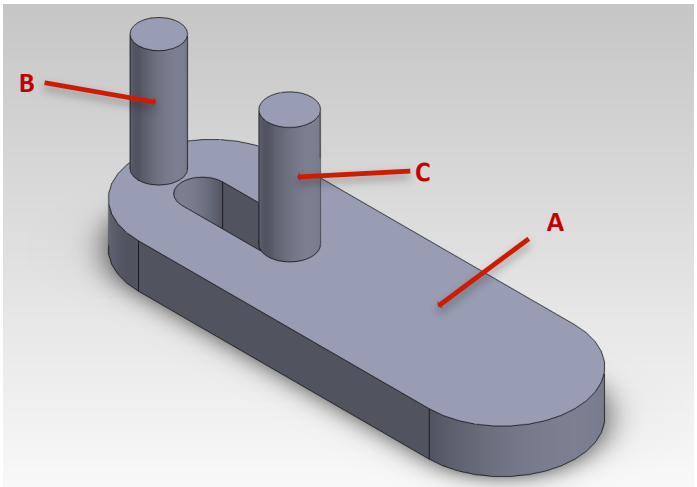

Figure 15: Fixed-pin device. (A) Handle section where the device can be held and allows for movement to various wells for testing. (B) Fixed Pin. (C) Moveable Pin. The ring would be placed around the fixed and movable pin and allowed to contract.

It will also be high throughput because a large amount of rings can be grown in wells and each ring's contraction can be quickly measured by moving this device from one well to the other. By measuring the initial diameter and then the new diameter of the ring after contraction has taken place, we can calculate the amount of force that the ring generated based on the time of contraction and the amount the ring diameter displaced. Thus, we will need to monitor the time it takes for the ring contraction to take place, most likely with microscopy or a high speed camera.

Another potential variation of this design is to use two fixed pins to a set diameter made out of a material with elastic properties instead of using a fixed pin and moveable pin. Thus, the concept will be the same as the PDMS micropost deflection, but this device can be handheld and portable. This way, contraction will induce deflection of the fixed pins and force can be measured from this deflection. This design offers an alternative to the many micropost models.

4.6 Hollow Tube Filled with Gel or Liquid

Another alternative design that we have been working on is a multifunctional design that allows the cells to be cultured in a well and aggregate into either a 2 mm or a 4 mm diameter ring. The design will be similar to the molds that are currently being used to grow the tissue rings in the laboratory. However, the cylindrical post that allows the cells to aggregate into a ring will be

hollowed out and filled with either a gel-like or liquid substance. After the tissue ring has formed, concentrations of chemical compounds can be exposed to the rings, eliciting contraction. The rings will contract around the post, increasing the pressure inside of the post and causing some of the liquid or gel to dispel from the inside. Thus, a new volume of liquid will be inside of the post once the ring is done contracting. The displaced liquid could be collected in a holding tray (as seen in Figure 16) or a one way valve could be used to collect the displaced liquid.

From the change in volume before and after contraction, we could calculate how much force the tissue ring contracted to dispel the liquid, similar to how a tube of toothpaste is squeezed to dispel the toothpaste. There are some concerns that the design may not be accurate in measuring the displaced volume because some of the liquid may remain trapped in the one way valve. To combat this, we could use a solidifying agent to turn the liquid into a solid, or we could measure the volume in the post before and after contraction, rather than measuring the volume in the valve or holding container. Although we are currently unsure if this design idea is entirely feasible, we plan to conduct some more research in order to get an idea of which materials could be used to make this idea possible. For the time being, we will keep it as a design alternative because this concept satisfies many of our main objectives. It could be made high throughput, multifunctional, and easy to use.

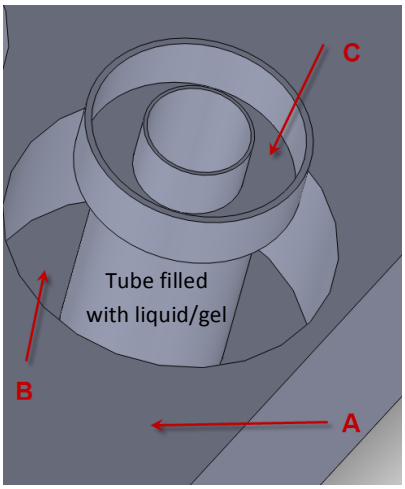

Figure 16: Liquid or gel displacement design. (A) Plate containing the wells where rings are cultured and tested. (B) Well where rings are cultured and slid up to be tested. (C) Mini well where the displaced gel, from the contracted rings, can be collected in the holding trays. The tube is in the center of the figure.

As outlined in this chapter, the team has devised several ideas for conceptual designs for a tissue ring contraction force measurement device. Although many of these designs are still only in the conceptual phase, we will begin to conduct several tests to verify which features of each design best complete each of our functions and objectives that have been outlined. This testing will enable

us to narrow down all of the conceptual designs and decide on the best features and aspects of each design idea in order to develop a final design idea. A detailed description of our experimental procedures and results for our alternative design testing are provided in Chapter 5.

Chapter 5: Evaluation of Design Alternatives

After devising several conceptual designs, the team brainstormed methods for testing those designs. The testing phase of this project has allowed us to use our metrics to gauge whether or not the features of each design successfully complete an objective. We first gathered all of our materials for testing, and devised our testing protocols. It was important that we tested for several factors relating to each design idea in order to get a clear idea of which features best completed our design objectives. Some of the initial factors that we tested for include: the flexibility of our microposts, how to build prototypes of our three pronged model and displaced volume (squeeze) idea, different materials that molds and microposts can be made of, the general handling and culturing of the tissue rings, the amount of ring adhesion to the posts, and different mechanisms to prevent ring slippage off of a micropost or the prongs.

We conducted tests on several of our design alternatives in order to determine how well they met our objectives and how easy or difficult they would be to manufacture for a working prototype. We conducted a large amount of conceptual testing, with materials that a working prototype would not be made of, but were inexpensive to obtain and would give us a good idea of the functionality of our designs. Based on our experimental testing, we have been able to create a numerical evaluation matrix, allowing us to eliminate some of the conceptual design alternatives discussed in Chapter 4 and decide upon a final design idea. This chapter contains both the experimental testing procedures, the results of our testing, and the conclusions that we can draw from these results. A complete list of materials needed for our all of our experimentation can be seen in Appendix E.

5.1 Simulation for Contractile Tissue Rings

In order to conduct contractile force testing on a variety of our designs, we elected to use various items to simulate the contractile tissue rings before we actually began to culture the rings. It takes time and resources to culture cells and assemble tissue rings, so we needed to first use substitutes for actual tissue rings in order to eliminate our designs that could not give us a proper means to measure contractile force. The items that we used for this purpose were both 4.8 mm and 7.9 mm diameter elastic bands, commonly used for braces and other orthodontic applications. Our rationale was that when stretched to a known diameter, the elastic bands would simulate a contraction force in the desire to return to their original diameter. Thus, we measured the

resistance to failure by the rubber bands at known diameters by using an Instron 5440 uniaxial testing machine (Figure 17). We stretched the elastic bands to a known length. The 4.8 mm bands were stretched to an extension of around 2 mm because they were going to be used for the testing of our fixed pin model. In this prototype, we planned to stretch the 4.8 mm bands an additional 2 mm and allow them to move the moveable pin in an attempt to return to their original diameter. The 7.9 mm bands were stretched an additional 7 mm because they were to be used in the four post prototype, where they would be stretched an additional 7 mm from their original diameter around plastic stirrers (the detailed procedure for this testing is outlined later in this chapter). This was done for five separate trials and then the results were averaged in order to obtain a known force, which could then be employed for various contractile tests on our design alternatives. We conducted these tests for both the 4.8 mm and 7.9 mm elastic bands. This data can be seen in Table 4 for the 4.8 mm elastic bands and Table 5 for the 7.9 mm elastic bands.

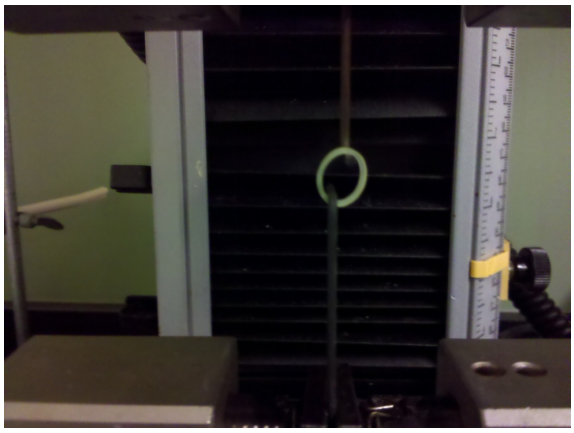

Figure 17: Tensile testing of elastic band using Instron machine.

Table 4: Forces produced by the 4.8 mm elastic band during Instron testing

Elastic Band Extension (mm)		Force Generated (N)	
	2.027		0.096
	2.059		0.260
	2.184		0.353
	2.066		0.408
	2.028		0.307
	2.033		0.395
Average:	2.066	**Average:**	0.303

Table 5: Forces produced by the 7.9 mm elastic band during Instron testing

Elastic Band Extension (mm)		Force Generated (N)	
	7.501		0.59
	7.68		0.595
	7.62		0.413
	7.68		0.53
Average:	7.620	**Average:**	0.532

However, we felt that it would be easier and more accurate to have a broad range of force/extension readings for any testing procedures we wanted to design. Thus, we did Instron uniaxial tensile testing of the elastic bands and decided to pull these elastic bands to failure. Figure 18 shows an example of the Instron testing of the orthodontic band. A total of five elastic bands were tested and stretched to around 55 mm in order to achieve a force versus extension curve (Figure 19). The bands displayed great elasticity, so it was difficult to pull them to failure. However, an extension of 55 mm was certainly greater than we would be using in any of our testing procedures, so we were confident that the range of values we obtained was sufficient. This testing allowed us to obtain data simulating a ring producing an inward force. Although the rubber bands were not really contracting, they were producing an inward force when they were stretched, similar to a ring contracting and producing an inward force. Additionally, this testing allowed us to obtain a wide range of force vs. extension values for the rubber bands. When we tested our prototypes with the rubber bands, we were able to see how a ring shaped structure would interact with the device and how well the device would be able to withstand an inward "contractile" force. A complete data summary of the elastic band Instron testing can also be seen in Table 6.

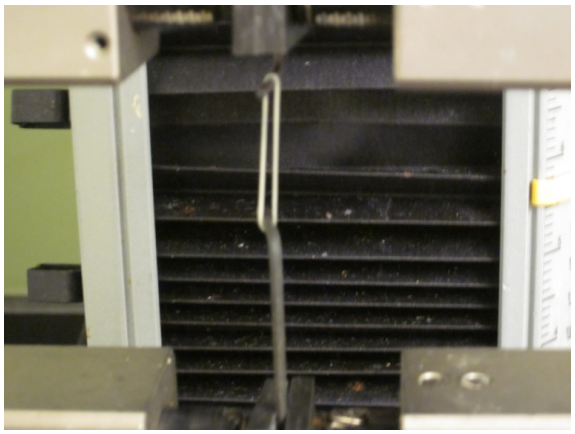

Figure 18: Elastic band undergoing Instron uniaxial tensile testing.

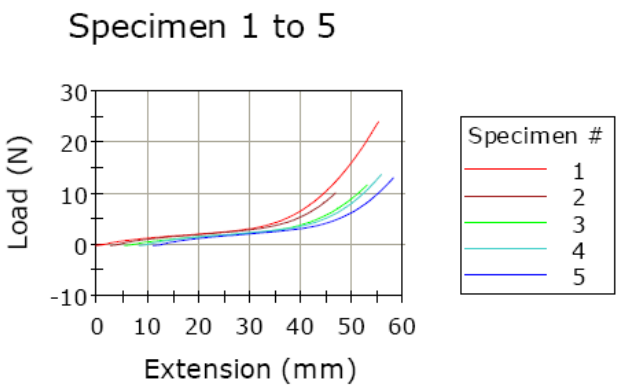

Figure 19: Raw data from the orthodontic elastic band Instron testing.

Table 6: Data summary of the elastic band testing

Sample	Maximum Force (N)	Maximum Extension (mm)
1	24.0	55.1
2	10.2	43.9
3	11.8	47.4
4	13.7	47.3
5	13.1	47.0
Average	14.56	48.14

The next item that we wanted to use to simulate the contracting tissue rings was a strain gauge, also sometimes referred to as a Mark 10™, as it is one of the most common brand names of these devices. The string on the gauge could be wrapped around the posts or the prongs, and tightened to a certain diameter. The other end of the string would be attached to a force gauge. Thus, we could tell how much force was being exerted on the posts at each change in diameter of the string. This would be another useful tool for simulating a contracting ring. However, this gauge is very expensive to purchase, and would virtually take up our entire project budget. Thus, we attempted to contact Mitralign, a company that some of our group members have worked with before, to see if they would let us use this tool. We also contacted various other sources, including the Physics Department, Robotics Engineering Department, and Mechanical Engineering Department, to see if they have any of these available for us to borrow for use. Unfortunately, we were unable to obtain the strain gauge, so we continued testing using the elastic bands to simulate our contracting rings, and from there we planned to move on to testing with actual cultured tissue rings for our final design.

5.1.1 Fixed Pin Model

One of the design alternatives that we thought about in Chapter 4 was the fixed pin model, which could possibly be a handheld device that had one pin that was free to move and one pin that

was fixed. These pins could be placed in the inner diameter of the rings, and the moveable pin would move in response to the ring contracting. From this movement, we could determine the change in the diameter over time, and thus calculate the force. However, we decided not to continue on with this model early in the testing phase of this project. We attempted to make several prototypes in order to start testing, but it was very difficult to assemble and was much more complicated than we anticipated because of the minuscule features of this device. The moveable pin experienced much more friction than expected and barely moved in response to the rubber bands. Thus, we did not think that it would be able to move at all in response to the much smaller forces that would be produced by contracting tissue rings. Also, we felt that this method could not really be made high throughput, and was going to be very difficult to get accurate measurements at such small sizes. It was found in the literature that many of the force gauges used to measure cell contraction use a two pin method very similar to what we had proposed. Therefore, we decided to move onto testing and prototyping with our other design ideas, and did not conduct any data resulting tests on this design, as we did not continue to try to develop a useable prototype for this design.

5.2 Three-Prong Design

One of the first designs that we tested for was the three pronged design. Ideally, our idea was that the tissue rings could be cultured and handled with forceps and placed onto wire or plastic posts. The ring would sit on the posts (at a known position) and then the chemical agonists could be added to induce ring contraction. Once contraction occurs, the ring will slide down the prongs and stop at a known diameter (known distance between the prongs). This idea is conceptually similar to that used by Jeffrey Morgan's lab, at Brown University (Morgan, 2010). In order to test the functionality of this design, we created a prototype with three metal wire prongs embedded in a Styrofoam base and then used a Spaghetti-O to act as a tissue ring (Figure 20).

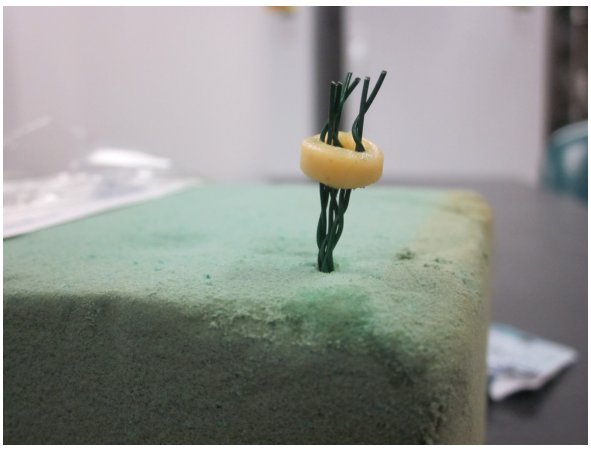

Figure 20: Spaghetti-O resting on our three-prong prototype.

5.2.1 Handling Testing

The first test we conducted was a sample handling test to see how much time it would take to handle and mount the rings onto the three prongs. Essentially, for our design to be high throughput, we would need to mount at least 24 tissue ring samples onto one microplate containing prongs and then induce contraction to all the rings simultaneously. Also, it was necessary to decide whether it would be beneficial to make this design multifunctional, meaning the cells would be cultured on the same array as the prongs. This way, once the cells aggregate into rings, they could be slid right up onto the posts. We tested the handling time by starting with the Spaghetti-O in a plastic weigh boat and using the forceps, picked it up and placed it onto the prongs. This was repeated 5 times and each trial was timed with a stopwatch and recorded. The results of these trials can be seen in Table 7. A picture of the handling experiments can be seen in Figure 21.

Table 7: Results of handling testing for non-multifunctional three-pronged design

	Time to Place Spaghetti-O on Prongs (sec)	Time to Do the Same on 24 Wells (min)
Trial 1	31.0	12.4
Trial 2	24.0	9.6
Trial 3	N/A (the Spaghetti-O ripped)	N/A
Trial 4	19.0	7.6
Trial 5	21.0	8.4
Average	23.75	9.5

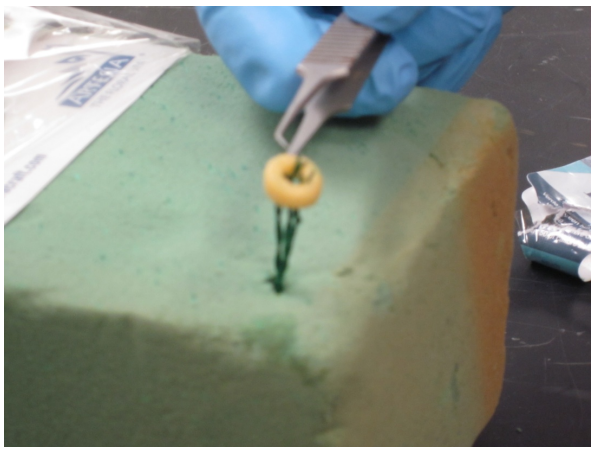

Figure 21: Sliding Spaghetti-O onto the three-prongs with forceps during testing.

The average time it took to place the Spaghetti-Os successfully on the prongs was around 24 seconds, which would translate to an average of about 9.5 minutes in total to place all of the tissue rings onto the posts before contraction could even be induced. It is important to note that during one of the trials, the Spaghetti-O ripped when it was being slid down the metal wire prong. This made it evident that some of our tissue ring samples could be damaged or even destroyed using this technique.

We then completed the same type of handling test, except this time to simulate the multifunctional design option. To begin, we had the Spaghetti-Os at the base of the prongs and then we slid them up the prongs until they were securely in place. We did this handling for five separate trials and timed each one with a stopwatch. The results from this testing can be seen in Table 8. The average time to slide the Spaghetti-Os onto the prongs was 6 seconds, which translates to 2.4 minutes for all 24 samples to be prepared in a high throughput arrangement. Obviously, this is much faster than the previous testing times, showing that the multifunctional design would be much more time efficient and allow us to test 24 samples more quickly. Additionally, none of the Spaghetti-Os were damaged in this testing procedure, so it is likely that this technique would produce less damage to the tissue ring samples. After the handling testing and timing experiments, it appears evident that the multifunctional three-pronged design would better meet some of our design objectives.

Table 8: Results of the handling testing with multifunctional three-pronged design

	Time to Slide Up the Prongs (sec)	Time to Do the Same on 24 Wells (min)
Trial 1	5.0	2.0
Trial 2	7.0	2.8
Trial 3	6.0	2.4
Average	6.0	2.4

5.2.2 Three-Prong Proof of Concept Testing

After the handling tests were complete, we chose to proceed with some proof of concept testing on our three pronged model. We again set up three wire prongs embedded in a Styrofoam base. Our main objective for this testing was to practice our calculations and determine the feasibility of this design alternative. We placed an elastic band on the prongs and slid it down to a known diameter, simulating what would happen when the tissue ring contracted. From the change in the diameter and the set angles that the posts were arranged, we could calculate contractile force. The process and examples of the engineering and calculations associated with this device can be seen in the following section.

First, we needed to do some calculations to determine how far up the posts the ring must originally be placed to reach a 4.8 mm diameter. To determine how far to originally place the elastic band up the post, we needed to perform several calculations derived from geometry. From a top view, the prongs could be thought of as the three points of an equilateral triangle that is inscribed inside of a circle (the elastic band or tissue ring) (Figure 22). Based on the diameter of the circle, formulas can be used to determine what the length (L) of the side of a triangle should be. We used an online calculator to help us simplify these calculations ("Sine Law Calculator and Solver"). The various lengths based on different diameters can be seen in Table 9. We know that our elastic band is 4.8 mm in diameter, so this means that the length (L) between the prongs is about 4.16 mm, and for a 4 mm diameter tissue ring, this distance would be 3.46 mm. However, this is looking at the prongs from a top view, so this still does not give us the distance to slide the prongs up the posts.

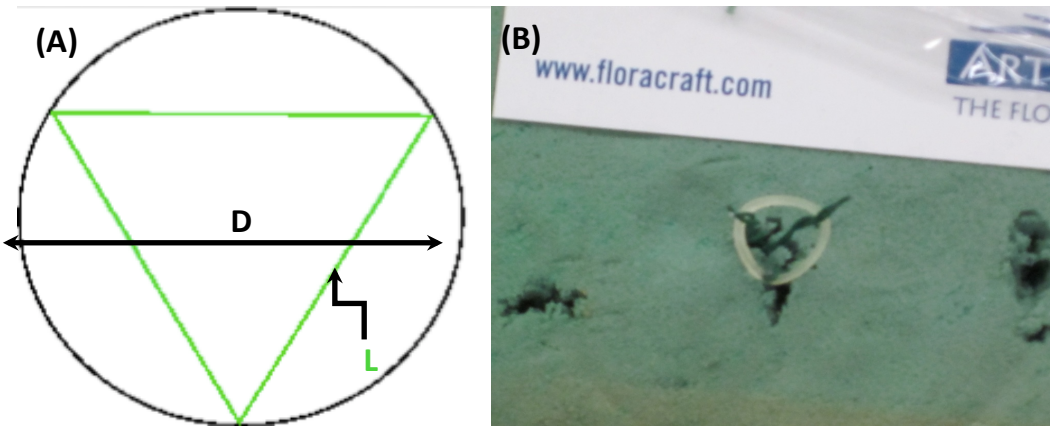

Figure 22: (A) A triangle inscribed inside of a circle. L = distance between two of the prongs; D = diameter of the elastic band (B) Elastic band around the three posts, in the same configuration.

Table 9: Lengths of triangle inscribed inside of circle based on diameter of circle

Diameter of Circle (D)	Length of Side of Triangle (L)
2 mm	1.73 mm
4 mm	3.46 mm
4.8 mm	4.16 mm
6 mm	5.20 mm

We then need to use the Law of Sines, which is shown in Figure 23 below. The posts were placed each at an angle of 60° with respect to the Styrofoam base, measured by a protractor. This arrangement can be seen in Figure 24. The length (a) in the Law of Sines is the same length (L) that we previously found and we know it is an equilateral triangle, so all of the sides and angles are of the same values. At 60°, the length we need to slide the ring up the prong is equal to the (L) value that we just found (4.16 mm), but this becomes more complicated if we do not set the prongs at an angle of 60° with respect to the base. Table 10 shows an example of the different lengths to slide the ring up the prongs based on various angles. The original placement of the tissue ring on the prongs depends on both the diameter of the ring and the angle that the prongs are at with respect to the base.

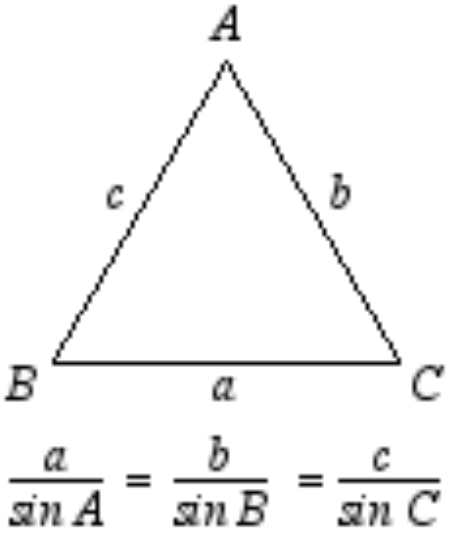

Figure 23: Law of Sines, lengths of sides of a triangle based on the angles between the sides.

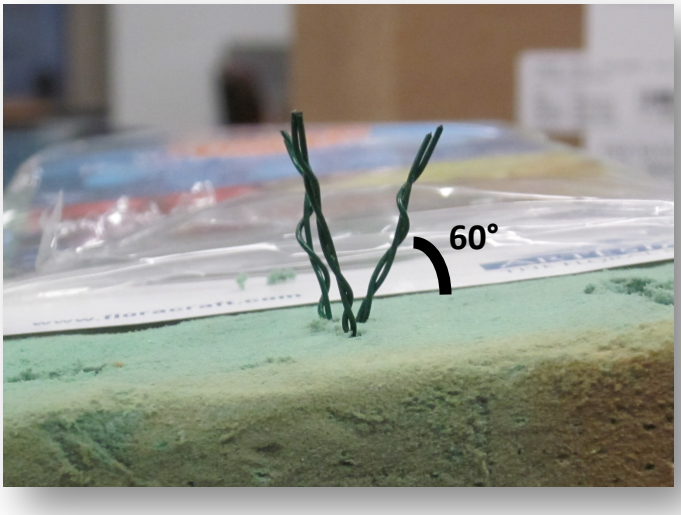

Figure 24: Initial set up of three prongs, at 60° angles with respect to styrofoam base.

Table 10: Lengths of sides of a triangle based on angles (60°) between sides

Angle (B or C)	Length (b and c)
40°	2.26 mm
60°	3.46 mm
80°	9.97 mm

Calculation of the contractile force depends on both change in diameter and time. The rings will ideally slide down the prongs as they contract, and the diameter will shrink to a new diameter.

Liu et al. (2008) has shown that force can be derived as a function of the change in diameter plotted vs. time. If the rings slide down the prongs at a faster rate, they would be contracting with a greater amount of force. Thus, we would need to incorporate a way to keep track of contraction time, such as a timer or stop watch. However, if only concerned with maximum contraction force, only the beginning and ending positions of the ring on the prongs is important. We were not able to test for the measurement of the contractile force with the elastic bands, because the frictional force from the prongs was too great and would not allow the elastic bands to slide down the prongs. Frictional force can be accounted for in our calculations, but the force of contraction is not able to be calculated if the frictional force is so great that it does not allow the rings to slide down the prongs at all.

After conducting this testing, we concluded that the three pronged method appears to be difficult in terms of both set up and calculation. It would be difficult to optimize the idea length of the prongs and angles to place the prongs at in order to obtain the most accurate force calculations. Although the multifunctional design would lower the set up time, there is a high possibility that the prongs could damage the interior of the tissue rings. Also, it is not known how well the rings would slide up and down the prongs. We would have to attempt to lower the frictional forces created on the interior diameter of our rings by the prongs. Additionally, this method would have to be viewed from a side perspective to see the small tissue rings slide down the prongs. This would be difficult to image all of our prongs at the same time in a high throughput array. All of these factors must be carefully considered and accurately measured in order for the force measurements to be correct.

5.3 Four-Post Design

The next design that we chose to test and evaluate was the four-post model. This can be developed into a multifunctional model, where the tissue rings are cultured and then slid up onto the four posts when properly formed. Then, chemical agonists could be placed on each of the tissue rings to induce contraction. Once the rings contracted, they would cause the posts to deflect and this deflection would allow us to calculate the contractile force of the tissue rings.

5.3.1 Manufacturing the Microposts

We experimented with several different methods and mold materials to make PDMS micropost arrays. We also tried a few different materials to construct the actual posts to gauge the stiffness of each post material and determine which material would give us the most accurate force readings.

Firstly, we used Crayola air-dry modeling clay to make prototype templates to make microposts. The clay was molded into blocks about 12.5 mm thick. To make holes, we used 0.5 mm and 0.7 mm lead from mechanical pencils as well as tips of Pasteur pipettes. We created PDMS by mixing SYLGARD 184 Silicone Elastomer Curing Agent and SYLGARD 184 Silicone Elastomer Base at a 1:10 ratio, degassing the mixture via a vacuum for 15 minutes, and curing it in the oven at 70°C for an hour. After several attempts, we concluded that the PDMS was incurable in the holes and around the periphery of the air-dry modeling clay; thus microposts were unable to be made via this method. A second mold we made conformed to the bottom of a weigh boat. This was to reduce the amount of PDMS wasted. Figure 25 below shows the structure if the air-dried clay molds.

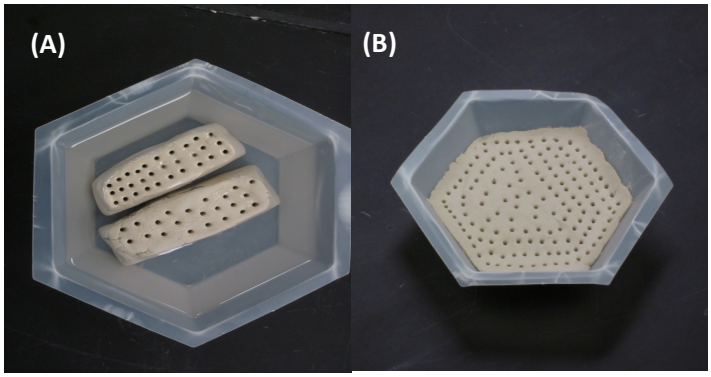

Figure 25: Initial PDMS post making trials. (A) First attempt, not enough PDMS was used to cover the clay molds. For this design, the entire weigh boat needed to be filled with PDMS for the post array to be molded. (B) Second mold attempt, so PDMS can be poured right on top of the mold.

To combat the mentioned complications, we then attempted to make posts out of bakeable terracotta clay. The clay was first molded into a 28.5 mm by 44.5 mm by 17.5 mm rectangular box and a recessed area (3 mm) was carved into one surface of the clay with a knife. A Pasteur pipette and 0.7 mm lead was used to make holes in the clay that were in sets of 4 and 4 mm apart. Figure 26 below shows how our clay mold was configured. According to the baking instructions, the clay needed to be baked for 15 minutes per ¼ inch of clay. Thus, we baked our clay at 275°F for approximately 2 hours. After we baked the clay, we found that it had a rubbery texture and we were skeptical of its success. We then let it sit in room temperature until it was cool to the touch. PDMS was then prepared and casted on the mold; syringes were used to ensure injection of PDMS into the holes. The mold was then cured in the oven at 70°C.

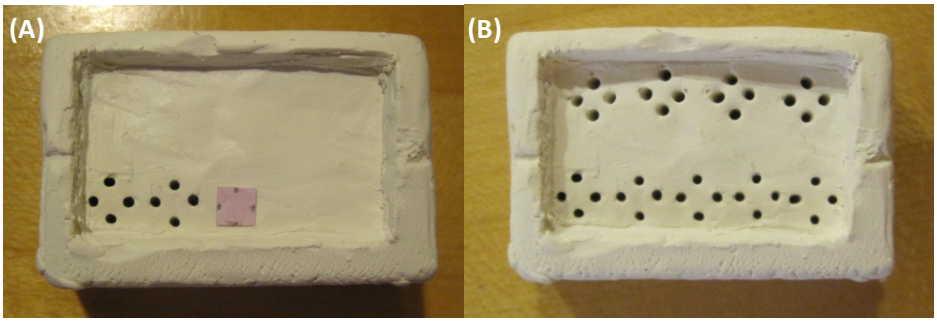

Figure 26: Baked clay mold. (A) Depiction of post spacing, opposite posts are spaced 4 mm apart. (B) Completed mold; Top row: 1 mm posts, Bottom row 0.7 mm posts.

After the PDMS was cured, we removed the posts from the mold. Since the mold had the recess, the PDMS posts came out in one piece. We found that the PDMS had actually cured in the holes, and retrieving them posed to be a simple process and fairly easy. Due to handling error, part of the PDMS was torn off. Thus, for future reference we learned to be more delicate when extracting the PDMS from our molds. Figure 27 shows our first successful PDMS micropost array. However, the mold proved to be too deep and the resulting posts were very long and flimsy, thus they need to be shortened for future testing. Nonetheless, it is evident that baked clay has shown to be an option for creating PDMS microposts.

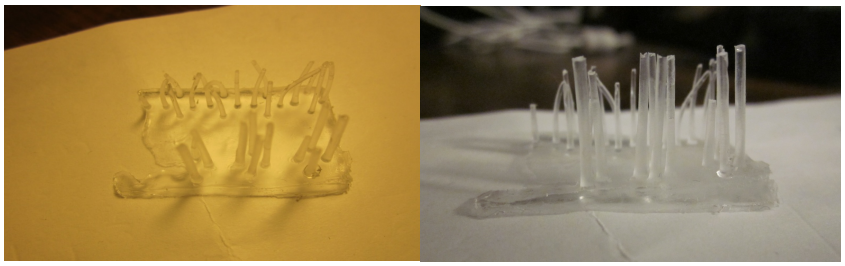

Figure 27: First successful PDMS micropost array.

5.3.2 Contractile Force Measurements

Preliminary calculations for this four-post design were made with the Equation 1 obtained from the study by Vandenburgh et al. (2008). From the literature, we found the range of expected force values from contractile blood vessels to be 10-30 μN (Murphy, 1974). We also found the range of Young's modulus values of PDMS to be between 200-800 kPa (Sasoglu, 2007). We also determined from the literature the desired radius of the microposts to be 350 μm and the lengths of our posts to be about 3 mm (Vandenburgh, 2008). After obtaining the predicted values for our various parameters, we calculated the expected deflections of 350 μm diameter posts with varying moduli. The expected deflections can be found in Appendix F.

Since the equation was meant to calculate the force exerted by a contractile tissue construct between two posts, a force reading can be calculated by measuring the deflection between each of the two posts. Then force values can be calculated from these deflections of opposite posts. From our experiment with the stirrer posts later described in Section 5.3.3, we concluded that the four deflection measurements could be averaged together and used in Equation 1 to yield one averaged force reading, as explained earlier. The equation only depends upon the deflection of one of the posts, and it can be expected that the rings will contract uniformly, as rings of uniform thickness will be tested and completely submerged in the chemical agonists.

5.3.3 Four-Post Proof of Concept Testing

To observe post deflection and to compare our measured values of elastic ring force with those from the Instron, we used 41 mm in length plastic coffee stirrers retrieved from Dunkin' Donuts on the WPI campus as a scaled up and crude prototype. A four-post set up was arranged by anchoring the stirrers in a square formation, with diagonals of 15.65 mm, into a PDMS piece that acted as the base. Figure 28 shows the set up of our prototype. Tiny incisions were made in the PDMS base by a blade where the posts were supposed to be fitted to prevent tearing in the PDMS. Four and eight tenths millimeter elastic bands were used to simulate contractile rings. A proportion between the diameter of the microposts and the diameter of the base was made to calculate the expected base post of our scaled-up model.

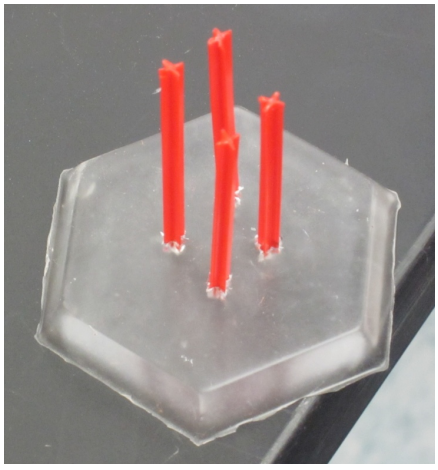

Figure 28: Four-post proof of concept testing.

After we created the prototype, we documented the location of the posts when they were straight. We then placed the elastic bands around the posts approximately 2 mm from the tips. Deflection of the posts was observed; however, the posts displayed a rigid deflection instead of an expected curved deflection. We then documented the relocated posts in respect to the straight posts

and measured the deflection. We recorded four measurements of deflection and averaged them to obtain an average deflection. Equation (1) presented in Vandenburgh's studies was used to calculate the force obtained by the deflection. Figure 29 below shows a top view of the straight and deflected posts and a representative image of how deflections were recorded.

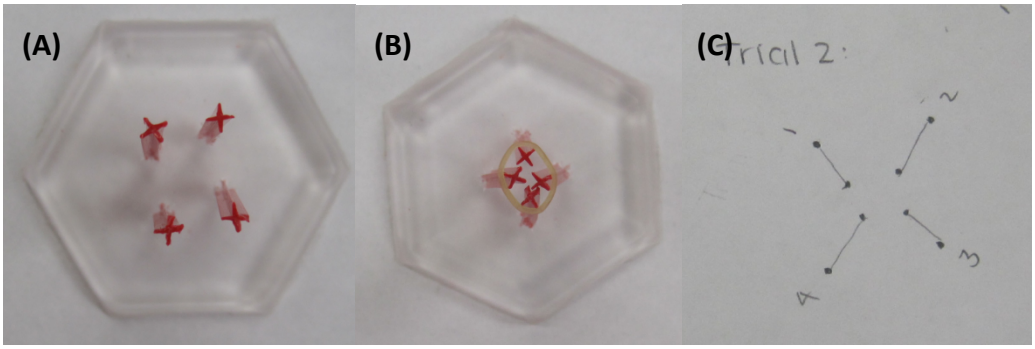

Figure 29: Representation of four-post deflection testing. (A) Posts are in initial, straight position. (B) Deflected posts. (C) Method of recording deflections.

Before we could calculate the force using Equation 1, we used a three-point bending test on the Instron to obtain data that would allow us to calculate the Young's modulus of the plastic stirrers. From the data, we found that the modulus of the plastic stirrers was about 8.9 MPa. From there, we calculated the force exerted by the elastic bands and found the average force to be 6.0 mN. When compared to the results of the elastic bands, with an average force of 0.532 N, measured from the Instron, the value we obtained was 100 times smaller than expected. We suspect that the length of the plastic stirrer posts and the potential misconception of the amount of deflection observed affected our results. At first, we expected the length of the posts to be normalized in the equation, thus we decided not to create a proportion for length of the posts. However, length of posts is inversely proportional to force; thus a long post will cause a lower force measurement. Since a more developed way of measuring deflection (in the form of a microscope or high speed camera) was unavailable at the time, the method to measure deflection consisted of flipping the posts over and marking their locations on a piece of paper. After deflection, the prototype was again flipped over and the deflected posts were marked. This was a very crude way of obtaining changes in deflection and subjected to much user error and variation. Additionally, the rigid deflection of the plastic stirrers may also be a factor causing the large amount of error in this experimentation.

5.3.4 Finite Element Modeling (FEM) for Micropost Arrays

Finite element modeling (FEM) or finite element analysis (FEA) is a technique for solving partial differential equations, and it can be used to model a variety of different factors including

static forces, fluid flow, aerodynamics, and magnetic fields ("Introduction to Finite Element Analysis", 1997). We were able to practice using ANSYS FEM software and were able to develop a preliminary model for one of our PDMS posts. A sample of the post model on the ANSYS can be seen in Figure 30. We felt that FEA would be a great tool for our group if we chose to make our final design based on the four-post method because it would allow us to make a functional model with the ANSYS software that can give us data about the forces produced based on the amount of post deflection. This will allow us to model a curve of post deflection vs. forces of contraction once we determine the mechanical properties of our PDMS posts. We received great instructional help from Dr. Adriana Hera from the WPI Mechanical Engineering Department, and learned how to create an accurate model of our multifunctional four post design using the ANSYS software.

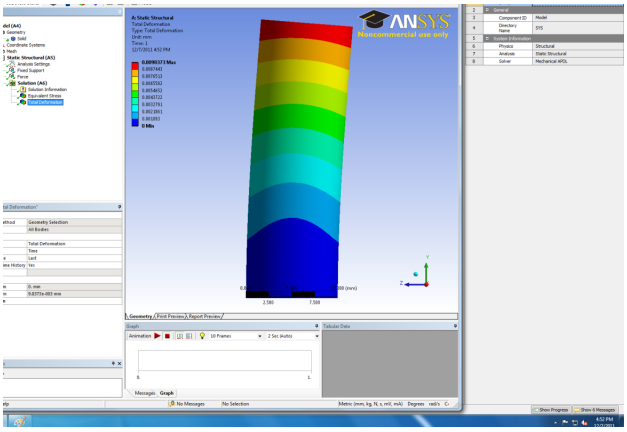

Figure 30: Sample of Finite Element Analysis (FEA) software showing a force on a post with a fixed base

5.4 Displaced Volume (Squeeze) Design

The next conceptual design we tested was the displaced volume, or "squeeze" design. We wanted to gauge if we could accurately measure the force that a tissue ring was contracting by allowing the ring to contract around either a post or a tube filled with liquid and measure how much of the liquid was displaced from the tube. In order to test this design, we purchased a one-way valve from Petco, normally used in home aquariums. To simulate the tube that would hold the liquid, we cut off a small portion of a latex laboratory glove. We believed that latex would give us a realistic simulation because it was an elastic material and not excessively rigid. We used a standard rubber band to create a seal between the latex and the one-way valve. Figure 31 shows the set up of our squeeze design prototype.

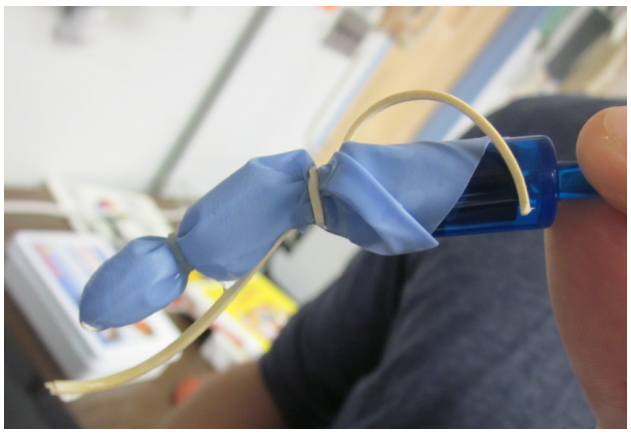

Figure 31: Squeeze design set up. Elastic band contracts around latex and causes water to be expelled out of the one-way valve.

For the experimentation, we filled up the latex glove with a known volume of water (4 mL). We then stretched the elastic band to a known diameter (13.7 mm) in order to fit snugly against the latex glove. Based on our tensile testing with the Instron machine, we know the force being exerted by the elastic band on the latex glove when it is stretched from its original diameter (4.8 mm), to its new diameter (13.7 mm). We created a proportion based on the extension force values on the Instron machine and the force created from the extension to 13.7 mm was determined to be 1.31 N. After the elastic band contracted around the latex glove, a certain volume of water was expelled out of the glove and through the one-way valve onto a plastic weigh boat. The volume remaining inside of the glove was then measured by pouring it into a graduated cylinder. We chose to measure the remaining volume left in the glove rather than the volume of water expelled into the weigh boat because we feared that some of the water was still trapped in the one way valve; thus, not all of the water expelled would be in the weigh boat. We conducted two trials of this experiment and the results of each trial can be viewed in Table 11.

Table 11: Results of the experimentation on the squeeze prototype

	Trial 1	Trial 2
Original Volume	4.0 mL	4.0 mL
Diameter of Stretched Band	13.7 mm	13.7 mm
Contractile Force of Band	1.31 N	1.31 N
Final Volume	2.8 mL	2.7 mL
Average Volume Expelled:	2.75 mL	

From our testing, 2.8 mL of water was expelled in Trial 1 and 2.7 mL was expelled from the latex glove in Trial 2. This data from the two trials was averaged, for a total of 2.75 mL of water expelled. Based on the data from the tensile testing of the 4.8 mm elastic band (as outlined at the beginning of this chapter), it was determined that the elastic band was creating a force of 1.31 N to

expel that volume of water. To determine how much water a contracting tissue ring would expel, we created a simple proportion from these data, of which the results can be viewed in Table 12. From our literature review, it was determined that a tissue ring 2 mm in diameter would contract with a force of about 30 μN (Murphy, 1974). From the data obtained in our testing, this force would expel about 0.63 microliters of water with a post of the same dimensions as our model (0.7 mm diameter and 3 mm height). This is an extremely small amount of water that would be expelled due to the relatively weak contraction force of the rings.

Table 12: Scaled down results of testing to actual size with a 2 mm tissue ring

	Testing	Actual Size
Force Produced	1.31 N	30×10^{-6} N
Volume Displaced	2.75 mL	0.00063 mL

After conducting functionality testing on the squeeze design, we were able to see that this design is in fact feasible to measure the force of a contracting ring. The force can be successfully calculated by determining the amount of volume displaced. However, there are several concerns that came about after our testing of this design. Perhaps the most glaring is that it will be very difficult to make this design high throughput. This would mean that we would need to create a device with at least 24 different one way valves to dispel the liquid. Also, we would need to mount all of the tissue rings individual tubes that will be initially filled with the water. This will make the set up time consuming and we were not able to gauge how easily the rings would slide onto the latex material. One possibility is to look into creating the tube out of a different material rather than latex, but latex would be the most practical material for us to use, as it is both readily available and cost effective. Thus, it is still a concern that the tissue rings could be damaged by sliding them onto the tubing material to induce contraction.

Our experimentation revealed that the expected forces of the rings would expel a very small amount of water. This will create large variations and errors in the calculations if the amount of water remaining is not measured correctly. We could perhaps look into using a solidifying agent to change the remaining volume of liquid into a solid, and make the calculation of force more accurate. Another option would be to change the material that is holding the water, so that it is not as strong and the contraction of the ring would perhaps expel more water. However, our group could not envision how we could make this design idea very high throughput and how we could ensure an accurate calculation with such a small amount of liquid dispelled. It appears that there are a large number of factors that would need to be controlled and specifically calibrated in order to make this design feasible.

5.5 Light Diffraction Design

Another design idea that we recognized later in our testing was the light diffraction design. The idea behind this design was to allow the user to visualize and track the change in diameter of a contracting ring at a projected scale. The ring would be set on a transparent petri dish with a light source above, which would produce a shadow. The shadow ring would be a known proportion to the actual ring thus allowing the actual change in diameter to be calculated. Figure 32 displays this light diffraction design as we used it in our testing.

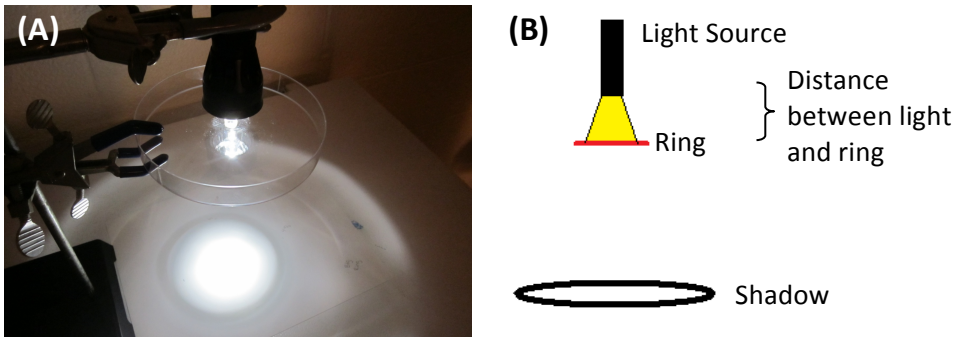

Figure 32: Light diffraction set up. (A) Metal ring is placed on a petri dish and a flashlight is positioned above the dish. The light then creates a shadow on the paper below (B). A schematic of how our light diffraction idea works. The light creates a shadow, and the shadow diameter/ring diameter can be calculated and changed depending on the distance of the light source.

We conducted an experiment to determine how height from the table, distance between light source and ring affects the shadow size, and the size of the ring affects the shadow size. We created a set up as seen in Figure 32 with the light source above a petri dish containing a ring and displaying a shadow outline of the ring below. First, we wanted to see how the distance from the table and distance between the light source and dish affected ring size. We did this by changing the height of the light and adjusting the dish until the shadow appeared in focus. We had to also vary the distance between the dish and the light to maintain a proper focus on the shadow. From this, we saw more variance in measured diameter when the distance from the table increased. Second, we wanted to see how the height from the table affected the shadow diameter. The further from the table and the increased space between the light source and dish resulted in larger shadow diameters. For each shadow, two diameter measurements (a vertical and a horizontal component) were measured. From this data, it appears that as the ring is magnified by the light source, the dimensions of the ring become slightly distorted. Our measurements of the shadow diameters indicate a slight ellipse shape in some of the shadows, rather than a perfectly circular shape. Lastly, we wanted to determine the ratio between the actual ring diameter and shadow diameter. We used the same 4 mm and 8 mm diameter metallic rings for all tests.

Table 13 shows the size ratios measured and calculated from the light diffraction tests. A force reading can be produced from this method by plotting the ratio of the area at an indicated time over the initial area as a function of time (Liu, 2008).

Table 13: Size ratios of ring size to shadow produced using light diffraction

Ring Diameter	Petri Dish Distance from Table	Distance Between Dish and Light	Shadow Diameter (Vertical, Horizontal)	Ratio Ring Size to Shadow
4 mm	21.3 cm	1.3 cm	134 mm, 130 mm	33.0 times
4 mm	6.7 cm	2.4 cm	100 mm, 100 mm	25.0 times
4 mm	10.4 cm	0.9 cm	66 mm, 65 mm	16.38 times
8 mm	21.3 cm	1.3 cm	172 mm, 167 mm	21.19 times
8 mm	10.4 cm	0.9 cm	81 mm, 83 mm	10.25 times
8 mm	6.7 cm	2.4 cm	133 mm, 132 mm	16.56 times

The ratios vary depending on the set up, but this could be avoided using a 4 mm metal ring as a way to calibrate the system. We also noticed that with the same experimental set up, the 4 mm rings produced a larger shadow relative to its size than the 8 mm. This means that when using our 4 mm rings, we will be able to track the change easier and the level of magnification was greater than if the rings were even larger. The elastic band contraction would occur too quickly for this method to be tested so we would need to come up with another way of testing the ability to get a force reading. From our data (Table 13), we can conclude that this light diffraction method could be a valid means of magnifying our tissue rings, as the 4 mm rings were magnified an even greater amount than the 8 mm rings. However, in order to ensure that this method is valid, we will have to conduct more experiments with multiple sample measurements to check for variance between both the ring measurements and the shadow measurements.

We will calculate force using the method by Liu et al. (2008). We will plot the change in diameter over time on a graph. From there, we will obtain acceleration from this curve, as it is the derivative, or the slope of the curve. The mass of the rings will be measured beforehand to allow for a force reading. We will take the acceleration that is the greatest and multiply it by the mass to give us the greatest force value the ring expressed, using the simple equation that force= mass times acceleration. Overall, this method has not been well cited in literature, but it appears to make the optical imaging of a small diameter tissue rings much easier to see. Thus, we will keep this design in mind as an option to incorporate with other designs, as a means to better imaging. We do not feel that it is a feasible design on its own, but that it can be used in association with some of the other designs to view the tissue ring contraction more easily.

5.6 Numerical Evaluation Matrix

A numerical evaluation matrix for our potential designs is shown in Table 14. The numerical evaluation matrix is used to evaluate how well our alternative designs meet our design objectives after we completed experimentation on them. This chart shows both the constraints and project objectives in the left-hand columns, while the scores assigned to each objective are shown in design-specific columns on the right. It should be noted that none of our designs are hindered by the constraints. Generally, any alternative designs that fail to meet the constraints must be removed from considerations, but all of our design alternatives adhered to the project constraints, so they could all be considered.

We decided to use our top four most important objectives to create this chart. Although all of our objectives are important, but we felt that using the most important ones would help us to better narrow down our alternative design choices. From our pairwise comparison chart, the objective of manufacturability received the least interest and importance. Therefore, it was not included in this matrix. We think that the four objectives compared below are of the most importance and we have both metrics and experimental data for these objectives.

Table 14: Numerical evaluation matrix for design alternatives. Note only four of six objectives originally identified is used.

Design Constraints (C) and Objectives (O)	Four-Post Model	Three-Pronged Post Model	Squeeze (Displaced Volume) Model	Light Diffraction Model
C: Under the budget				
C: Biocompatible				
O: Successful in Measuring Contractile Force	80	30	50	70
O: Easy to Use	70	60	30	70
O: High Throughput	80	80	30	80
O: Versatile	80	40	40	80
TOTALS	310	210	150	300

The four-post multifunctional model received the highest score, followed by light diffraction, the three-prong post model, and the displaced volume ("squeeze") model, respectively. From the obtained results of initial testing, the team generated these scores for each model. The scoring was on a scale of 10-100 with 100 being the best score and 10 being the worst, and the designs were ranked according to how well they met each objective. The four-post model seems to be our best design with the light diffraction closely following. These models have shown to be the most accurate in successfully measuring contractile force. We feel that these designs could most

accurately and easily measure the contractile force of our tissue ring samples, based on our experimental testing.

The three-pronged and "squeeze" model received the lowest scores in this aspect due to complications the team encountered during testing. These models are also able to measure the contractile force, but they are a bit more tedious to do so, and there is a higher chance for calculation error or inaccuracy, especially on a smaller scale. Tissue rings can potentially slide down on the three-prong design during testing and the collection of displaced liquid in the valve of the "squeeze" design can lead to inaccurate data. Additionally, these designs received low scores on versatility and ease of use. The light diffraction and the four-post model were also the easiest to use in terms of experimental set up and calculation procedure, as well. The other two designs would be a bit more difficult and take a longer amount of time for the initial set up. All of the designs seemed able to be made high throughput, but the "squeeze" design would be much more difficult to make high throughput, thus earning it a much lower score.

Lastly, the light diffraction and the four-post designs earned high scores for versatility because a variety of cell types could be tested with them. Also, the four post design could be made multifunctional, meaning that the tissue rings could be cultured and tested in the same device. Thus, the four-post model seems to provide us with the best completion of the objectives and the best chance to complete the metrics that we have outlined for these objectives.

5.7 Conclusions

After conducting a variety of testing procedures and analysis and constructing our numerical evaluation matrix, we were able to agree on which design ideas best achieve all of our objectives and adhere to our functions and specifications. The multifunctional four-post model scored highest on our numerical evaluation matrix. It appears to be the best design in terms of measuring contractile force, ease of use, and it can also be made very high throughput. Additionally, we predict that we can elaborate on this design to make it able to culture and test tissue rings on the same device. The light diffraction model was promising in our experimental testing, but there is not a sufficient amount of literature existing on light diffraction techniques for measuring cell contraction to help verify our calculations and procedures. We could attempt to couple the light diffraction technique with our four post design to help with the visualization of the contraction. After our experimentation to evaluate our design alternatives, we have decided to move forward with our four-post design. We have now shown that we are successful in creating molds and posts

for PDMS, and that our PDMS posts have the potential to successfully measure the forces produced by elastic bands when they are stretched to various extensions.

Our plan after this evaluation was completed was to validate our final design and make minor changes to our design if needed. We continued to manufacture more PDMS posts and conduct testing with actual smooth muscle cell tissue rings. We also completed some more testing to make this design multifunctional. We did some experimenting with making molds completely out of PDMS as well as making the tissue culture well parts out of agarose and the posts out of PDMS. After choosing our final design, we completed design validation and verification testing, which can be seen in Chapter 6.

Chapter 6: Final Design Verification and Validation

This chapter highlights all of the testing done on the multifunctional four-post design to validate its use and verify that it meets our main project objectives. Additionally, these tests helped us to optimize the design to achieve the best functionality within the given time constraints. This chapter also gives a detailed description of our final design.

6.1 Four Post and Two Post Contraction Simulation

Although we knew that the multifunctional post design was the best choice for our final design, it was still uncertain whether or not this design would best measure contraction with either a two post or a four post array. Based on some studies, deflection of only one post is necessary to observe and calculate the contractile force (Vandenburgh, 2008). However, very few studies using tissue rings to induce post deflection have been conducted, and we believed that a four-post array would help the ring maintain its structural integrity better than two posts. SMC strips and individual cells have been more commonly tested on micropost arrays (Kim, 2011; Legant, 2009) In order to measure the contraction of the tissue rings on this array, we observed the deflection between the posts situated directly across from each other, and we could average these values together to get a force reading. We conducted a series of experiments to observe how contraction would occur on both a two post and four post arrays, and which array would be easier to both observe contraction and calculate contractile force.

6.1.1 Two Post and Four Post Molds with Elastic Band Contraction

In order to determine which of these methods would be more accurate for measuring force, we created a mold allowing for a two-post array and a four-post array to be tested (Figure 33). The mold consisted of 1 mm diameter posts that are 4 mm in height. The posts were spaced 6 mm apart. To simulate a contracting ring, we used 4.8 mm orthodontic rubber bands.

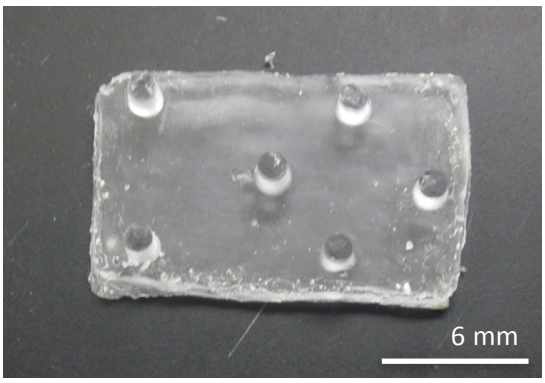

Figure 33: PDMS mold designed with both the two-post and the four-post arrays for contraction testing. The overall mold is 5 mm X 9 mm.

After completing the Instron testing of the elastic bands (as outlined in Chapter 5), we were able to determine the average force for each maximum extension of the samples. Based on the spacing of the posts, the elastic bands were stretched a total of 11.6 mm in order to fit tightly around the posts. The values from the Instron extension of the rubber bands were used to predict the force produced from an 11.6 mm extension of the bands, which was 3.51 N. The elastic bands were placed around the posts and the amount of deflection of the posts was measured. Figure 34(left) shows the elastic band placed around the two-post configuration of the mold.

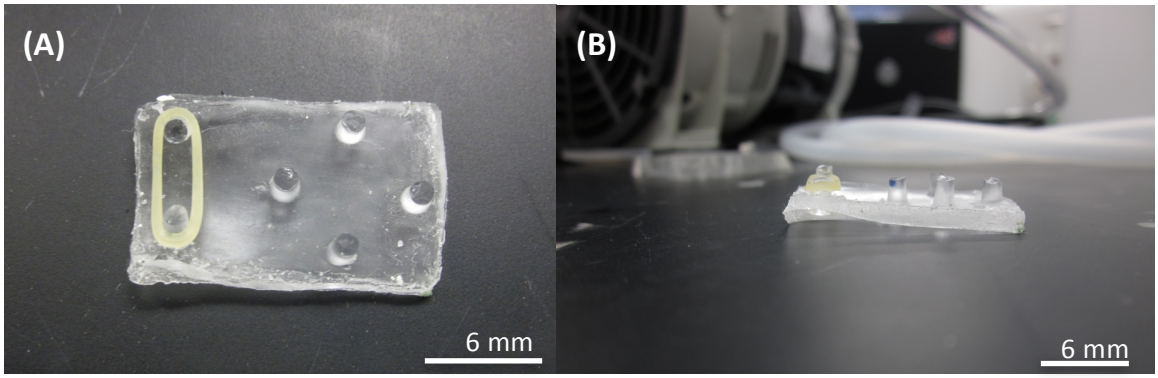

Figure 34: Rubber band placed around two PDMS posts to simulate a tissue ring contracting (A). The force of the rubber band was too large and caused the base of the mold to curl up off of the lab bench (B).

Unfortunately, many problems were encountered during this time, as the force produced was proven to be too large for the posts to withstand. The most prominent problem was the fact that the base, which the posts were protruding out of, was folding upwards, as seen in Figure 34(right). This caused an inaccurate deflection reading and thus, the force calculation from this deflection was incorrect. In order to combat the large force of the elastic bands, we attempted this testing procedure again but with 7.8 mm elastic bands. These bands would not have to be extended as far as the 4.8 mm bands, and thus, we would not expect as large of a contraction force. However,

we observed the same results, with the force of the elastic bands causing the base of the mold to fold upwards. Alternatively, after discussion with our project advisor, we decided to simulate the contractile force on the PDMS using our ANSYS finite element modeling software. We also attempted to see how actual tissue rings fit around and contracted in response to the different post arrays, which is discussed later in this section of the report.

6.1.2 Contraction of Tissue Rings on Two and Four Post Arrays

Further along in our testing, we were able to successfully make tissue rings from rat aortic smooth muscle cells. The tissue rings were made by seeding 1 million SMCs into the previously made 4 mm diameter agarose molds (Gwyther et al, 2011). The cells were first seeded into the molds and allowed to aggregate and form rings over a period of one week. After a week's time, a majority of the cells that we had seeded had formed 4 mm diameter rings, many of which displayed uniform ring thickness. We decided to practice handling and observing the structural integrity of the tissue constructs on both two post and four post molds. Although the elastic band simulation did not work as well as we expected, testing the different arrays with actual tissue rings allowed us to observe a situation much closer to the actual contraction testing procedure. Figure 35 shows the tissue rings place on both the two post and four post molds.

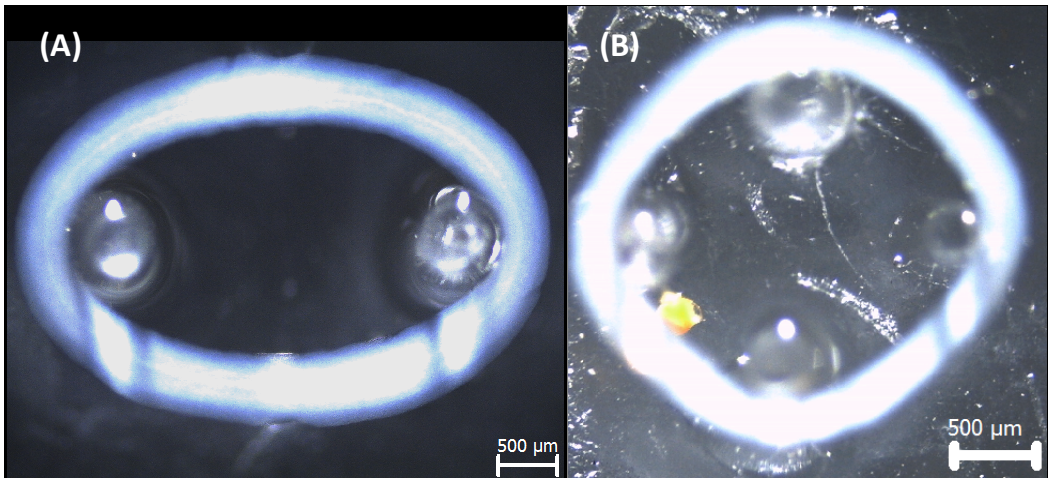

Figure 35: Tissue rings placed on two-post (A) and four-post (B) PDMS arrays. In each array, the microposts were 0.7 mm in diameter and 3 mm tall. They were spaced 4 mm apart from each other. Note: yellow dot in (B) is a small dust particle that was attached to the bottom of the four post mold.

When placed on the two-post array, the rings were shaped like an ellipse, while on the four-post array the ring maintained a circular structure. Also, it appeared that the ring was in more tension on the four-post array, making it easier to view the contraction and the deflection of the posts. For this experimental procedure, the tissue rings were soaked in physiological saline

solution (PSS), composed of 99.1% deionized water and 0.9% NaCl for 30 minutes. They were then picked up with forceps and carefully placed around the microposts with the forceps. Potassium physiological saline solution (KPSS) at a concentration of 99.1% deionized water and 0.9% KCl was then added via pipette to induce contraction. The rings sometimes tended to slip down the two posts because the tension was not as great, but they remained fixed at the top of the four post arrays, as the four post structure provided more structure to support the ring. This allowed for easier visualization of the post tips to check for deflection. Thus, after witnessing our SMC rings placed on both types of arrays, it appears that the four posts help the rings maintain a circular shape, which more closely mimics a native vessel segment structure. Also, the four posts allow the ring to experience more initial tension, ensuring that they will not slide down the posts and helping with visualization of contraction. Based on these observations, we decided to employ the four-post design as our final contraction force measurement device.

6.2 Elastic Modulus Calculations for Our PDMS (Post Calibration)

Our next challenge in validation testing was to ensure that we had an accurate way of measuring the modulus of our PDMS. The calculation for contractile force depends on the modulus of the post material, and the elastic modulus of PDMS can vary depending on how it is mixed and cured. Therefore, we decided to conduct a series of tests using both mechanical and manual testing to discover the modulus of our PDMS and calibrate our PDMS posts. We also extensively reviewed the literature to verify that our calculations were providing us with modulus data similar to that found in other studies.

6.2.1 Instron Tensile Testing

In order to use the ANSYS software to simulate the contractile forces on our PDMS posts, it was necessary for us to determine the mechanical properties of our posts. Using previous literature, we learned that the elastic modulus of PDMS varies depending on the curing process and the ratio of curing agent to elastomer base. For our posts, a 1:10 ratio, or a 10% concentration of curing agent, was used. Generally, the larger the concentration of curing agent used, the higher the value of the elastic modulus (Sasoglu, 2007). The procedure that we used to make our PDMS is detailed in Appendix G.

To determine the elastic modulus of the PDMS produced in the lab, Instron tensile testing using strips of PDMS samples was performed. For our first testing procedure, we selected six random rectangular pieces of PDMS from various molds that had been previously made. These

pieces were of various lengths, widths and thicknesses (Figure 36). Our rationale for using random PDMS samples was that the elastic modulus should not vary among our samples, because elastic modulus is a material property determined from the manufacturing process, and all of our PDMS had been developed in a similar manner. However, we did need to pay attention to cross sectional area of our samples, as a larger cross sectional areas would take greater forces to pull to failure. During tensile testing, the samples were clamped at both ends and pulled to failure. The initial data from the Instron testing can be seen in Figure 37.

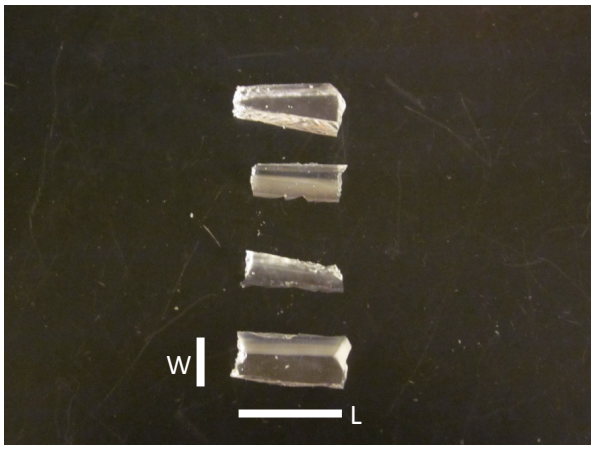

Figure 36: Various PDMS strips of different dimensions for Instron testing. Cross-sectional area of each sample was calculated as length (L) x width (W) of the face of each sample, as shown.

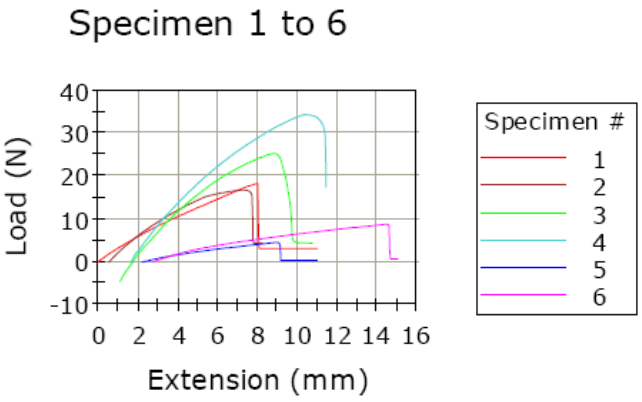

Figure 37: Raw data from the Instron testing of the individual PDMS strips.

The readings from the Bluehill software displayed curves of each sample for force versus extension. The software also provided information about the maximum extension achieved and the force reading at the maximum extension. From this data, Microsoft Excel was used to determine the stress (force/area) and strain (extension/original length). Cross sectional area was calculated as length x width of the face of each sample placed between the clamps on the Instron machine.

The elastic moduli of the samples were then determined from the stress-strain results. A summary of this data can be seen in Table 15.

Table 15: Data summary of the PDMS testing for samples of various sizes

Sample	Length (m)	Width (m)	Force (N)	Area (m^2)	Extension (m)	Stress (Pa)	Strain	Modulus (kPa)
1	0.02	0.003	18.2	8.2E-05	0.008	221698	0.3469	639.04
2	0.02	0.009	16.8	0.00022	0.006	73367	0.2750	266.75
3	0.03	0.009	25.2	0.0002	0.007	84312	0.2555	329.91
4	0.02	0.01	34.3	0.00034	0.008	98428	0.3283	299.81
5	0.04	0.005	4.6	0.00026	0.006	17463	0.1401	124.58
6	0.06	0.01	8.8	0.00080	0.011	10962	0.1828	59.94

The average modulus calculated for the samples was 286 kPa, which is fairly accurate to the range of values found in the literature about PDMS properties. However, it is evident that the data from each sample greatly varies, and that the calculations for modulus were quite different for each sample. It should be noted that all the samples broke towards the grips of the Instron machine and that Sample 6 slipped before it failed. Unfortunately, this set of data is shown to be imprecise. Also, the samples greatly in cross-sectional areas, so the need existed for more consistently shaped samples to be tested. Figure 38 below shows a graphical representation of the variation between the modulus values of each single PDMS sample used.

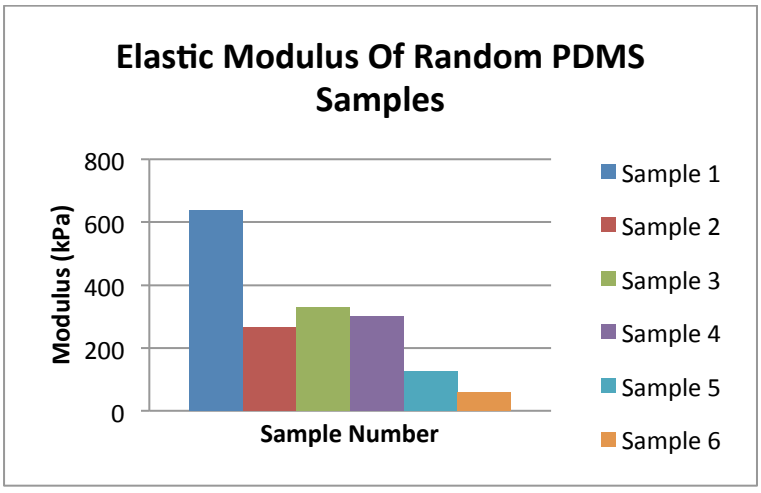

Figure 38: Elastic modulus of each of the PDMS samples.

To combat this precision and slippage problem, uniaxial testing was performed again with PDMS strips developed all in the same conditions. The conventional standard shape for conducting a tensile test is the "dumbbell" or "dog bone" shape (Figure 39), with a thin rectangular middle section and thicker sections at the ends to allow for better adhesion to the grips during testing

(Venkatraman, 2003). Our PDMS was cut for this experiment to model this shape, and we called our samples "end strips." Four PDMS end strips were shaped, each 30 mm in length. The strips were pulled to failure and data was collected by the Bluehill software. However, we again noticed that most of our PDMS samples fractured at the sites where they were attached to the grips (Figure 40).

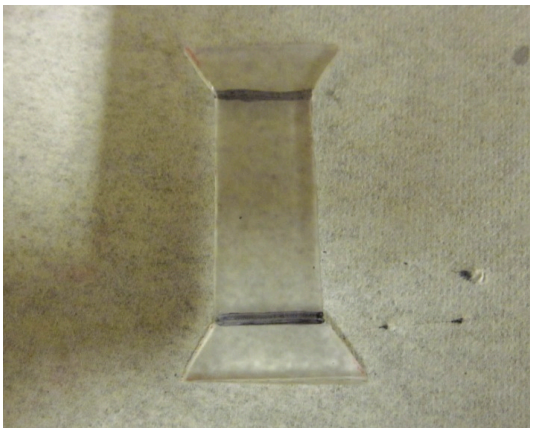

Figure 39: A PDMS "dog bone" shaped sample that was prepared for Instron testing. Since this is slightly different from the true dog bone shape, we called our samples "end strips."

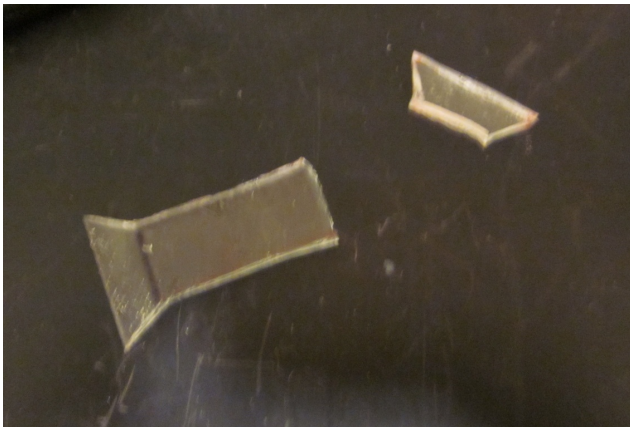

Figure 40: A PDMS end strip sample that was ripped after uniaxial tensile testing.

A summary of the data obtained during the end strip shaped testing can be seen in Table 16 below. Overall, more precise valves between the samples were obtained, meaning that there was less deviation between the elastic modulus values in the end strip samples, as seen in Figure 41, than in the random samples. On the other hand, the average modulus value obtained from the testing was only 88.2 kPa, a lower value than in literature. One main factor that potentially caused this was the fact that the PDMS did not cure fully. This batch of PDMS did not become fully hardened and was tacky upon testing. Incomplete curing of the PDMS was thought to be due to using PDMS that was not fresh. We cut the PDMS end strips with a scalpel, which may have caused

variation in dimensions between samples, but there was certainly less variation between these samples than in the previous round of Instron testing. The properties of the PDMS may have been affected due to age. Also, as stated previously, all of the samples fractured at the sites of the grips, which is not where the ultimate maximum force should be achieved. The ideal site of fracture in a uniaxial tensile test is the middle of the specimen. Thus, the fracture point of the end strip samples may have caused a lower reading for the elastic modulus value.

Table 16: Data summary of the PDMS end strip uniaxial testing

Sample	Length (m)	Width (m)	Force (N)	Area (m^2)	Extension (m)	Stress (Pa)	Strain	Modulus (kPa)
1	0.03	0.015	22.2	0.0005	0.018	42187	0.5297	79.64
2	0.03	0.015	14.4	0.0005	0.009	27068	0.2724	99.34
3	0.03	0.016	15.3	0.0005	0.011	28235	0.3369	83.79
4	0.03	0.014	17	0.0004	0.013	35420	0.3927	90.18

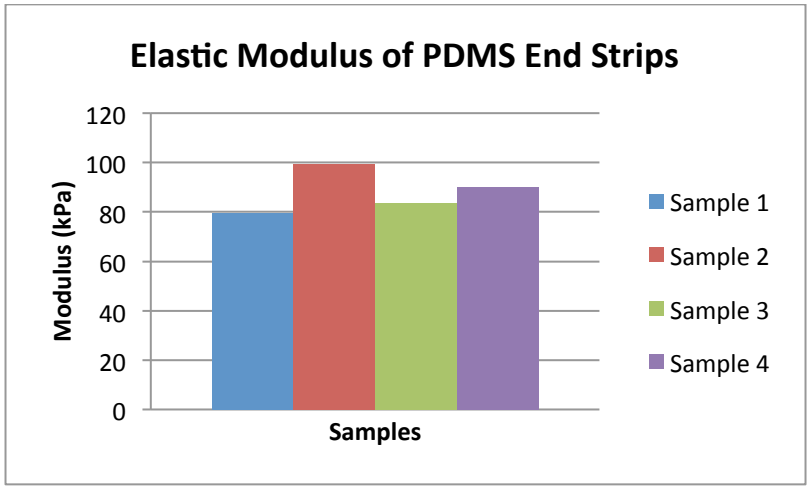

Figure 41: Elastic moduli of each of the PDMS "end strip" samples.

In order to obtain another more accurate reading, we decided to conduct another round of Instron testing with well-cured PDMS rectangular strips. For this final set of uniaxial tensile testing, four rectangular strips were cut to the same dimensions (15 mm width X 25 mm length) and all samples were developed from the same batch of PDMS. The strips were pulled to failure on the Instron machine and the data was recorded. Figure 42 below displays one of our rectangular strips in position prior to being pulled to failure.

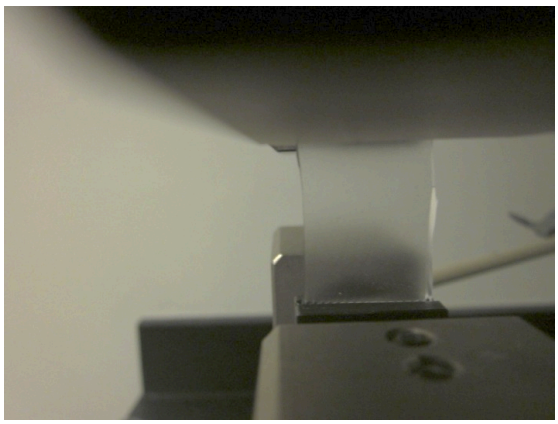

Figure 42: PDMS rectangular strip prepared for Instron uniaxial testing.

These rectangular strips cured properly and thus they were stronger than the "end strip" samples previously tested. Also, the rectangular strips failed towards the middle, which gave us more confidence of the accuracy of the force readings. Table 17 summarizes the data obtained from this round of testing. Overall, the precision between each sample was much better than our first round of testing. All of the pieces were similar in dimensions, and the force versus extension curves were all similar, suggesting that the manufacturing process was creating PDMS with uniform mechanical properties. The average elastic modulus obtained from this testing was about 160 kPa. This value was slightly lower than the expected values from the literature of 10% curing agent, but we believed that this was our most accurate value because the strips were uniform and well-cured.

Table 17: Data summary of the PDMS rectangular strip testing

Sample	Length (m)	Width (m)	Force (N)	Area (m^2)	Extension (m)	Stress (Pa)	Strain	Modulus (kPa)
1	0.035	0.02	73.2	0.0008	0.0147	90811	0.419	216.71
2	0.035	0.02	45.9	0.0008	0.017	56789	0.484	117.18
3	0.035	0.02	44.8	0.0007	0.019	57345	0.555	103.16
4	0.035	0.02	64.7	0.0008	0.014	79704	0.424	187.65

After extensive Instron testing, an elastic modulus value for the PDMS produced in the lab was obtained. Several reasons may be why the calculated modulus, 160 kPa, was less than the moduli found in the literature, 200-500 kPa. First, much of the variablilty of elastic modulus is dependent upon the manufacturing process. No indepth information on how PDMS was manufactured was provided in the literature, other than the concentration of curing agent used. Thus, our degassing time and curing time could vary quite differently than those of other researchers. Also, even though the literature review provided us with a range of values that we expected to obtain, all articles reviewed seemed in consensus on the fact that the value for the elastic modulus varies greatly. Thus, it is possible that the modulus value obtained from testing

could be slightly lower than that found in the literature articles that we reviewed. In order to maintain the best results for our future testing, it was vital that we replicated the same manufacturing process and adhered to this process for all of the PDMS we made.

Another reason that may have caused a yield of a lower modulus value was the method of acquiring the modulus. Instron tensile testing is more suited for tougher materials, such as strips of leather, which breaks uniformly in the middle of the samples. All of our samples failed close to the grips because this was the area where the PDMS was secured. After observation, it appeared that the grips most likely weakened the sections of our samples that were clamped; thus, we decided to develop another method of testing to determine an elastic modulus value. As an alternative to Instron testing, we manually submitted our posts to a known force and measured the deflection of the posts, as seen in section 6.2.2.

6.2.2 Manual Post Calibration

The goal of these tests was to obtain an additional elastic modulus value of the PDMS produced in the lab to compare to the values obtained from Instron testing, with the hopes of obtaining more consistent data. Many labs used precise micro indentation techniques with force transducers to calibrate their PDMS arrays—more information can be found in Appendix H (Sniadecki & Chen, 2007). However, this technology is costly and inaccessible to us, thus a simple and more cost effective method to calibrate the posts was devised. A previously produced mold was super glued to a solid plastic base for stability. A wire was attached around the tip of one of the posts. On the other end of the wire, a plastic cup was attached that served as a platform to add weight. The post was held at the edge of a table with the plastic bucket hanging off the edge of the table, as shown in Figure 43. The rationale behind this method was the weight that caused the post to tear could be measured, allowing us to calculate the elastic modulus of the PDMS. Although more crude than Instron testing, the modulus calculated from this test would confirm or refute the accuracy of our results from the tensile tests performed with the Instron.

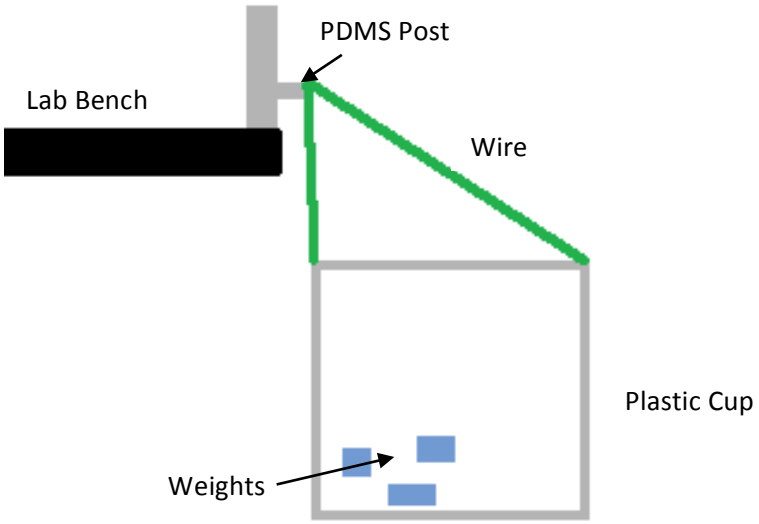

Figure 43: Experimental set up for our first manual post calibration. The plastic cup is attached to a PDMS post (set on a lab bench and held in place manually) with a wire and weight is added to the wire until the post breaks.

Weight was continually added to the plastic cup (in the form of metal screws that had been previously weighed on a scale) and the final deflection of the PDMS post was recorded. However, this experimentation did not go as planned, due to the fact that the amount of weight placed in the cup greatly exceeded the expected value; and the weight still did not cause the post to tear. This caused our calculation of the post modulus value to be about a 10-fold value higher than the results from Instron testing. Figure 44 shows the post bending under the weight in the cup.

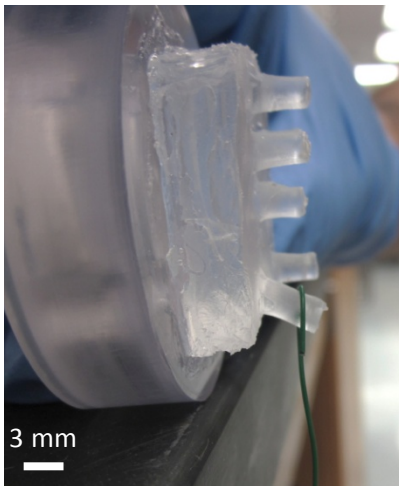

Figure 44: Post deflection from the weight of the items in the plastic cup.

The overall conclusion of this trail was that the experimental set up was the flaw causing the abnormal results in modulus values. A second trial of this test was performed. Instead of

pulling the post to failure and collecting the deflection at the end of the experiment, the deflection of the post was measured at each addition of a known, consistent weight. From this data, a force versus deflection curve was created and used to calculate the elastic modulus of the PDMS post. The experimental set up of this procedure can be seen below in Figure 45.

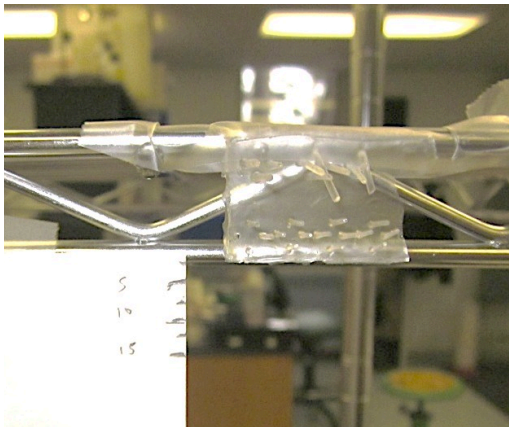

Figure 45: Experimental setup of manual post calibration (scale to the right is in millimeters).

The posts were 3 mm in height and had a diameter of 0.7 mm, the same dimensions as the posts we planned to use in our final design for measuring ring contraction (based on literature and vascular ring size). A scale bar in millimeters was also constructed using calipers and used as a reference (Figure 45). A wire segment was cut, weighed, and bent into a hook shape that fit securely around the post and allowed for the addition of elastic bands on the free end. Then, each individual 7.8 mm elastic band was weighed using a scale. Each band weighed about 0.025 g. For the experimental procedure, the elastic bands were added one at a time and a picture was taken from the same position to view the deflection of the posts. Calipers were used to precisely measure the deflection by hand with the addition of each band. This allowed us to witness the deflection of the post from a known external force. A total of 8 rubber bands were added to ensure a sufficient sample size and elicit a significant deflection of the posts. This experiment was completed three times and the measurements were taken from both a front view (Figure 46a) and a side view of the posts (Figure 46b). The modulus resulting from these acquired data yielded a value still much higher than the results from Instron testing, about 803 kPa.

A possible reason for this modulus value that is much higher than expected was that the wire hook was not properly placed at the tip of the PDMS post for testing, seen in Figure 46b. The wire was halfway along the length of the post, resulting in the deflection of the posts to be much lower than if the wire was properly placed at the tip of the posts. With this set up, it was difficult to

secure the wire at the tip of the post without it slipping off upon the addition of elastic bands. Unfortunately, this limitation was the main reason why the post underwent minimal deflection and thus, affecting the elastic modulus result.

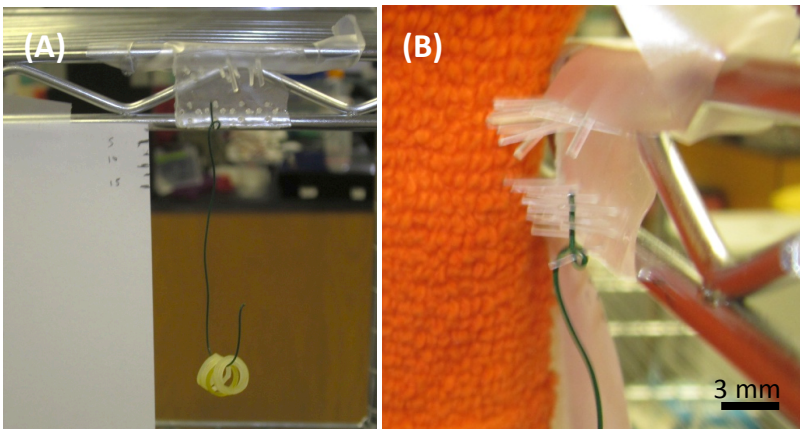

Figure 46: (A) Front view of the post deflecting in response to the weight of the elastic bands. (B) Side view of the post deflection. Measurements were taken from both front and side views during the experiment.

In order to combat this experimental flaw, an elastic band was glued around the tip of the post as shown in Figure 47a to ensure more accurate data collection. Eight other elastic bands were cut and placed onto the secured ring. Deflection of the post was measured with calipers after each addition of an elastic band. Three trials were performed and deflection was measured from a front and side view to ensure accuracy. The elastic bands that were added served as the uniform weights in this experiment. The results of each trial of deflection can be seen in Table 18 below.

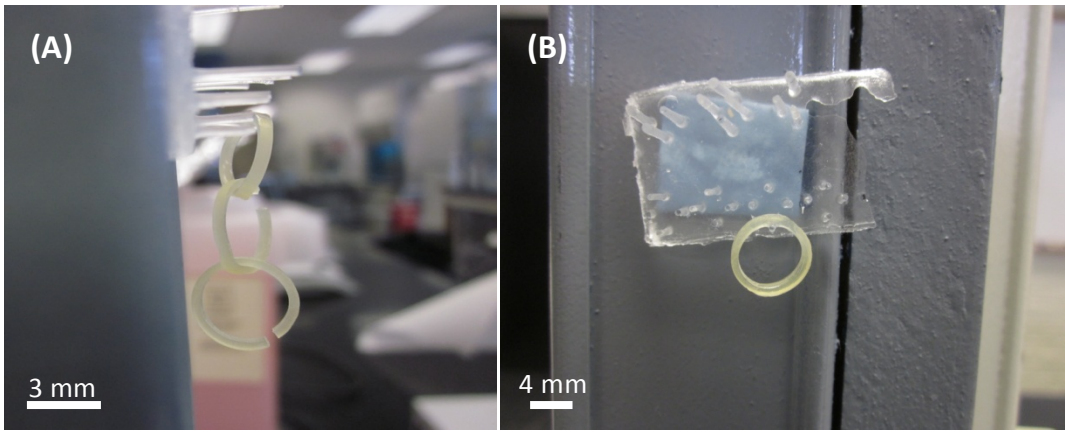

Figure 47: (A) Front view of experimental set up with elastic band glued to tip of the PDMS post. (B) Adding bands to witness post deflection. Measurements were made from both front and side views.

Table 18: Deflection of the post in response to the added rubber band weight

Deflection (mm)	Trial 1	Trial 2	Trial 3
Band 1	1	1	1
Band 2	0.8	0.9	0.8
Band 3	0.6	0.7	0.8
Band 4	0.8	0.8	0.9
Band 5	0.7	0.8	0.9
Band 6	0.6	0.8	0.8
Band 7	0.5	0.6	0.5
Band 8	0.5	0.5	0.4
Totals	5.5	6.1	6.1
Average Deflection (per rubber band)	**0.69**	**0.76**	**0.76**

The average deflection for each elastic band added was 0.69 mm for the first trial and 0.76 mm for both the 2nd and 3rd trials of the post calibration. Plots of force vs. total deflection of all 3 of these trials can be seen in Figure 48 below.

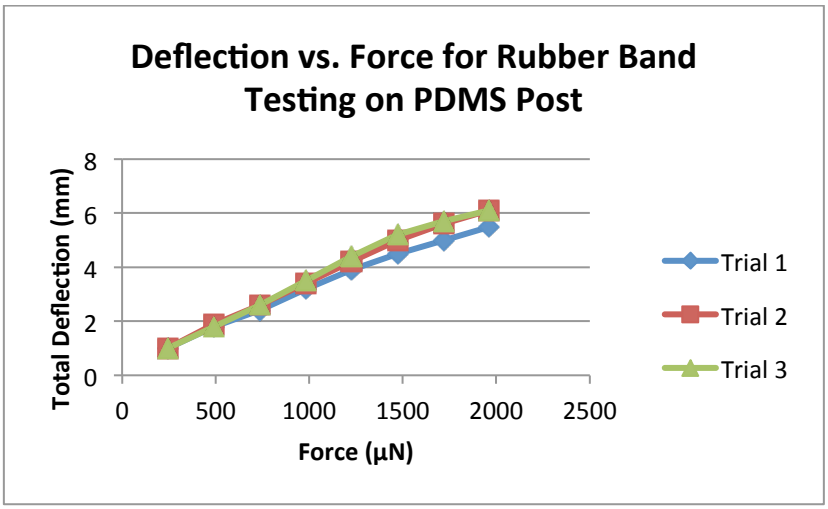

Figure 48: PDMS post deflections in response to the addition of rubber bands. All three trials are shown. Each data point represents a new rubber band being added (for each trial a total of 8 rubber bands were added).

The overall deflection with the addition of eight total elastic bands was 5.5 mm for Trial 1 and 6.1 mm for both Trials 2 and 3. Addition of elastic bands one at a time helped visualization of fairly uniform deflection of the posts from each trial of testing. It should be noted that as more weight was added, slightly less deflection was experienced. Also, the rubber band weight was still a much larger force than expected from tissue ring contraction. The deflection curves seemed to follow the same trend for all three trials. From this data, deflection of the PDMS post in response to various external forces was observed. This allowed for the use of the bending equation (described in Chapter 2) to solve for the elastic modulus of PDMS in a Microsoft Excel spreadsheet (Table 19).

This model was a very powerful tool, which allowed for the effective utilization of the ANSYS finite element modeling system. The deflection is expressed in millimeters and the force in μN.

Table 19: Calcuation of PDMS post modulus based off of known deflection and force during the rubber band testing. The bending equation was manipulated to solve for elastic modulus.

Length of Post (m)	Radius (m)	Deflection (δ) (m)	Force (N)	Modulus (Pa)	Modulus (kPa)
0.003	0.00035	0.0001005	3.331×10^{-5}	253100	**253.1**
Equations		**Total Weight Used (kg)**		**Force (μN)**	
$F = \frac{3\pi E R^3 \delta}{4L^3}$		0.000025		33.31	
$E = \frac{4FL^3}{3\pi R^4 \delta}$					

As seen in the above table, a modulus value of 253.1 kPa was yielded from this equation. This value was more comparable to the elastic modulus of PDMS in the literature than the values obtained in the previous tests and the data obtained from this testing provided a lot less variation for modulus values than the Instron testing.

6.2.3 ANSYS Finite Element Model

After this testing was completed and a modulus value was acquired for the PDMS posts made in the lab, the ANSYS FEA model was modified. A post with dimensions parallel to our final design (0.7 mm diameter, 3 mm height) along with accurate mechanical properties was modeled. This model was used to predict the expected deflection of the posts when induced by ring contraction.

One aspect that was investigated was whether or not a two-post array or a four-post array yielded a more accurate contractile force calculation. By experimenting with the ANSYS software and discussing with Dr. Adriana Hera of the WPI Mechanical Engineering Department, it appeared that the calculation would be the same in either array. As long as the tissue ring contracts uniformly, which had been confirmed by testing actual tissue rings and observing them under a Leica EZ4D stereomicroscope, the calculation would depend on the deflection of one post. Thus, it was only necessary to model a single post in the ANSYS software. Table 20 displays some expected deflection values from various forces. From this model, we were able to find that the upper limit of accuracy is about 1 mN of force for our PDMS posts of the specified dimensions. Any force higher

than this will cause too much deflection and not yield an accurate measurement. Figure 49 shows a screenshot of the ANSYS post model undergoing deflection from a simulated force.

Table 20: Expected deflections from various generated forces (based on ANSYS software)

	Force Generated (N)	Maximum Expected Deflection (mm)
Example 1	30 x 10^{-6}	0.092
Example 2	0.000245	0.76
Example 3	0.002 (upper limit of accuracy)	too large for detection
Example 4	3.51	N/A (too large for detection)

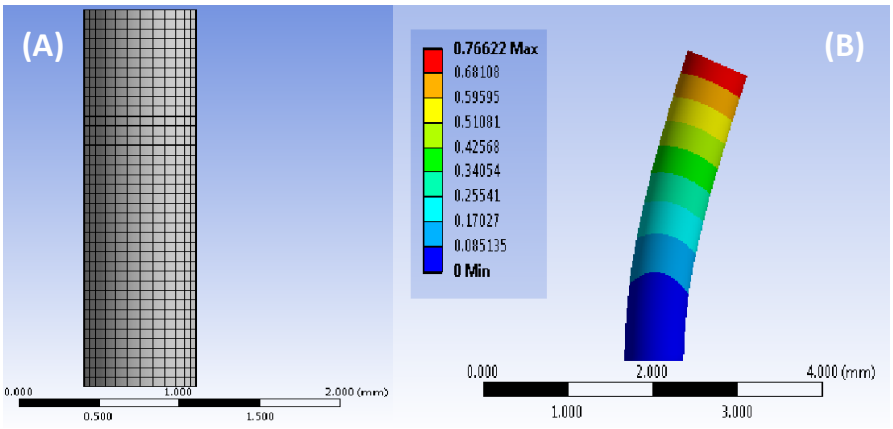

Figure 49: (A) ANSYS finite element model of a PDMS micropost. (B) Simulation of a 245 microNewton force being exerted on the top of the PDMS post, with expected deflections given.

Based on the modulus values in the literature, about 30 μN of force was expected to be experienced from a contracting SMC ring. As seen in Table 19, our expected deflection from this force based on our post calibration model would be around 0.092 mm, a small amount of deflection, but can certainly be viewed under a stereomicroscope, which offers a 4.4:1 zoom capabilities and allows for 3 Megapixel color images to be taken (Leica, 2012). Another interesting finding from the ANSYS model was that the force generated by the orthodontic elastic bands, 3.51 N, was too large to be accurately modeled. This force was far too great and caused too much deflection of the posts for an accurate measurement.

A force value of 245.25 μN was also inputted in the ANSYS model, because this was the equivalent force produced by addition of elastic bands to induce post deflection. For this force value, an expected deflection of about 0.766 mm was observed. This value was very similar to the average deflection observed during the final post calibration test, which was 0.74 mm. This confirms that the ANSYS post model accurately represents the data obtained during post calibration testing and can accurately predict expected deflection from known forces. This data also indicates

that the device is specific for measuring small forces. Based on the ANSYS testing, any forces larger than about 2 milliNewton produces too much deflection and thus cannot provide an accurate force calculation. Thus, had we added any more rubber bands onto our post for calibration testing, they would have caused too much post deflection.

This simple method of adding weight to the post tip and measuring deflection was a powerful tool for contraction force measurement. The force of a contracting tissue ring can accurately be calculated based on the deflection of PDMS posts. Additionally, if the approximate number of cells that compose a ring is known, the contractile force exerted by a single cell could be calculated. This could be important in studying the effects of various drugs on the expression of contractile proteins by vascular cells.

6.2.4 Calibration Testing of Our Final Design Mold

After we had ensured that our post calibration testing had been validated, we wanted to test our final design molds using the same calibration, by placing the rubber bands of known weights onto the tip of one of the microposts. In order to ensure that the manufacturing of our molds was consistent and did not change the properties of the PDMS, we tested two separate posts each on two of our manufactured molds. Additionally, to ensure that autoclaving the PDMS did not disrupt the mechanical properties; we tested two separate posts on one of our autoclaved molds. Also, for consistency, we used the same eight rubber bands on each of the posts during this round of testing (Figure 50).

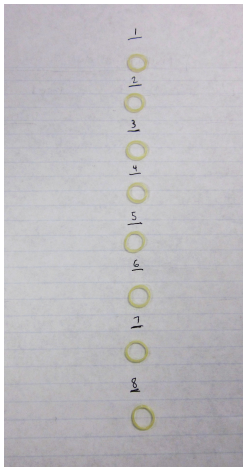

Figure 50: The same eight rubber bands were used in all testing to ensure for the same amount of weight to be added to each post.

The walls of the final design molds were cut, so that the posts were easily exposed. Then the base of the molds were super glue onto the side of a plastic weigh boat and allowed to hang off the edge of the lab bench (Figure 51). Rubber bands were added one at a time, with each deflection being measured by calipers and recorded to the nearest tenth of a millimeter.

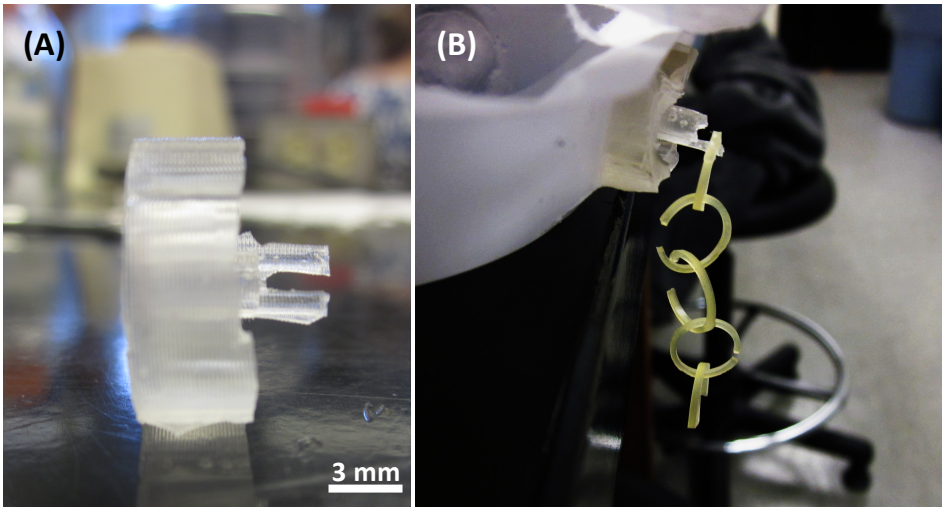

Figure 51: Post calibration testing. Wall of mold was removed to expose microposts (A). The experimental set up: the mold was glued to a weigh boat and allowed to hang off the edge of the lab bench (B).

The total deflection experienced was recorded for each post of all of the molds and used to calculate the elastic modulus of each post. Since the same rubber bands were used in all testing procedures, the total force exerted on each post was the same for all trials. The values obtained for the two posts tested on each mold were then average for comparison. Table 21 below provides a data summary of all of the testing conducted.

Table 21: Data summary of the calibration testing on the final design molds

	Total Deflection (mm)	Total Force (µN)	Elastic Modulus (kPa)
Non Sterile Mold 1 Post 1	5.6	1962	201
Non Sterile Mold 1 Post 2	5.3	1962	212
Average	5.45	1962	206
Non Sterile Mold 2 Post 1	5.4	1962	208
Non Sterile Mold 2 Post 2	5.3	1962	212
Average	5.35	1962	210
Sterile Mold Post 1	5.3	1962	212
Sterile Mold Post 2	5.2	1962	216
Average	5.25	1962	214

Based on the data obtained from testing, the average elastic modulus for the first non-sterile mold was 206 kPa and the modulus for the second non-sterile molds was 210 kPa. These values are in close proximity to one another, helping show that the manufacturing process of our molds is consistent and not greatly changing the mechanical properties of each newly made mold. The average elastic modulus found in the autoclaved mold was 214 kPa, which was also in close proximity to the posts of the two non-sterile molds that were tested. This provides us with data showing that autoclaving our molds does not greatly change the mechanical properties of the PDMS posts. Although the values obtained during this testing for elastic modulus were slightly lower than we obtained in the prior testing on a PDMS mold of an earlier design, the numbers obtained in this mold were still within the limits of some values found in literature (Sasoglu, 2007).

Although this was a reliable method of calculating a modulus value, the resolution of the measurement led to us questioning the calculations, as human error with the calipers could greatly change the overall modulus value. Therefore, we decided to repeat the experimental procedure with both the sterile and non sterile molds. However, instead of using calipers to measure the deflection of the PDMS posts, we took images of the posts from a side view as each rubber band was added to the posts. We then used the Leica software package, which is essentially equivalent to ImageJ, to measure the deflection of the posts as each rubber band was added (Figure 52).

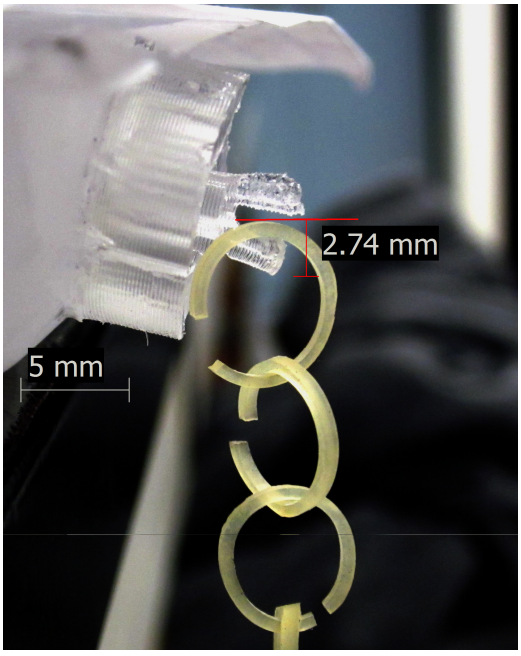

Figure 52: Post deflection measurement made with the Leica software package. Using this software allowed us to make measurements with less resolution and less chance of human error.

This allowed us better resolution for our deflection measurements, as tenths of a millimeter can make a large difference in the overall force calculation. The new data for the rubber band post calibration testing can be seen in Table 22.

Table 22: Modulus calculations of all tested microposts based on average post deflection in response to the addition of a rubber band

	Average Deflection (mm)	Modulus (kPa)
NS Mold 1 Post 1	0.71	262.85
NS Mold 1 Post 2	0.70	268.09
NS Mold 2 Post 1	0.71	263.31
NS Mold 2 Post 2	0.70	267.54
Sterile Mold Post 1	0.72	261.67
Sterile Mold Post 2	0.69	272.90
Average	0.70	266.06
Standard Deviation	0.01	4.25
Coefficient of Variance (%)	1.58	1.60

The average elastic modulus value found for our PDMS microposts based on the deflection measured by the Leica software was 266.06 ± 4.25 kPa. This value was still within the range of the previously reported literature (Sasoglu, 2007). Also, there was little variation between the calculations, showing that our manufacturing process of the PDMS molds was consistent and did not cause a large change in mechanical properties of the posts. Figure 53 shows that the force versus deflection curves follows a linear trend and all PDMS post samples showed data that followed this trend. This testing method for the preliminary experimental rounds was primitive and prone to human error, as calipers were the only tool used for the measurement. However, using the Leica software package to make the measurements gave us more confidence that our elastic modulus values were calculated correctly and with better resolution. There was little variation between the modulus values calculated in the various posts and molds, ensuring us manufacturing of our molds was consistent and not greatly changing the mechanical properties of the posts. Additionally, autoclaving the PDMS does not seem to alter the mechanical properties of the posts. In the future, more advanced means of calibration, such as mechanical force transducers should be used, but with the budget and equipment constraints of the project, this method allowed us to determine a value for the elastic modulus of the PDMS microposts.

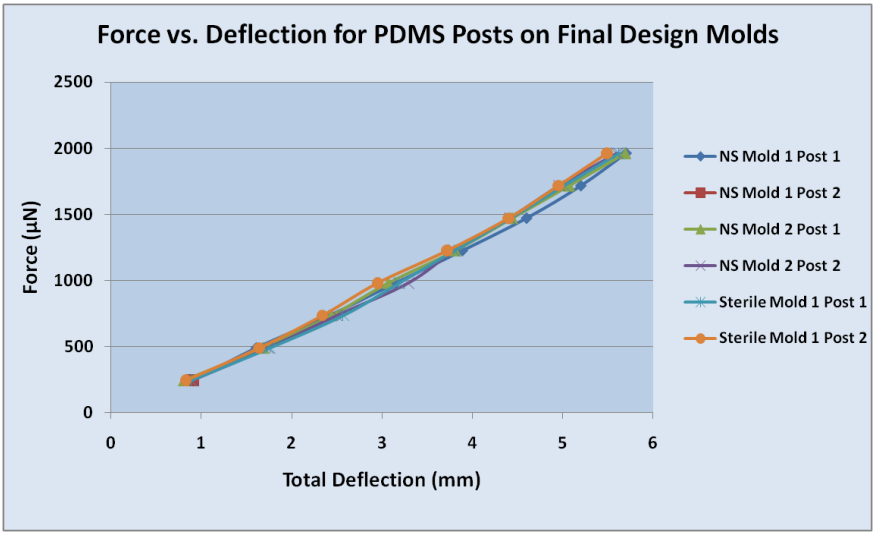

Figure 53: Force vs. deflection for all PDMS posts tested on the final design molds. Notice the force vs. deflection curve seems to follow a linear trend.

6.3 Multifunctional Mold

After doing several rounds of testing on the mechanical properties of the design, it was necessary to experiment with making our PDMS micropost molds. We needed to first design a negative template that the PDMS could be poured into and cured. A multifunctional design model was created in order to create properly scaled PDMS molds. The dimensions used in this model were specific to our findings in literature, which allow for it to be applied to cell culture experiments. A total of four equivalent parts were assembled to create the full template as seen in Figures 54 and 55 below. This four-part design is beneficial because it allows for easy PDMS removal upon polymerization, as the PDMS tends to slightly stick to its negative template material. This design was first modeled using SolidWorks software, then rapid prototyped with ABS to create a negative template to make a PDMS mold used for testing. The mold design allows for a 4 mm base with four attached microposts (0.7 mm in diameter and 3 mm in height) with small "caps" on top of each micropost to help prevent the rings from sliding off the top of the posts during contraction. The overall diameter between the posts is 4 mm. The well is smooth and rounded to allow for cell aggregation into a ring and is 1.50 mm wide.

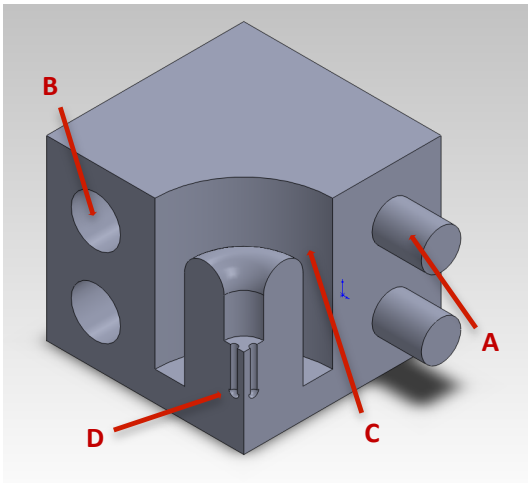

Figure 54: CAD of one part of negative template for multifunctional mold. The PDMS is poured into this mold and allowed to cure to form our device. Peg inserts (A) that fit into gaps (B). (C) Well where cells are seeded and cultured (D) Microposts with caps.

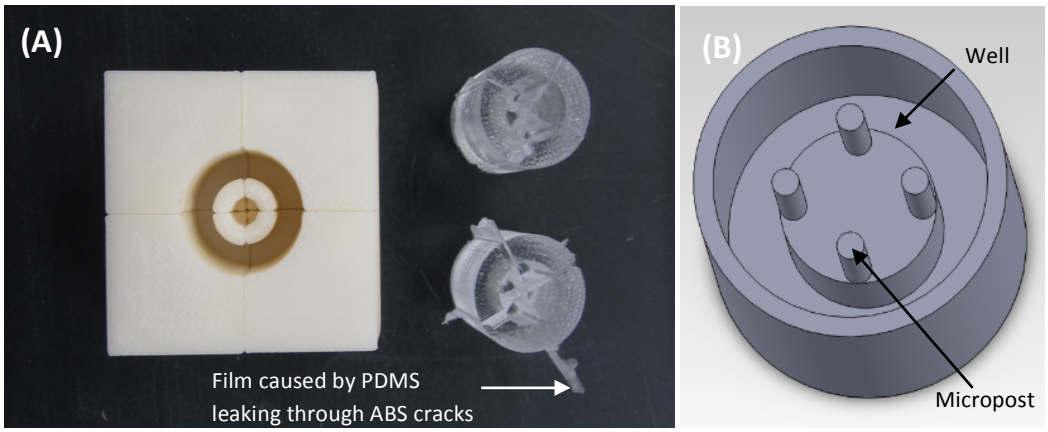

Figure 55: ABS negative template and resulting PDMS molds (A). A close up top view of the PDMS mold, with components labeled (B).

As seen in Figure 54, the PDMS molds had films within the seeding well, compartmentalizing the well. This design limitation posed a problem due to the fact that the well was to be used to culture cellular rings; with the PDMS films, cell seeding could not be done. Although an elastic band was used to tightly hold the four parts together as the mold was degassing and curing in the oven, the PDMS seeped through the cracks in between the individual ABS pieces creating thin PDMS films (Figure 55).

Even though there were a few major problems, it should be noted that this negative template did result in a successful mold. The microposts were completely intact upon removing the PDMS from the template.

As one solution to the problem of the cracks in the molds, Silicone vacuum grease, used to create a tight seal in vacuum desiccators, was used to coat the inner surfaces of the individual pieces of our ABS rapid prototype with the grease. A rubber band was tied tightly around the four pieces as well, in an attempt to limit crack size and PDMS leaking into the cracks of the negative template. The vacuum grease allowed for a much tighter seal of the cracks while still allowing the PDMS to cure properly. However, it did not get rid of the cracks entirely, especially in the center of the mold. This was still concerning, as the posts needed to be able to deflect freely. Surgical scissors were used to carefully remove the undesired PDMS films on all the PDMS molds developed with the ABS template. Figure 56 below shows the mold created from the vacuum grease coated ABS template.

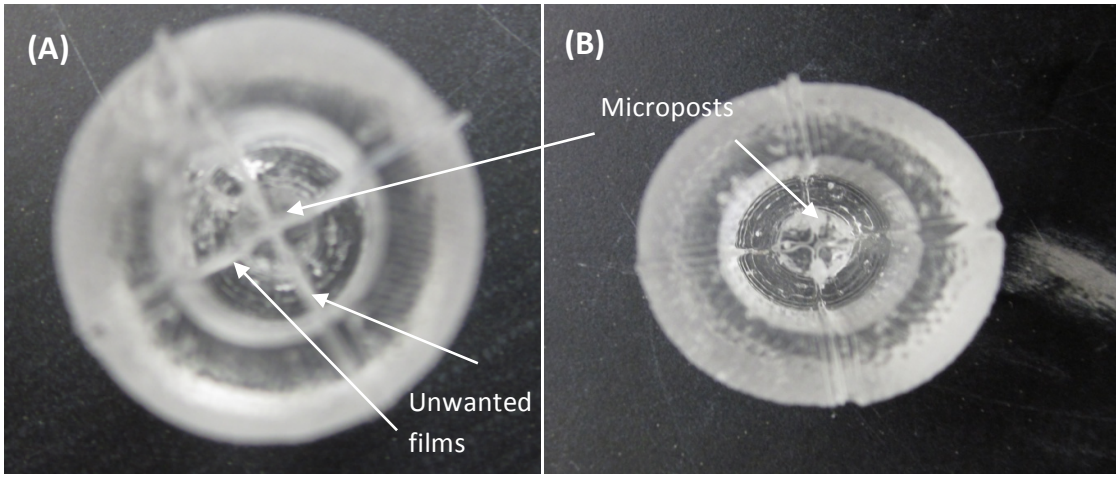

Figure 56: PDMS mold before (A) and after (B) coating negative molds with vacuum grease to limit the size of the cracks. Note the reduction of the unwanted films, especially in the inner diameter around the microposts.

As another solution to the problem with the cracks, a one piece CAD model was designed and rapid prototyped (Figure 57). This model would completely eliminate any cracks, as all of the PDMS would be poured into one individual well. The model had the same sized posts and an overall base diameter of 4 mm, like the four piece mold. However, this mold was much smaller in overall size, as it was only 10 mm length by 7 mm width. This was done because the previous mold with four pieces used a lot of excess ABS, as it was 16 mm x 18 mm. It also had the potential to be more easily manufactured and allow for even faster PDMS mold creation, as it is less complex than the four-piece model. However, some concerns existed with this model. First, it was much more difficult to remove the PDMS from this ABS template successfully in one piece. It was difficult to separate the PDMS from the ABS template. Through all the attempts, the PDMS was torn to pieces. Also, caps could not be added to the tips of the microposts in this model, as they would simply tear

off when the PDMS was lifted out of the template. From this experimentation, it was verified that the prior negative template with the four separate pieces was more successful in making a PDMS mold. Thus, we decided to optimize the four-piece design and make some changes to allow for easier removal of an intact PDMS mold, which can be seen in our final design section.

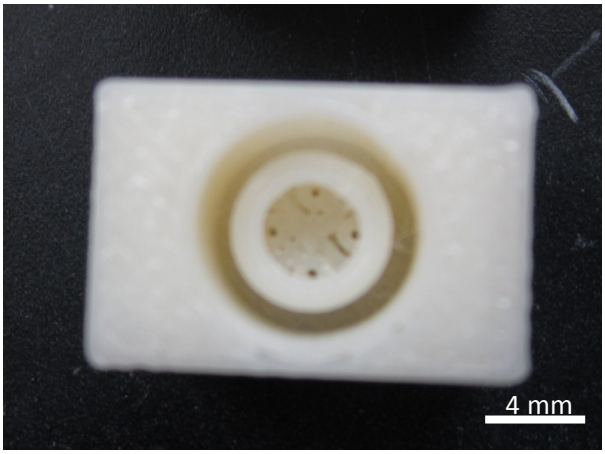

Figure 57: The one-piece multifunctional negative ABS molds.

Visualizing Ring Contraction

In order to induce contraction of the tissue rings, it is necessary to completely submerge the posts in the proper chemical agonists. Six-well plates were used to contain the micropost molds and chemical agonists. With this set up, it was uncertain whether or not the submerged posts would be difficult to view or whether the deflection of the posts would be distorted under a liquid.

Therefore, observations and images of posts submerged in water were obtained using a standard digital camera. From a top view, the molds could be seen clearly. However, one concern we did discuss was the fact that the PDMS was clear and when the clear chemical agonist was added, it may be difficult to visualize the posts. Thus, we experimented with dyeing the posts of the molds different colors to provide more contrast (discussed later in this section). Forceps were used to manually move the posts to simulate deflection (Figure 58). After induced post deflection, the posts could be seen clearly and without distortion from the top view. In our actual experiments, a camera with a higher resolution was used to acquire images and data.

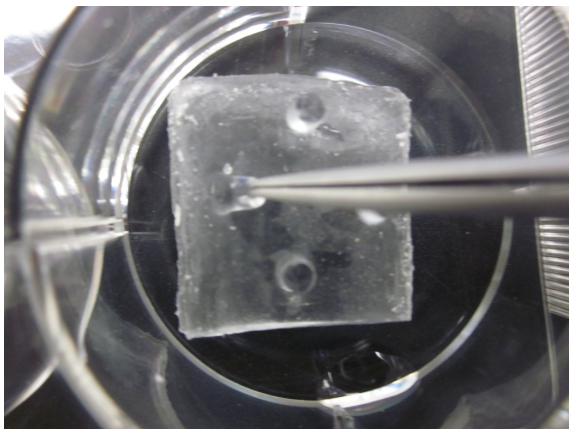

Figure 58: Top view of simulated PDMS post deflection under water.

PDMS post deflection was also observed at a side view (Figure 59). It was more difficult to view the posts clearly from the side because of the plastic walls of the six-well plates. However, the deflection of the posts was not distorted from a side view either. This testing suggested that post deflection could be successfully imaged in solution from both a top and side view.

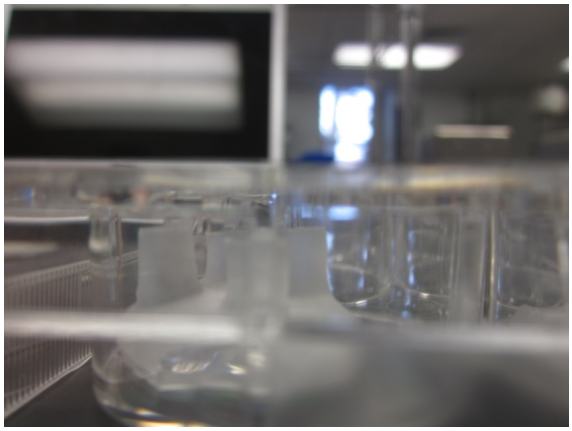

Figure 59: Side view of PDMS post mold. Note that it is more difficult to see the mold in this picture because the 6 well plate covering blocks the view.

To better contrast the posts from the PDMS mold base, the posts were dyed with red food coloring and the base was kept clear, Figure 60a. When observing molds under a stereomicroscope, shown in Figure 60b, it was evident that dyed posts allowed for more prominent visualization of the dyed posts. The tips of the PDMS posts can be seen very clearly when they are dyed a red color under the Leica stereomicroscope. This makes visualization of the post deflection very easy. However, it is not absolutely necessary, because the Leica is equipped with several different brightness capabilities and can provide lighting from both a top and bottom light source, allowing for the ideal contrast of the posts and the base to be viewed even without a dye. If a quick manufacturing process for dyeing and curing the molds was developed, the dyed molds can be a

viable option for optimizing the viewing of the tissue ring contraction. It was also easier to manually focus on the posts when visualizing the dyed post under the Leica microscope.

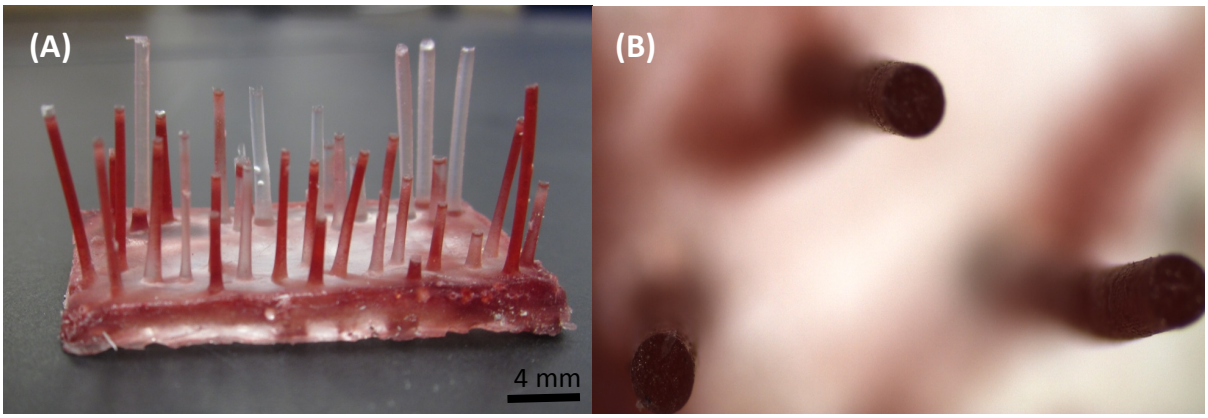

Figure 60: (A) Dyed PDMS mold. Note: the lengths of the posts came out of the mold all different, so the posts needed to be trimmed to 3 mm length. (B) Image of individual posts as seen under a Leica EZ4D stereomicroscope, magnification 16X.

6.4 Growing Tissue Rings and Testing the Molds

The final step in validating our final design was to grow functional tissue rings, allow them to contract, and successfully measure this contraction with our molds. It was important to be able to practice and develop techniques in cell culture and handling of the tissue rings prior to advancing on to our device composed of PDMS.

6.4.1 Cell Culture Techniques

In order to have viable tissue constructs for testing, rat aortic smooth muscle cells (rASMCs) were used for tissue ring formation. Using the negative template available in Professor Rolle's lab, 2% agarose in DMEM molds that contained viable wells for cell seeding were made (Gwyther, 2011). The complete protocol for our cell culture techniques can be seen in Appendix I.

Once the molds were fully gelled, they were removed from the template and cut into individual wells. As shown in Figure 61 below, the agarose molds were placed into 12-well plates. One million rASMCs at a concentration of 5 million cells per mL were seeded into each 4 mm well and placed into an incubator (one million cells/ring). Media was changed every other day. The cells aggregated into viable tissue rings and were cultured for 7 days.

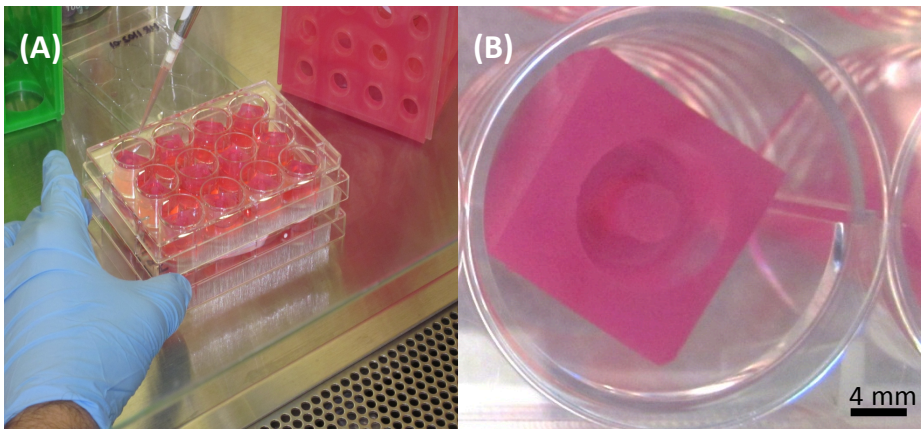

Figure 61: Seeding rASMCs onto agarose wells (A). Close up view of one of the agarose wells (B).

Proper rings did not form in all the wells. Of the 36 wells seeded with cells, 20 resulted in successful tissue ring formation, with all but 2 of the 20 samples showing uniform ring thickness. However, the rings were still used for contraction experiments and observation. A tissue ring sample can be seen in Figure 62.

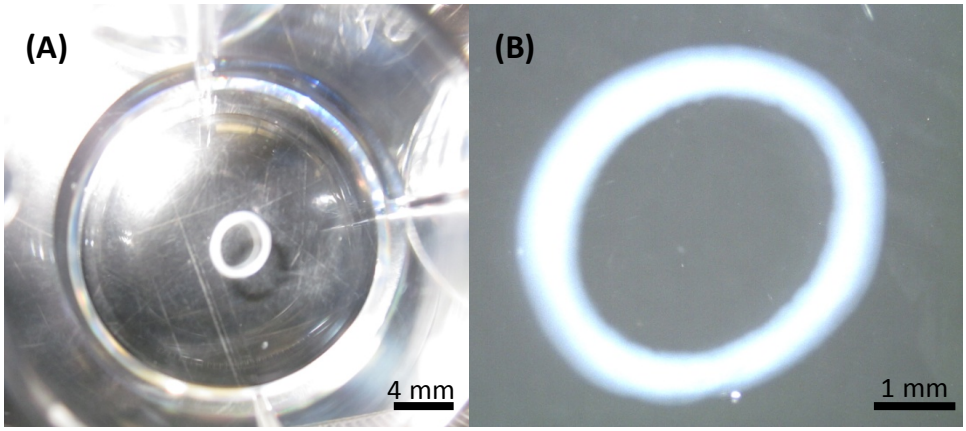

Figure 62: (A) Formed tissue ring placed in phosphate buffered saline solution (PBS) in one well of a six well plate. (B) Formed issue ring, magnification 16x.

6.4.2 Tissue Ring Contraction Procedure

The viable tissue constructs were induced to contract using potassium physiological saline solution (KPSS) made to a concentration of 0.9% KCl and 99.1% deionized water, as cited in prior literature (see Appendix J). According to prior research, KPSS was the best chemical agonist to induce maximum contractile response from SMCs (Scholar Chemistry, 2008, 2008; Spires, 2005). For example, SMCs contract in response to acetylcholine, potassium chloride, and phenylephrine while vessels contract *in vivo* due to hormones such as epinephrine and norepinephrine (Gentile, 2008; Hecker, 2008; Zheng, 2000; L'Heureux, 1998). The KCl allows for the cell membrane of the

SMCs to become depolarized, leading to contraction (Gentile, 2008; Hecker, 2008; Zheng, 2000; L'Heureux, 1998). For initial contraction testing, three rings were removed from the agarose and placed into separate wells of a six well plate. First, the rings were submerged with physiological saline solution (PSS), which was composed of 0.9% NaCl and 99.1% deionized water for 30 minutes in order to normalize the rings prior to contraction and images were taken by a Leica EZ4D stereomicroscope (Spires, 2005). The Leica allows for high quality 4.4:1 zoom ratio and a 3 megapixel camera for imaging and measurement. Also, it includes 7 LED lights for various contrast and brightness settings.

The PSS was then removed from one well and KPSS was added until the tissue ring was completely submerged with the KPSS. Images were taken of the ring with both digital cameras and the camera on the Leica EZ4D every five seconds for five total minutes. However, contraction was only observed for the first 2 minutes after the KPSS was added. This procedure was repeated for the other two rings. The ultimate contraction distance observed during this test was 143.43 µm for the first ring (Figure 63) and 114.98 µm and 140.23 µm for the second and third tissue ring samples, respectively. Table 23 displays the total contraction experienced by the tissue ring samples when placed in the cell culture wells.

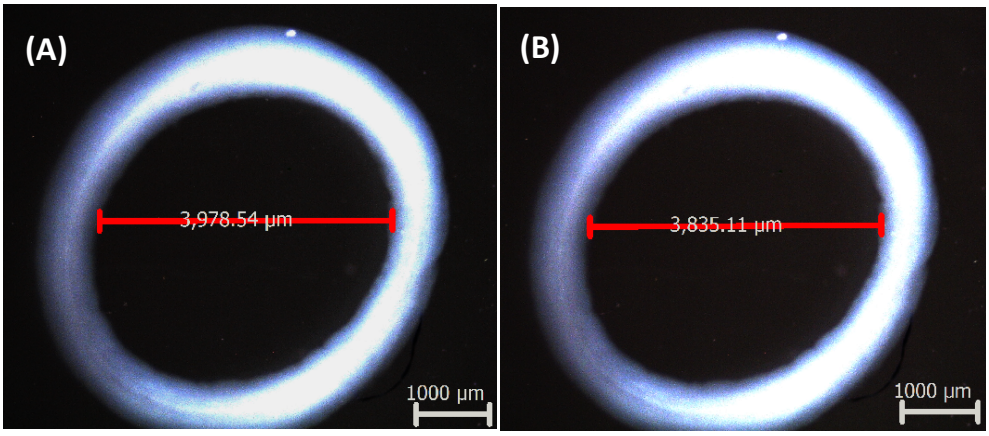

Figure 63: (A) Tissue ring sample before KPSS addition. (B) Tissue ring after KPSS addition

Table 23: Summary of the KPSS induced contraction

Ring Sample	Original Diameter (µm)	Final Diameter (µm)	Total Contraction (µm)
1	3978.54	3835.11	143.43
2	3982.43	3867.45	114.98
3	3972.24	3832.01	140.23
		Average	132.88
		Standard Deviation	12.72

As seen in Table 20, the average difference in diameter was 132.88 microns. This is a relatively small change in diameter, indicating that the stereomicroscope is capable of detecting miniscule changes in length, allowing the use of this technology to observe post deflection. In this initial test, tissue rings were successfully grown and induced to contract in plates. Although this experiment showed that the KPSS induced tissue ring contraction, we now wanted to use our PDMS microposts to measure contraction force of the tissue rings. Thus, this experimental protocol of adding KPSS was used to induce rings to contract around PDMS posts. However, we also needed to ensure that it was the KPSS causing the rings to contract. As a controlled experiment, we also tested several rings on our final design molds and added only PSS to measure contraction. This testing will be described in detail in the next section of the report.

6.4.3 Contraction Force Measurements with the PDMS Posts

The PDMS mold consisting of microposts, created from a clay negative template, was used for further contraction testing. The rings were all normalized prior to being placed around the PDMS posts. It should be noted that tests were conducted using a two-post and four-post interface in order to verify thorough handling and force readings, which was more suitable for data collection. An analysis of the two-and four-post arrays can be seen in Section 6.1. Rings were placed around the posts using forceps and initiated to contract with KPSS. First, the tissue rings were placed on the PDMS posts and allowed to equilibrate in PSS solution for 30 minutes. Then the PSS was gently pipetted out as not to disrupt the rings from their positions on top of the posts. KPSS was gently pipetted into the plate to replace the PSS. Images were taken approximately every 10 seconds during contraction using the Leica stereomicroscope, for 4 minutes in total. However, maximum contraction was experienced after about 2 minutes. From the previous testing, it was determined that after this time point, very minimal contraction was witnessed (Table 24). Thus, for the remainder of our testing, we decided to take photographs for a total of four minutes and were confident that maximum contraction of the rings would occur within this time frame.

Table 24: Contraction of a SMC ring samples submerged in KPSS in a 6 well plate from the previous testing over time

Time elapsed (seconds)	30	60	90	120	150	180	210	240
Average total deflection of posts (mm)	0.33	0.67	1.02	1.28	1.31	1.34	1.34	1.34

Figure 64 shows a tissue ring initially placed on a four-post array.

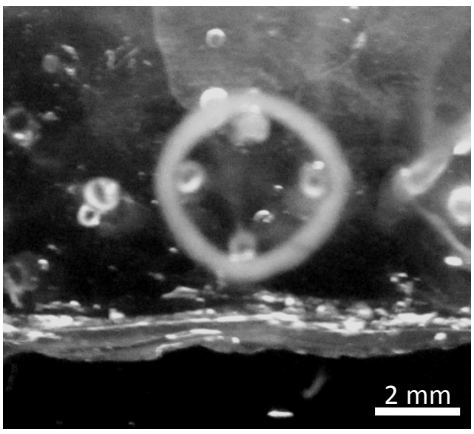

Figure 64: A rAMSC tissue ring mounted on PDMS micropost mold.

In total, eight ring samples were tested; four on the two-post arrays and four on the four-post arrays. Figure 65 shows an example of the contraction of a tissue ring on the four-post array over time and Figure 66 gives an example of a tissue ring contracting on a two-post array over time. Measurements were made by first calibrating the scale on the photograph with the known diameter of each micropost (0.7 mm) using the Leica software. A distance line was then drawn between the two sets of posts on the four post arrays. The change in diameter was averaged for both sets of microposts to get a value for total deflection. Table 21 shows the data summary of all total deflections observed in tissue rings placed on the four-post arrays. We then used these deflection values to calculate the contraction force using the force bending equation (Equation (1)) in Microsoft Excel.

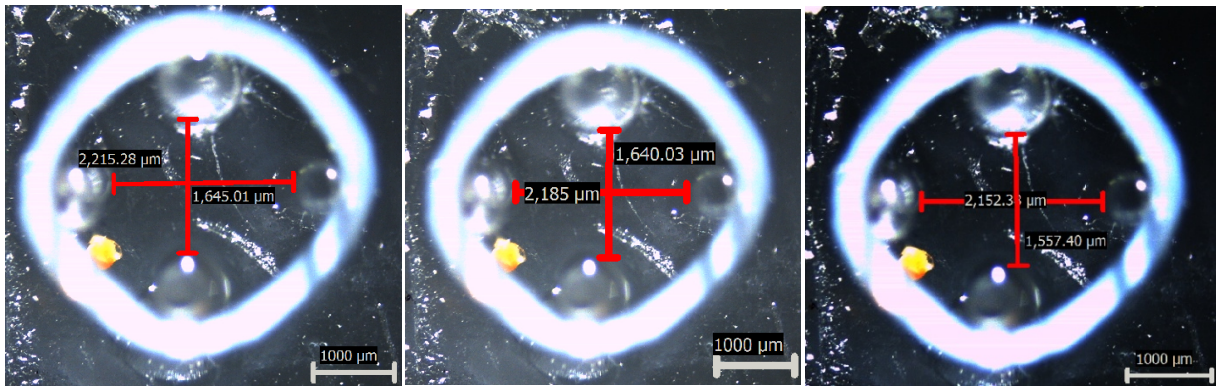

Figure 65: Contraction of a rASMC tissue on a four-post array. The samples were analyzed using the Leica EZ4D software package.

As seen in Figure 65, contraction was minimal on the four-post molds. Maximum contraction of our ring samples seemed to occur between 1 to 2 minutes after the addition of the KPSS. It is also important to note that the rings that were allowed to contract freely in the tissue

culture wells showed more overall contraction than the rings placed on the microposts. This is most likely due to the fact that the PDMS posts resisted the contraction of the rings. The average deflection seen on the four post molds from the four sample tissue rings was 0.057 ± 0.01 mm. To the naked eye, it was very difficult to notice contraction, but using the Leica software, a deflection was detected. Deflections were measured from the inner diameters of each of the two posts and the deflection values were averaged to obtain a final deflection. Vandenburgh, et al. (2008) measured the post deflection from a side view, so our approach did not have precedent in literature.

However, as long as the measurement is taken from the same place at all time points (inner diameter, outer diameter, or center of the post), the only important aspect is the change over time in the position. Thus, we chose to continue to measure the distance between the inner diameters of the posts over time, as this position was easier and clearer to visualize on the Leica photographs, and correlated with the way deflection was measured in our ANSYS model. The outer diameter and point where the ring was touching the outer diameter of the post were not as clear to see in all of the pictures, so we chose now to use the outer diameters for measuring. Microsoft Excel was used to calculate the maximum contractile force due to these deflections. A complete summary of the data obtained during the contraction of the rings on four posts can be seen in Table 25.

Table 25: Data summary deflections of tissue ring contraction on four-post arrays

KPSS Trial	$Distance_0$ 1 (microns)	$Distance_F$ 1 (microns)	$Distance_0$ 2 (microns)	$Distance_F$ 2 (microns)	Deflection 1 (mm)	Deflection 2 (mm)	Average Deflection (mm)	Maximum Contraction Force (μN)
1	2135.24	2076.11	1867.34	1809.34	0.05913	0.058	0.0586	19.39
2	2269.85	2232.4	1876.43	1828.9	0.03745	0.04753	0.0425	14.22
3	2418.22	2361.25	1789.27	1736.98	0.05697	0.05229	0.0546	18.10
4	2215.01	2152.38	1640.03	1557.4	0.06263	0.08263	0.0726	24.06
						Average	0.0571	18.94
						Standard Deviation	0.01204	4.06

The average maximum contractile force for the four rings placed in the four-post array was 18.94 μN. This value of maximum contraction seemed to be similar to values seen in the literature, 30 μN. The Leica software, along with our force/deflection equation, enabled the calculation of this maximum force contraction value exerted by the tissue rings on the four-post array.

As previously mentioned, four tissue ring samples were also tested on a two-post array with the same procedure. The rings on the two post arrays were more elliptical in shape, but still contracted. A complete data summary for the testing on the two post arrays can be seen in Table 26. The rings on the two posts caused an average of 0.074 mm of deflection, which was more than

the deflection caused by the tissue rings on the four-post arrays. This may be due to the fact that the rings were under greater tension on the four post arrays, so there was more resistance. However, the four post arrays also helped the rings keep their structural integrity better and some of the tissue rings on the two-post arrays slid down the posts rather than remaining in place.

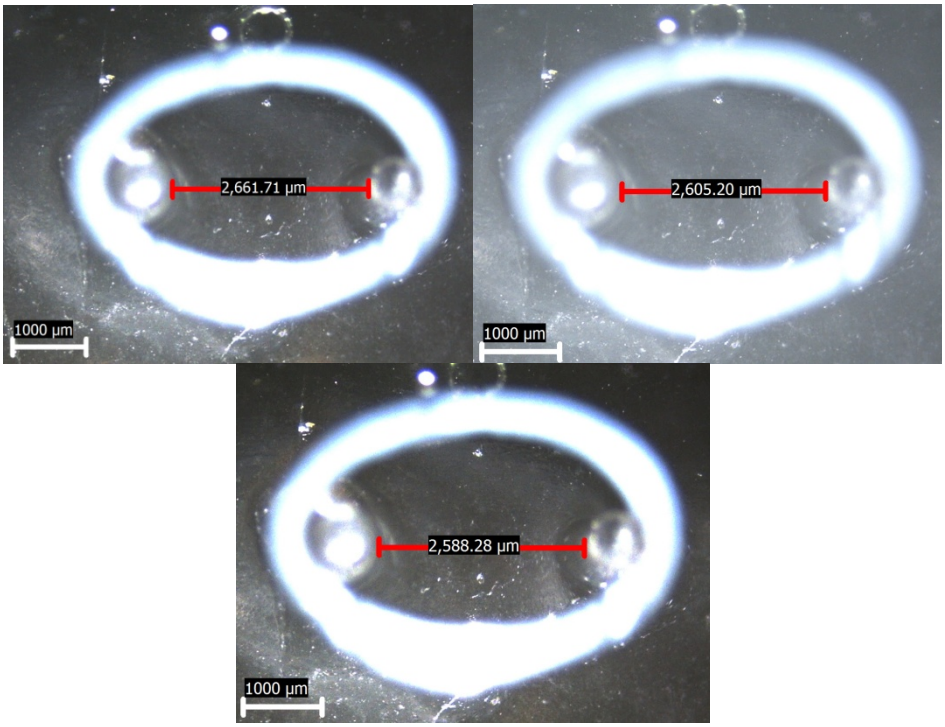

Figure 66: Contraction of a rASMC placed on a two-post array. Measurements were made using Leica stereomicroscope software.

Table 26: Data summary of tissue ring contraction on the two-post arrays induced by KPSS

KPSS Trial	$Distance_0$ (microns)	$Distance_F$ (microns)	Deflection (mm)	Maximum Contraction Force (µN)
Trial 1	2057.58	1967.41	0.09	29.89
Trial 2	2661.71	2588.28	0.07	24.33
Trial 3	2744.39	2685.20	0.06	19.62
Trial 4	2550.39	2474.42	0.08	25.16
		Average	0.07	24.75
		Standard Deviation	0.01	4.21

The average deflection caused by these tissue rings corresponds to an average contractile force of about 24.75 µN, which was slightly more than the force exerted by the rings on the four post arrays. This force output was also used to in our ANSYS model to verify our Excel calculations as see in Figure 67.

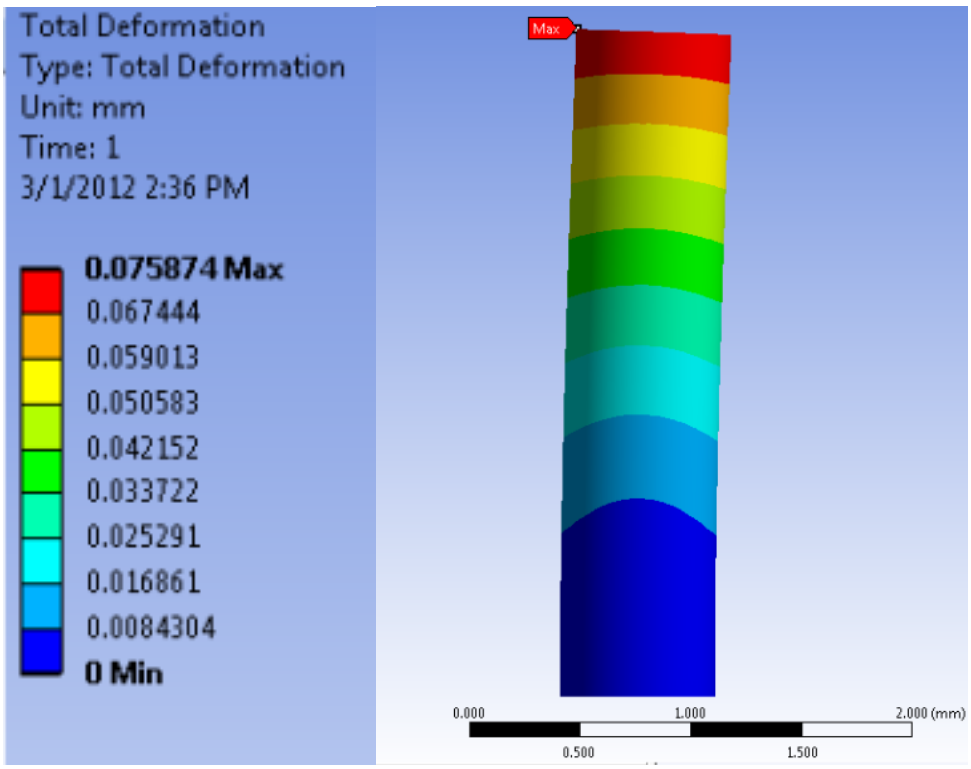

Figure 67: ANSYS model of the average contraction force generated by the tissue rings on the two-post molds.

For a force of 24.75 μN, the ANSYS model displayed that the maximum deflection of the PDMS microposts would be around 0.075 mm, which was only a 0.001 difference than the value of observed deflection during testing. This confirmed that the manual calculations for contractile force were accurate. Two ring samples were also tested on the posts of the PDMS multifunctional molds that were made from the ABS negative template. This test is described in the following section. Overall, fairly consistent force readings to values seen in literature were obtained via the tests outlined in this section.

6.4.4 Culturing and Testing rASMC Rings on the PDMS Molds

After successfully obtaining contraction force outputs from the deflection of PDMS microposts, the functionality of the multifunctional molds were tested. RASMCs were seeded into the wells of sterilized multifunctional molds coated with 1% bovine serum albumin (BSA). BSA was used to coat the PDMS surface to prevent cell adhesion to the PDMS surface—a detailed procedure can be found in Appendix I. Unfortunately, viable tissue rings were not formed in the either of the two trials performed. RASMCs were seeded in three different BSA-coated PDMS molds and incubated for 24 hours. Cells balled up, bunched together and adhered to the bottom of the PDMS well as shown in Figure 68.

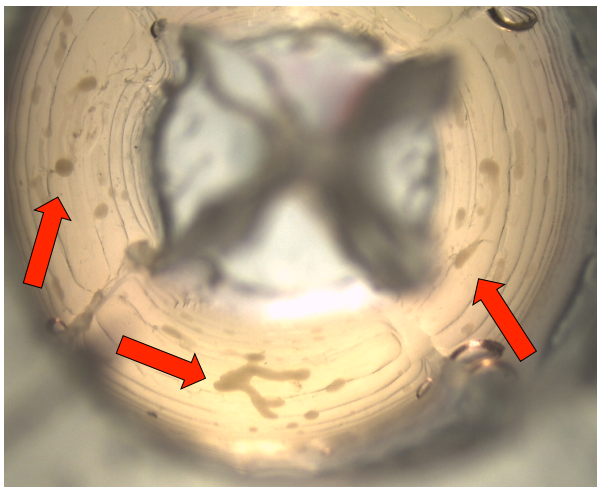

Figure 68: rASMCs failed to form a ring on the BSA-coated PDMS mold. Some balled up cells indicated by red arrows.

As another experiment in attempt to grow our rings on our PDMS molds, we plasma treated three molds in the laboratories at Gateway Park. Our advisor had informed us that the plasma treatment would make the surface of the PDMS much more hydrophilic than normal, possibly allowing the BSA to adhere more easily and uniformly to the wells in our molds. Immediately after plasma treatment, we again coated the molds with BSA and then seeded rASMCs into the wells. Unfortunately, tissue rings did not form on any of the three molds that we had plasma treated. There are still some other options and techniques that can be used to help cells grow on PDMS, but we did not have sufficient time or money to try all of these methods. We still believe that our final device has the potential to be made multifunctional, so that cells can be grown and tested on the same device.

To test whether or not the microposts on these molds were functional, tissue rings that were cultured in agarose were tested for contraction testing on the PDMS posts of the multifunctional device. Two PDMS multifunctional molds, one consisting of a two-post array and the other a four-post array, were placed into separate cell culture plates. The two post array mold was made with the same ABS negative template as the four post mold, but two of the posts were cut off. A tissue ring was positioned around the PDMS posts in a PSS solution, and the mold was focused under the stereomicroscope (Figure 69). Images were taken with the stereomicroscope and the PSS was replaced with KPSS after 30 minutes of normalization. Images were taken of the micropost deflection until ultimate contraction was observed as shown in Figures 70 and 71. Deflections of the posts were further measured and analyzed from the images using the LEICA software, and the data can be viewed in Table 23.

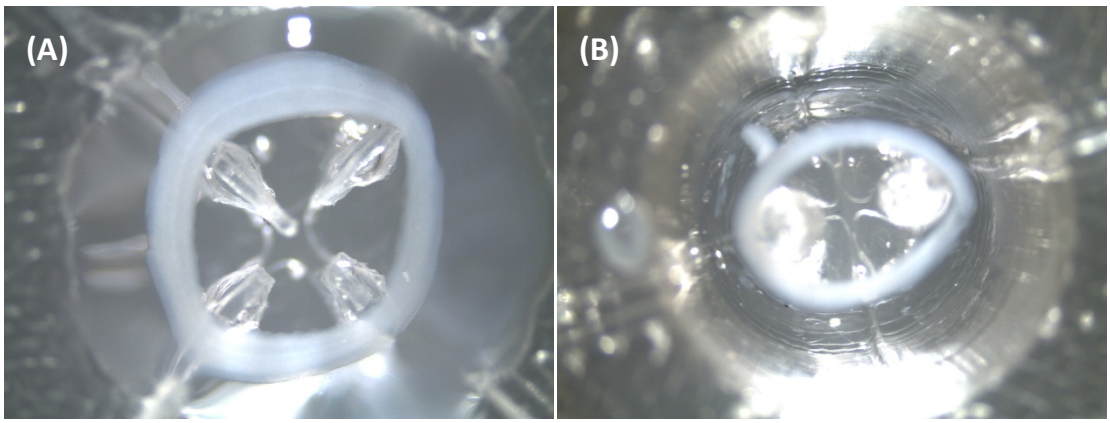

Figure 69: (A) Tissue ring placed around the four-post mold, magnification 16X. (B) Tissue ring placed around the two-post mold, magnification 8X.

We decided to continue the rest of the testing with a four post design, as the four posts helped better keep the circular structure and integrity of the tissue rings. Since testing has never previously been done in ring constructs with microposts, there was no precedent of the most effective way to conduct the testing procedure and calculations. Based on all of the initial ring contraction testing as described above, we were able to devise an effective experimental protocol to test vascular ring contraction on our final design molds.

For the testing of contraction on our final design, we first soaked rASMC tissue rings in the PSS solution for 20 minutes. Using forceps, we gently placed the rings onto the tops of the PDMS microposts. As we had witnessed in earlier testing, the rings maintained their position around the posts at the tops, without sliding down or popping off the top of the posts during testing. Using a pipette, we then added 0.8 mL of KPSS into our final design mold, ensuring that the tissue ring was completely submerged. We then took photographs every ten seconds for a total of four minutes with the Leica EZ4D. For all final testing rounds, 16X magnification was used. A total of ten ring samples were tested with this procedure.

To ensure that the KPSS was the cause of ring contraction, we repeated this procedure, but we pipetted PSS into our molds rather than KPSS. Once again photographs were taken every ten seconds for a total of four minutes at 16X magnification. A total of 10 ring samples were tested with this procedure as well.

Lastly, we wanted to ensure that the deflection of the posts was caused by the action of the smooth muscle cells, and not by the extracellular matrix that made up the ring structure. As a negative control, we lysed the cells by soaking our rings in deionized water for a total of 30

minutes. We then placed the rings onto our microposts with forceps and added KPSS to our molds. We took pictures every ten seconds for a total of four minutes at 16X magnification. A total of nine ring samples were tested using this procedure.

To analyze the ring samples, the Leica software was used to measure the distance between opposite posts. This was done for every picture, as total deflection was calculated as the difference between the original and final distance between the posts. The vertical and horizontal deflections were averaged because the deflection of a post is thought of as independent of the other posts, and this value plugged into Equation (1) to calculate maximum contraction force (Tan,2010). A complete data summary of all samples tested can be seen in Table 27.

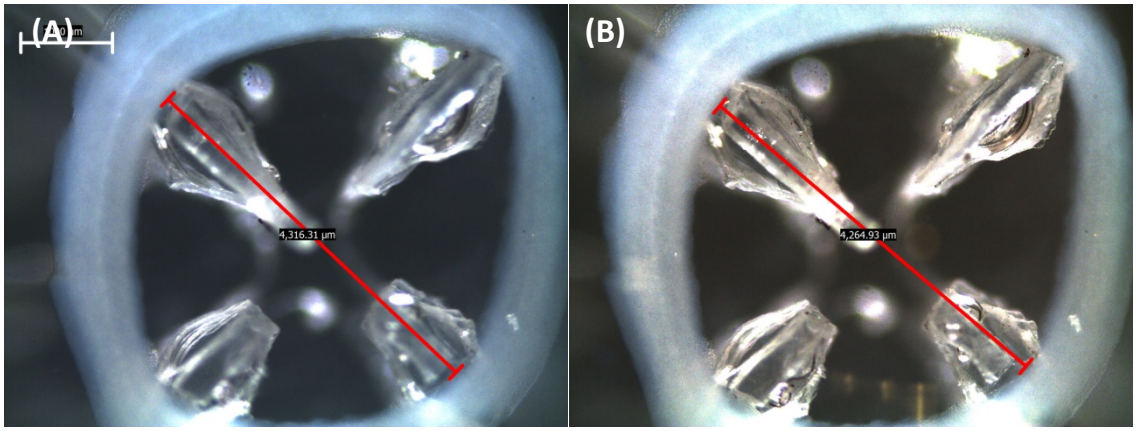

Figure 70: Contraction of a tissue ring sample on the four-post array (Scale bar=1000 µm).

Table 27: Data summary of the contraction testing on four-post multifunctional PDMS molds, with KPSS treatment, PSS treatment, and lysed cells

KPSS PDMS Trials	Original Diameter1 (mm)	Final Diameter1 (mm)	Original Diameter 2	Final Diameter 2 (mm)	Average Deflection (mm)	Maximum Contractile Force Produced (µN)
Sample 1	3.95	3.89	3.86	3.76	0.08	27.87
Sample 2	3.92	3.83	3.83	3.74	0.09	31.36
Sample 3	3.97	3.90	3.91	3.79	0.10	33.10
Sample 4	3.84	3.7	3.82	3.72	0.12	41.81
Sample 5	3.90	3.81	3.69	3.60	0.09	31.26
Sample 6	3.84	3.78	3.65	3.59	0.06	20.91
Sample 7	3.91	3.82	3.63	3.56	0.08	28.87
Sample 8	3.96	3.87	3.77	3.68	0.09	31.36
Sample 9	3.84	3.72	3.73	3.64	0.11	36.88
Sample 10	3.90	3.77	3.67	3.59	0.105	36.58
Average	3.90	3.81	3.76	3.67	0.09	32.00
Standard Deviation	0.05	0.07	0.10	0.08	0.02	5.71

PSS Trials						
Sample 1	3.94	3.91	3.75	3.70	0.04	13.94
Sample 2	3.93	3.90	3.63	3.55	0.055	19.16
Sample 3	3.84	3.79	3.64	3.61	0.04	13.94
Sample 4	3.93	3.88	3.73	3.68	0.05	17.42
Sample 5	3.81	3.78	3.75	3.71	0.035	12.19
Sample 6	3.96	3.94	3.82	3.81	0.015	5.23
Sample 7	3.92	3.90	3.82	3.80	0.02	6.97
Sample 8	3.91	3.91	3.8	3.78	0.01	3.48
Sample 9	3.96	3.94	3.89	3.88	0.015	5.23
Sample 10	3.97	3.96	3.92	3.90	0.015	5.23
Average	3.92	3.90	3.78	3.74	0.03	10.28
Standard Deviation	0.05	0.06	0.10	0.11	0.02	5.72
Lysed Cells Trials						
Sample 1	3.84	3.82	3.67	3.64	0.025	8.71
Sample 2	3.96	3.95	3.78	3.75	0.02	6.97
Sample 3	3.95	3.94	3.89	3.88	0.01	3.48
Sample 4	3.96	3.94	3.70	3.67	0.025	8.71
Sample 5	3.91	3.90	3.73	3.71	0.015	5.23
Sample 6	3.87	3.85	3.77	3.74	0.025	8.71
Sample 7	3.89	3.88	3.69	3.67	0.015	5.23
Sample 8	3.94	3.93	3.78	3.76	0.015	5.23
Sample 9	3.88	3.87	3.85	3.84	0.01	3.48
Average	3.91	3.90	3.76	3.74	0.02	6.19
Standard Deviation	0.04	0.05	0.07	0.08	0.01	2.15

The average maximum contraction force calculated for the ring samples treated with KPSS was 32.00 ± 5.71 μN, which is consistent with values found in prior literature (Bramley, 1995; Murphy, 1974). The average maximum contraction force calculated for the ring samples only treated with PSS was 10.28 ± 5.72 μN. Using a 95% confidence interval, this is a significantly lower value of contraction force than the samples treated with the KPSS ($P \leq 0.05$). The average maximum contraction force calculated for the negative control samples where the rings were lysed was 6.19 ± 2.16 μN. This is also significantly lower force than was calculated for the KPSS treated samples ($P \leq 0.05$). Figure 71 shows a summary of the contraction force testing in a graph and Table 28 provides another summary of the average maximum contraction forces obtained.

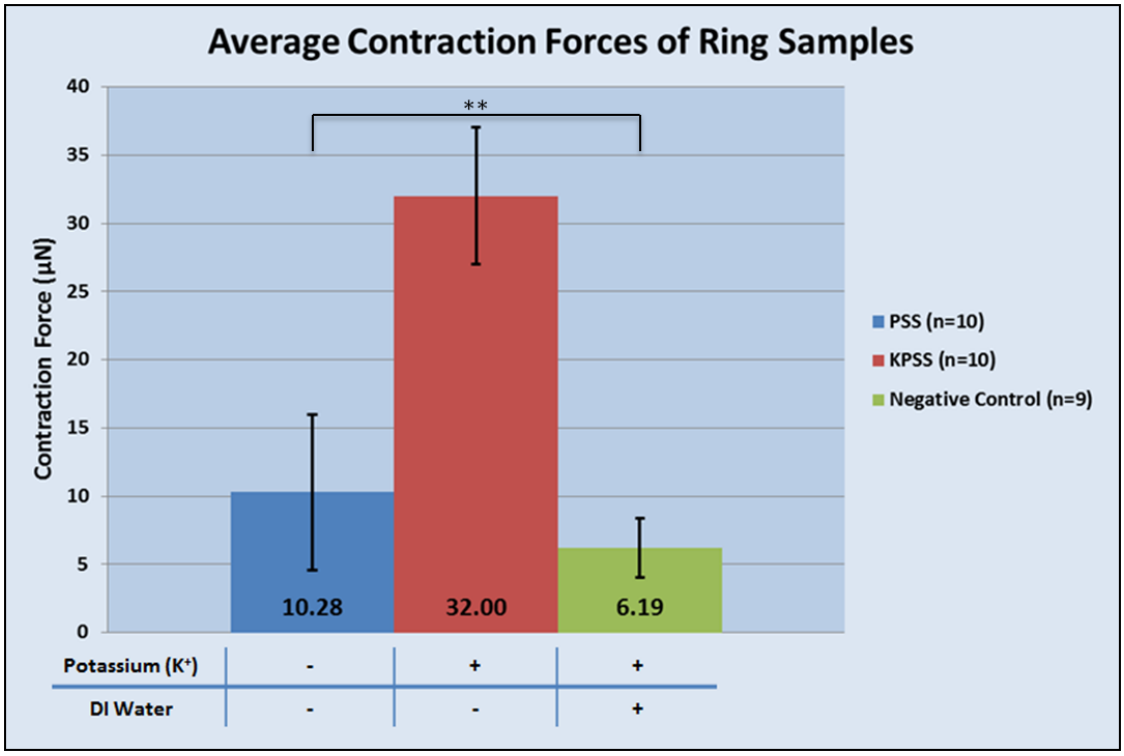

Figure 71: Maximum contraction forces calculated in experimental ring testing (indicates statistical significance P≤0.05). The table below the bars indicates whether or not potassium and/or deionized water was added to the tissue ring samples.**

Table 28: Average contraction forces obtained in the tissue ring contraction experimentation

	Average Contraction Force (µN)	Standard Deviation	Coefficient of Variance (%)
KPSS (n=10)	32.00**	5.71	17.84
PSS (n=10)	10.28	5.72	55.60
Negative Control (n=9)	6.19	2.15	34.77

**indicates statistical significance (P≤0.05)

Based on the results of this testing, we can conclude that the KPSS did induce contraction of the SMC tissue rings, and that the contraction was due to the action of the SMCs. It must be noted that we were restricted in the resolution of the images, as we used a 3 Megapixel digital camera that was included on the Leica stereomicroscope. With higher resolution images, more precise measurements could be made, perhaps obtaining a more accurate force reading. On such a small scale, relatively small changes in post deflection can result in large variations in the total contractile force value. Also, there is no precedent in the literature for expected values of 3D ring constructs, as these are exclusively made at WPI. However, it was clear from our testing that KPSS treated rings created significantly more post deflection than those kept in PSS, and that our device allows for a reliable platform to test our tissue rings on. Our advisor informed us that the tissue rings are

only expressing a small amount of contractile proteins (based on immunohistochemical analysis of smooth muscle alpha-actin). Thus, in future experiments, rings may be able to contract with even more force.

This testing indicted that rings were not able to be properly cultured on the PDMS. However, situating the rings around the microposts did not seem to pose much of a challenge. Additionally, the well in our multifunctional molds served as an excellent reservoir for adding the chemical agonist. Rather than adding enough agonist to fill an entire tissue culture plate, the amount of agonist used was minimized by adding it directly into the well of the mold. Based on our data, the agonist still elicited contraction, so this seems like another positive function of our design. If the PDMS can be altered to successfully form and culture viable tissue rings, then this device will be able to meet the multifunctional objective of the design.

6.4.5 Testing C2C12 Cells on the PDMS Molds

Another objective for our project was to be able to test multiple cell types on the device. Fortunately, one of the other project groups working in the Biomedical Engineering Department was working on creating rings out of C2C12 mouse myoblast cells. These are progenitor cells that have the potential to differentiate into skeletal muscle fibers. The project group had a few extra C2C12 rings for us to test on our device for contractile force. However, the other group had done histology on the rings and found that the C2C12 cells were not expressing myosin heavy chain, one of the essential proteins for cellular contraction. Thus, we were uncertain whether or not we would be able to witness any contraction by the C2C12 cells.

We tested the C2C12 cells by the same protocol that we tested the SMCs; first soaking them in PSS for 30 minutes and then pipetting KPSS into the final design mold. We took pictures of the rings around the posts every ten seconds for five minutes. We were only able to test 2 of the C2C12 rings, as that was all that was available to us. We then used the Leica software package to measure the post defection over time and then we calculated a contraction force value from the total deflection. Table 29 shows a data summary of the contraction testing with the C2C12 mouse myoblast rings.

Table 29: Data summary for the C2C12 contraction testing

	Original Diameter 1 (mm)	Final Diameter 1 (mm)	Original Diameter 2 (mm)	Final Diameter 2 (mm)	Average Total Deflection (mm)	Average Contractile Force (μN)
Sample 1	3.87	3.86	3.81	3.79	0.015	5.23
Sample 2	3.96	3.95	3.90	3.89	0.01	3.48
				Average	0.013	4.36

As shown in the data table, we did not find much contraction in the C2C12 cells. This was somewhat expected, as the cells were not expressing contractile proteins. Additionally, we witnessed some interesting differences between the C2C12 cells and the SMCs that we tested. The C2C12s did not seem to have as much structural integrity in a ring shape as the SMCs. They seemed to be more "flimsy" than the SMC rings when handling them. They did not remain in a ring shape around our posts, taking more of a diamond or square shape (Figure 72). Also, when we used the maximum magnification on the Leica stereomicroscope, we were able to notice that some of the individual cells were breaking away from the ring, especially near our PDMS posts. It seemed that the C2C12 cells did not form as stable of a ring structure as the SMCs.

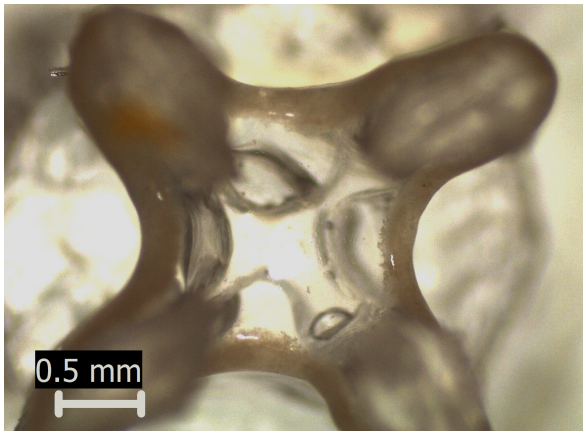

Figure 72: C2C12 ring around our PDMS posts once the chemical agonist was removed.

Nonetheless, this testing with another cell type shows that other cell types can be tested on our device. If various cell types can be made into a ring structure, they can be placed onto our PDMS micropost device and tested for contraction. However, as seen with the C2C12 cells, some cell types do not form very stable ring structures or have not been made into rings that display contractile properties. Our device is versatile in the fact that various cell types can be tested on it and various chemical agonists can be added to the wells in order to induce contraction. Testing

with another cell type helped us to achieve another project objective, showing that our device has the potential to test rings of various cellular compositions.

6.5 Final Design

After conducting several rounds of verification and validation testing, a final design was developed for our vascular ring contraction force measurement device. The following section outlines the specifications and components of our final design.

6.5.1 Detailed Description of Final Design

To manufacture the final design, a negative template developed using SolidWorks CAD was sent to the Mechanical Engineering Department at WPI to be rapid prototyped. The negative template is composed of four parts; the four detachable parts allow for a means of removing the PDMS mold without damaging the microposts. Each part is composed of two extruding pegs (that extrude 3 mm and are 3 mm in diameter) on one side and two intruding holes (3.1 mm in diameter) on the other side to allow for adjacent part attachment (Figure 73a). These pegs are used to lock the four components of ABS negative template locked into place as shown in Figure 73c below.

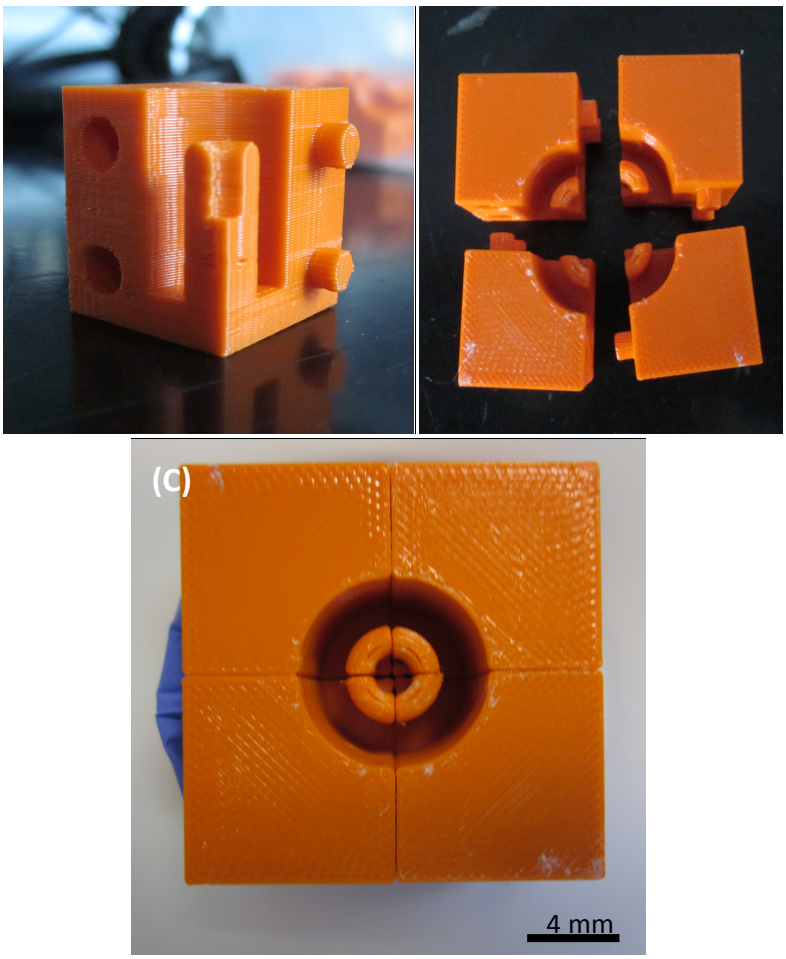

Figure 73: Negative ABS template for our final design. (A) Single component. (B) Piecing the individual pieces together to make the final product. (C) Final product, ready for PDMS to be poured into it.

PDMS was mixed, initially degassed, poured onto the negative template, degassed again, and placed in the oven for about an hour at 70°C to acquire proper polymerization. Finally, the PDMS mold was carefully removed from the template, yielding the final device.

Figure 74 is a CAD drawing of the final design with hidden lines and a solid model. The entire mold is 18 mm in height, 26 mm in length, and 13 mm in depth. Each micropost is 0.7mm in diameter and the base that the microposts are attached on is 4mm in diameter. Additionally, the outer diameter and inner diameter of the well are 18mm and 12mm, respectively. Figure 75 shows an isometric view of the final device

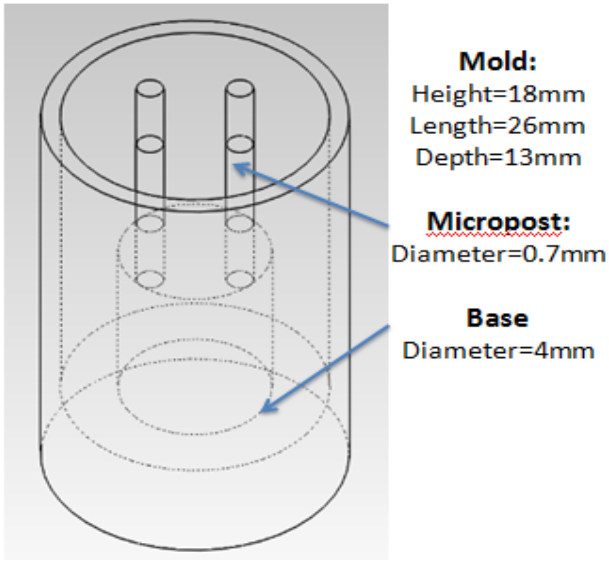

Figure 74: A model of our final PDMS mold.

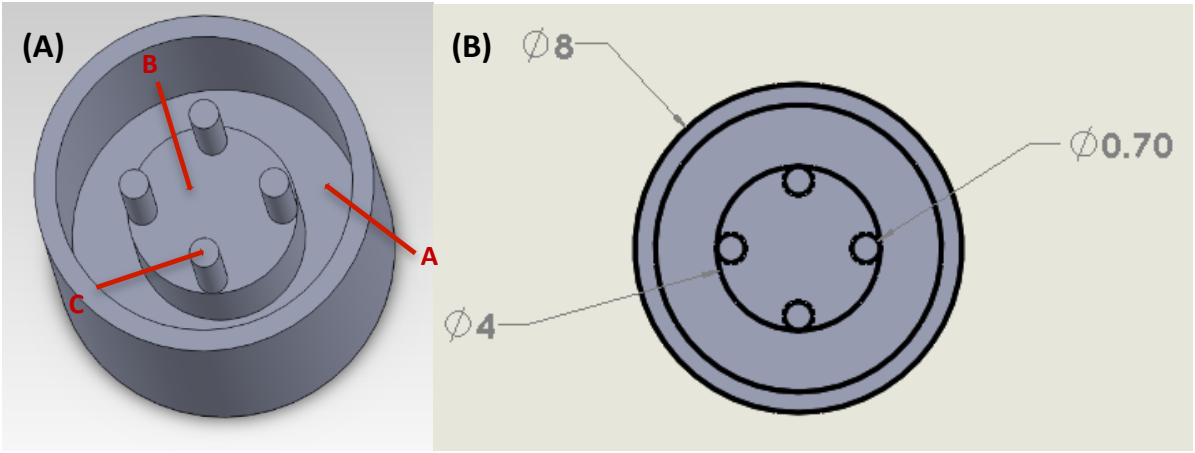

Figure 75: Top view of final PDMS mold design. [A] Seeding well where cells are seeded and agonists are added. The well is rounded to allow for proper SMC aggregation into a ring. [B] Base post where rings aggregate around [C] Micropost where rings are tested (A). Top view of the final PDMS mold design with dimensions (in mm) included (B).

6.5.2 Projects Objectives Achieved

Based upon our initial client statement and research on published literature, we developed the following main objectives for our device: measure contractile force, easy to use, versatile, high throughput, and easy to manufacture. Through extensive laboratory testing we were able to fully meet the metrics outlined for all of the aforementioned objectives except for versatile and high throughput.

Our device successfully provides an indirect contractile force reading upon contraction, as verified by our ANSYS finite element modeling system. Although this type of testing has never been done before, values for contraction force were similar for all SMC ring samples that we tested by adding KPSS chemical agonist. With regards to slippage, there was only one trial where we observed the tissue ring sliding up on the 4-post design. We also observed that the rings seemed to slide down on a couple of tests executed on the 2-post design. In contrast, there was no downward slippage upon contraction on the 4-post design and all testing samples except for one remained on the posts without sliding up or down.

Although our device was determined to be easy to use through laboratory testing, it could be improved upon. For set-up time it takes about 20 minutes for each ring to normalize with PSS, an additional 3-5 minutes to place the rings on the PDMS posts, and then KPSS was added and within 2 minutes the rings were fully contracted. Thus, we successfully achieved the set-up time within an hour, which was our standard metric based from the DMT myograph. Moreover, the entire testing procedure including set-up, inducing contraction, and obtaining readings were completed in less than 3 hours, comparable to the DMT myograph. The DMT myograph allows for testing of four rings at a time, and we only tested one ring at a time.

However, complete set up and testing for the DMT takes about 3 hours, and we found that our complete testing set up and data acquisition could be completed in 30-40 minutes, allowing four samples to be tested and contraction measured in less than 2 hours. It should be noted that the user develops skills (in ring handling and imaging acquisition and measurement) through numerous tests, which results in better time management. In order to obtain force readings, stereomicroscopic images of the posts undergoing contraction had to be analyzed with the Leica Software. This software does take some time to get used to, but allows for deflection measurements to be taken in minutes. Once deflection measurements are taken, they can be plugged in to an Excel spreadsheet and forces can be calculated instantly. Our PDMS posts can be manually calibrated to measure the elastic modulus.

Due to time constraints, we were unable to completely achieve our versatile objective. We were unable to successfully develop SMCs into tissue ring constructs directly on the PDMS molds coated with BSA , even with plasma treatment. However, we did show that our device was able to maintain the structural integrity of rings from both smooth muscle and skeletal cells. Future experiments can focus on creating PDMS post arrays to allow for the testing of 0.5-6mm diameter rings. Ideally, the device should be able to test the contraction of smooth muscle cells, cardiac

myocytes, and even skeletal muscle cells, as *in vitro* contraction studies may be desirable for all three of these cell types.

We wanted to create a PDMS micropost array that consisted of at least 24 separate wells to accommodate for simultaneous testing. This would allow for the testing of different concentrations of chemical agonists on these samples and the large amount of force data from an assortment of chemical agonists in a relatively short amount of time. However, our single device can be manufactured in bulk and be placed in separate wells, thus, allowing for high throughput potential as it is, with a separate mold being placed in every well of two 12-well plates and separate contraction being induced in each well. Additionally, we could not find an adequate imaging source that would allow for the acquisition of post deflection of multiple tissue ring samples at the same time. This still allows for various agonists to be added in each well. Another benefit of our molds is that each well is self-contained and small, so only 800 μL of chemical agonist needed to be added to each well to induce contraction. With better manufacturing technologies, our single mold could be designed into a one piece mold with 24 wells to be manufactured all in one piece. This way, a mold with 24 wells could be made in a similar way that we make our one well mold.

Of all of the project objectives, easy to manufacture was the most successfully accomplished even though we were unable to explore alternative manufacturing methods. Our device is one solid part and is very inexpensive to manufacture. The negative ABS template to complete our mold consists of four identical parts that can be easily pieced together. Additionally, both the negative ABS template and the PDMS cast from the template were produced in a short amount of time. Even with a long wait due to other students needing to use the rapid prototype 3D printer, our negative template was completed in just a few days, and the PDMS mold can be made in less than 2 hours. Moreover, our PDMS device is reusable, and we observed that around 15-20 PDMS molds can be cast from a single ABS template before the template surface begins to become sticky, making the PDMS difficult to remove.

The ease of use of our device was confirmed through by meeting our metrics developed with respect to the DMT myograph. The Leica software took some time to get accustomed to and learn to use, but it becomes more natural as the user practices and becomes familiar with the procedure and software. Due to time constraints, we were unable to fully achieve the versatile objective and this should be a focus for future studies and improvements. Additionally, we did not produce a single device that contained 24 wells for testing, but our current device is still available

for a high throughput assay. It should be noted that our single device could be created in bulk and be placed in separate wells of two 12-well plates, allowing for a high throughput application.

Chapter 7: Discussion

7.1 Project Discussion

The main focus of this project was to create a device that measures the contractile force of SMCs aggregated into the form of rings in response to chemical stimuli. Our device is made of PDMS, a silicone-based elastomer that is molded into a well consisting of a center base post along with four small microposts extruding from the base. SMCs are seeded into the well and are allowed to aggregate around the base post to form a ring. When the cultured ring is ready to be tested, it is slid up to the tips of the microposts and induced to contract with agonists. The amount of deflection of the microposts in response to ring contraction is used to indirectly calculate the force of ring contraction. We developed a software model to predict contraction force in response to a known deflection. We also conducted validation testing to determine the mechanical properties of our PDMS and the viability of creating tissue constructs in a PDMS mold. Ultimately, we created a multifunctional device that is both inexpensive and easy to manufacture, and allows for a calculation of the contractile force of tissue ring constructs. Based on the standard costs of rapid prototyping, it costs $4.73 to have our negative template machined out of ABS. PDMS kits containing 1.1 lb. in total on Amazon.com or the Dow-Corning™ website cost about $50, so it only costs us slightly more than 50 cents to make one of our molds. Our device also has the potential to be made high throughput and test rings of various sizes and diameters from various cell types.

Upon completion of this project, we have successfully developed and prototyped a device that measures the force of engineered vascular tissue ring construction. We conducted extensive background research on relevant tissue contraction assays and procedures, and developed several project objectives and metrics to define those metrics in conjunction with our project advisor. We then conceptually developed several design ideas to meet our project goals and completed bench top testing to evaluate these designs. Using information and results obtained from both background literature and bench top testing, we decided to employ a PDMS micropost device to best measure the force of tissue ring contraction. From there, we designed and executed several experiments to validate the functionality of our device and verify that it properly met our main project objectives. Overall, our device aims to contribute to the field of toxicology testing on 3D tissue constructs and eventually developing new drugs to combat a variety of cardiovascular diseases.

There are several important advantages to our newly developed device that could help advance the field of *in vitro* testing on 3D vascular tissue constructs. Foremost, it is very inexpensive and easy to manufacture. The negative ABS template can be prototyped and machined in less than 3 days and the PDMS device can be made in a little less than two hours. This allows for several modifications to be made if needed and allows for a large number of molds to be made in a short period of time. PDMS is not overly expensive (as a 1.1 lb. or 499 gram kit can be ordered on a website such as Amazon.com for around $50) and can be bought in bulk, and our device is small so it does not require a large amount of PDMS to manufacture. One of our molds requires 4 grams of elastomer base and 0.4 grams of curing agent, for a total of 4.4 grams of PDMS. Additionally, very little to no PDMS is wasted in the manufacturing process if poured carefully and this process only requires a few specific equipment items (vacuum pump with plastic tubing, desiccator, weigh boats, stirrers, oven that can reach 70°C, forceps, and oven mitts). Our PDMS microarray design was also reusable.

There are also several limitations to our contractile force measurement device; some of which pertain to budget and manufacturing limitations that we experienced as part of our project constraints. The device allows for the potential of several improvements that could make it even more efficient and effective in measuring contractile force of vascular tissues. Through numerous experiments, we were unable to successfully have smooth muscle cells aggregate into a uniform tissue ring when seeded onto the PDMS wells. Due to our time constraint, we were also unable to successfully make our device high throughput. Ideally, we would like to test 24 tissue ring samples simultaneously on one device without contamination in order to obtain accurate and precise results. Our device can easily be placed in the wells of a tissue culture plate, so a high throughput assay is still feasible to conduct with several of our devices each placed in a separate well.

Unfortunately, our manufacturing limitation did not allow us to properly create PDMS posts with caps located at the tips. Although we made our ABS template with caps on the posts, the posts did not remain intact upon PDMS removal. However, the caps did not seem to be necessary, as we did not witness the rings contracting so much that they slid off the top of the posts. Due to this constraint, we were only able to create our negative ABS template by rapid prototyping in the Mechanical Engineering Department. Although this was a fairly cheap and easy process, it did not allow for a precise template for PDMS casting. Thus, we were unable to create posts with caps at the top. This limitation resulted in some slippage during tissue construct contractile testing. However,

it should be noted that a large majority of the tissue ring samples did not slip at all during our contraction testing on the posts.

Another limitation of our device that should be discussed is the maximum force that can be detected by the microposts. Once the microposts deflect to a certain point, the calculation of contractile force based on deflection is not longer valid. Based on our ANSYS model, the current limitation of our PDMS microposts is a maximum force of 2 mN. It should also be noted that the SMC rings developed for this project did not show as high a level of contractile protein expression when compared to native vessels. However, if a TEBV was developed and optimized to mimic the contractile forces of native vessels, the dimensions of our device can be altered to measure larger contractile forces. Since the variables in Equation 1 include the length and elastic modulus of the micropost material, these parameters can be adjusted to measure varying contractile forces. For example, stiffness of PDMS microposts can be increased depending on concentration of elastomer base to curing agent. A stiffer post would not deflect unless acted upon by a larger contractile force. Also, the length of the micropost could be adjusted, as a shorter micropost would not deflect as much as a taller micropost. Thus, our device still has a purpose in a potential of quantifying the physiological responses of vascular tissue rings and can be manufactured to best meet the specifications and contractile properties of the rings that will be tested.

One of the most beneficial aspects of our device is the fact that it addresses the current gap in toxicological research. Pharmacological and toxicological *in vitro* testing with human cells provides a method to "bridge the gap" between animal testing and full-scale human clinical trials. Our device allows for *in vitro* testing to be conducted on chemical compounds in a short amount of time to screen the functional effects of unknown compounds. The present limitations, once improved on, can allow for an even more successful device to be integrated into toxicological research. Chapter 8 of this report provides a discussion of future recommendations to further the advancement of our current device.

7.2 Impact Analysis

In the development of our novel tissue ring contraction force measurement device, it is important and necessary to analyze the various impacts that this device and new technology may have on various facets of society and the world in general. As with any new technology, advancement is just one part of the larger spectrum. If a technology is advancing the medical field, but having negative effects on other aspects of society, than it is not a very successful technology.

Therefore, it is vital that we thoroughly evaluate the overall impact of our new device and measurement technology.

7.2.1 Economics

The design and development of any new medical device will have a significant and substantial economic impact. Our device was specifically designed for the purpose of measuring the contraction of 3D tissue ring constructs in response to various chemical compounds. Currently, a huge economic opportunity exists for drug testing on 3D human tissue constructs *in vitro*. This allows for an important step of discovery between 2D cell culture experimentation and animal studies. Testing on 3D tissue constructs derived from human cells can allow for more accurate results than testing on animal cells, and can save large sums of money in the long run. For instance, if a drug does not produce the desired result in a 3D tissue construct, there is no need to move on to *in vivo* animal studies, which are very expensive.

A large economic sector exists for the design, manufacturing and sales of measurement devices for toxicity testing on tissue engineered constructs (McKim, 2005). Our design simply addresses one facet of blood vessel structure and function, but the need exists for tissue constructs of several other organ functions and structures to be tested. Although testing is always an expensive process, *in vitro* testing is much cheaper and faster than *in vivo* studies. The development of a new drug requires up to 15 years of research and development, at an estimated cost of nearly $1 billion (McKim, 2005). This cost increases significantly during preclinical animal testing for safety and in clinical trials. The National Institutes of Health (NIH) spends more than $8 billion a year on animal testing. However, the cost of testing a single substance using animals is frequently in excess of $2 million (Sklarew, 1993). Moreover, the field of *in vitro* testing is still expanding and has potential for very lucrative business in the near future.

As for the economic impact of our actual device, the cost of manufacturing is very low. Our project had an overall cost constraint of $524 meaning all of our manufacturing and testing had to be conducted under this budget. PDMS is a relatively cheap material, as a 1.1 lb. kit can be ordered on a website such as Amazon.com for around $50, and our molds only require 4.4 total grams of PDMS to make. Thus, one of these kits would allow us to make nearly 100 total molds. Additionally, our molds are reusable for a certain number of tests, meaning that new molds do not have to be made for each contraction test. The machining of our negative molds was done with ABS, which is a very cheap plastic, and seemed to work well in forming the PDMS. However, to make an ideal PDMS mold, it would be better to use a smooth plastic such as polycarbonate, which would only slightly

raise the cost of manufacturing. In fact, polycarbonate has virtually the same cost as ABS, but has much stronger mechanical properties, including tensile strength and impact strength. ABS and polycarbonate both cost about $14 for a 12 inch X 12 inch and 0.625 inch thick sheet. However, ABS has a tensile strength of 36 MPa and polycarbonate has a tensile strength of 68 MPa (Interstate Plastics, Inc., 2012). The cost of chemical agonists is beyond the researcher's control, but our device is small, so fortunately it does not require a large amount of chemical agonist to be added during testing (only 800 μL). Our device is certainly much cheaper than any type of force transducer or wire myograph, but it does not give a direct force reading. A complete comparison of the specifications of our device vs. the "gold standard" DMT wire myograph can be seen in Table 30. Overall, our multifunctional post design seems to be a very economically smart device.

Table 30: Comparison of our device to the DMT Wire Myograph "gold standard"

	DMT 620M Wire Myograph[1,2]	Our Device
Cost	Not available	$5.50
Number of parts	30	1
Experimental set up time	3 hours	1 hour
Calibration	Every time turn machine on	Once
Reading	Direct	Indirect
Samples tested at once	4	1
Longevity	Service recommended yearly, known to last 10+ years	Depends on creep/hysteresis of PDMS microposts
Measurement Range	200-1600 mN	0.01 μN-2 mN

[1] Danish MyoTechnology. (2011). DMT. Retrieved September 25, 2011, from http://www.dmt.dk/
[2] Danish MyoTechnology. (2008). Multi Wire Myograph System 610M: User manual 2.2. Atlanta, GA.

Our device is only composed of one part and obviously requires no servicing. However, over time, the posts may not return to their original positions after deflection due to creep and hysteresis of the PDMS. In some other studies, the posts have lost their mechanical stability after around 70 repetitions of testing (Vandenburgh, 2008). In this case, the device should not be used anymore for testing. Our device allows for much smaller force readings to be obtained than the DMT myograph, but our device will not produce accurate force readings above 2 mN. With the resolution of the Leica stereomicroscope, the lower limit of measurement for force is 0.01 μN, but even smaller forces could be calculated with a higher resolution imaging and measurement system. Experimental set up and testing only takes about one hour with our device. Additionally, we were only able to test tissue ring samples one at a time and of one diameter during the timeline of this project. However, our design can be easily made to accommodate tissue rings of various sizes if various size ABS negative templates are machined. Additionally, our device only costs about $5.50 to make, including the ABS negative template. We were not able to find pricing for the DMT 620M

wire myograph, but it is certainly not as cost effective as our device. Still, our device is both easy to manufacture and easy to use.

7.2.2 Environmental Impact

It is also vitally important to analyze the impact of our device on the environment. Any medical device should be expected to be environmentally friendly both to manufacture and to use. The fact that our contractile force measurement device is reusable has a positive impact on the environment. Fewer raw materials will have to be harvested than if we needed to make a new device for every round of testing. PDMS or its degradation products have been observed in the environment and are proven to have no effect on seed germination, plant growth or the plant biomass (Dow-Corning, 2012a). Additionally, PDMS has no effect on terrestrial life even under high exposure (Dow-Corning, 2012b). Therefore, if our device were to be discarded, and the PDMS were to enter the environment as a component of industrial waste it should have no adverse effects to the surrounding environment (Dow-Corning, 2012a). Moreover, if the waste is incinerated, then PDMS will be degraded into its inorganic components, which are eco-friendly. PDMS fluids are not considered hazardous wastes (Dow-Corning, 2012b). That being said, efforts should be continued to make the disposal process even more environmentally friendly and strive to one day make the substance completely recyclable.

7.2.3 Societal Influence

This device design has the potential to have a tremendous impact on society in the United States. As we have previously addressed, this device allows for the accurate testing of 3D tissue rings, which can be used to study the effects of numerous drugs on blood vessel structure and function. Using our device to measure tissue function could potentially lead to the discovery of new drugs to address such problems such as atherosclerosis, coronary artery disease, and general blockages or arterial plaques that may lead to myocardial infarction and stroke. Cardiovascular problems have become a huge problem in the United States and around the world, and have continued to increase at an alarming rate.

With an increase in problems and disease comes an increase in the demand for new cures and remedies. Pharmacological testing is vital for the discovery of new drug therapies, and this goes not only for the field of cardiovascular medicine but a plethora of other medical fields. Therefore, we feel that this device is an example of a device in an industry that has the potential for

an impact on society. Furthermore, the increase in this industry could lead to the need for more jobs, creating a positive impact on society by creating more employment opportunities.

7.2.4 Political Ramifications

Currently in the United States, the government has given a large backing to the medical field and medical research. Predominantly, stem cell research and regenerative medicine have been areas of interest and importance to the government, especially in recent years ("Removing Barriers to Responsible Scientific Research Involving Human Stem Cells"). The government has also been very supportive of health and fitness, in an attempt to lower obesity in America. They most certainly want to promote cardiovascular health. As part of the bigger picture, our device also aims to improve the overall cardiovascular health of society by making it easier and faster to discover cures and remedies for a wide range of arterial ailments.

As previously stated, the field of research in 3D tissue constructs is still relatively new and unexplored, which has the potential to become an incredibly lucrative field. However, the field of 3D tissue construct research also will be very expensive to invest in and help to thrive. Thus, continued government support is vital. Advances in health and medicine follow more quickly when more money is given to support research and development. The potential of our device is great in medical research, but it is not possible without sufficient government backing. We feel that the potential benefits and long term possibilities of 3D tissue construct testing outweighs the cons of any negative initial costs. Economic support is an essential factor in any type of medical research and development, and this is no different in the case of our device.

7.2.5 Ethical Concerns

One of the most beneficial aspects of our device is the fact that it addresses the current gap in toxicological research. This allows for a great deal of *in vitro* testing to be conducted on chemical compounds before moving on to animal studies. One of the most ethical concerns with any type of drug research is testing on animals. Our device does not completely eliminate the need for animal studies to be conducted, but it does allow for alleviation on animal studies. *In vitro* results on tissue engineered constructs from human cells will give researchers a great deal of information that would otherwise have to be discovered by animal testing. Prior to testing on 3D constructs, if the 2D cell culture experiments showed promising results, then the therapy could potentially be tested in animals. This will help to save many animals from tests that would have been faulty and very

harmful. Thus, if the effectiveness of a potential drug therapy does not produce results on *in vitro* constructs, more research and studies will need to be conducted before animal testing can proceed.

Another main ethical concern in developing our device is the source of the human cells for tissue culture. Obviously, embryonic stem cells are one source for a plethora of human cells that could be utilized to produce a wide variety of tissue engineered constructs for testing. Embryonic stem cells are still an enormous ethical concern, and so it is important to try to create 3D tissue constructs from other sources of cells. Specifically, our tissue engineered vessel rings were created from cultured rat aortic smooth muscle cells. Another option is to use adult human stem cells, which can be harvested from a number of sources in the adult body. The cells can be harvested and then allowed to proliferate and form the desired construct for potential testing. Cells can even be harvested from a specific patient and then used to form a construct and tested, giving an even more accurate representation of how a drug might affect an organ in the body of patients with known vascular diseases.

Our device itself does not elicit as many ethical concerns as the actual testing procedure. The device is composed of a silicone-based polymer, meaning it is a synthetic material. The overall process of creating the polymer is fairly straightforward and a well-known procedure. The negative templates to make our molds can be made from common plastics. In the following sections, we will address the health concerns and the sustainability concerns associated with our device.

7.2.6 Health/Safety Issues

In general, PDMS is a relatively safe material. It does not cause damage to the skin (but skin should be washed with soap if contact occurs) and can be breathed in without any toxic or harmful side effects. PDMS is colorless and has a slight odor, and can be irritating if it comes in contact with the eyes. If this occurs, eyes should be flushed with water for several minutes (Dow-Corning, 2012b). It is also important to handle the PDMS with proper laboratory safety equipment (gloves and goggles) when mixing it. Also, PDMS must be cured in the oven at high temperature (approximately 70 degrees Celsius), so it is important to wear proper protection when handling the PDMS, as it will be extremely hot. Also, PDMS is extremely sticky before it has been cured in the oven, and it can be rather messy, so caution should be used when handling it. PDMS can be removed from surfaces using household cleaners, such as Goo-Gone™.

Another health and safety concern comes with the testing that our device is involved in. We use our device to test the contraction of living cells (either animal or human cells). Therefore, there

is a health risk of blood borne pathogens associated with any type of cell culture and testing procedures. In order to complete our project, we needed to take training courses in laboratory safety and the handling of blood borne pathogens. Laboratory gloves must be worn at all times and caution must be taken when handling cells, changing media, and seeding cells to form rings. All cell culture and ring seeding experiments must be done in a sterile hood and the PDMS molds must be autoclaved to limit the risk of bacterial contamination of the cells.

In order to induce contraction, chemical agonists must be added. Our device allows for a wide variety of chemical compounds to be added and for post deflection to be observed. The chemical compounds that we used were relatively mild (although high concentrations of KCl are lethal to the cells, so care must be taken when preparing the KPSS) and did not pose severe health or safety risks, but proper lab technique is always necessary. It is important to first research the Material Safety Data Sheet of any chemical compound being used, and to follow all necessary precautions when handling any chemical compounds. Also, it is vital to dispose of any materials in their proper disposal containers when testing is completed and use the proper protocol when cleaning up any chemical spills. The device and entire testing procedure is not difficult and not very dangerous if proper technique and common sense are utilized at all times.

7.2.7 Manufacturability

Manufacturability is a major factor in both the scientific and commercial success of any device used for testing. Our device is relatively simple in terms of manufacturability. We used a specific concentration of curing agent to make our PDMS. The entire process to manufacture and cure the PDMS is not long and overall takes about an hour and 20 minutes (see Appendix H). Our negative template molds were made from ABS plastic, which was manufactured from the Dimesion SST 1200E rapid prototype 3D printer in the WPI Mechanical Engineering Department. This process is quick and easy, as the model can be made using SolidWorks™ CAD software and sent in to the rapid prototype queue. Usually, our negative ABS templates were received about 3 to 4 days after being sent in to the rapid prototype machine. However, ideally, the negative mold could be made out of polycarbonate plastic, so that the surface is a lot smoother and the machining of the plastic could be even more precise. The Dimension SST 1200E printer only allows for the machining of ABS plastic.

Additionally, another method of manufacturing would have been to use the MakerBot Thing-O-Matic™ 3D printer to machine our negative template mold. However, this machine was not functioning properly and we ran out of time for our project deadline before it was up and running

for us to use to make some negative templates. There was a Thing-O-Matic™ available on campus, but it needed to be debugged. We did make one piece of our negative mold with the Thing-O-Matic™, but the resolution was worse than all of the molds we had rapid prototyped. Table 31 displays some of the key features of both machining options.

Table 31: Comparison of the Maker-Bot Thing-O-Matic™ with the Rapid Prototyping Machine available in the WPI Mechanical Engineering Department

	Thing-O-Matic ™[1]	Dimesion SST 1200E Rapid Prototyping Machine[2]
Cost	$1,099	$32,900
Dimensional Accuracy	XY resolution of 0.02 microns, Z resolution of 0.005 microns	± 0.006"
Materials that can be used	ABS Plastic/PLA	ABS Plastic
Machine Size	12" X 12" X 16"	33'' X 29" X 45"

[1] MakerBot Industries (2011). MakerBot Thing-O-Matic Kit. Retrieved December 7, 2011, from http://store.makerbot.com/thing-o-matic-kit-mk7.html.

[2] "Dimension 1200es series." Stratasys, Inc. 2011 viewed 22 March 2012 at http://www.dimensionprinting.com/3d-printers/printing-productspecs1200series.aspx

Overall, the rapid prototype machine is much more expensive, but the Thing-O-Matic™ has a bit better resolution. Additionally, the rapid prototype machine can machine much larger pieces than the Thing-O-Matic™. The Dimension SST was readily available to us on campus, and was more convenient and reliable. Thus, we chose to use this method of machining. Many labs that make micropost arrays use more advanced techniques, such as photolithography, to manufacture the PDMS microposts (Cheng, 2010; Sniadecki, 2007). These fabrication techniques allow for even microscopic features to be manufactured with great accuracy, but are extremely expensive and were not available to us.

Overall, we experienced a large amount of manufacturing difficulties when trying to perfect our final device design. However, many of these problems were encountered due to the time and budget constraints of our project. With more available resources and time, manufacturing would be relatively easy and quick. Also, because our device is reusable, less overall devices need to be manufactured. Thus, the raw material and manufacturing costs should remain low.

7.2.8 Sustainability

Our device by itself meets the sustainability criteria. Poly(dimethylsiloxane) (PDMS) is the most commonly used silicone-based organic polymer; therefore, creating our micropost arrays out of this material does not require the use of large amounts natural resources. The components are similar to those of many common types of plastics. It is both resourceful and easy to manufacture.

Currently, there is no way to recycle PDMS, but the disposal method is not harmful to the environment. Efforts are currently being made to develop a method of recycling. Additionally, our PDMS molds are reusable and continue to give accurate results until they start to experience creep or hysteresis. Thus, this contributes to the sustainability of the device and limits the depletion of resources. If a high throughput negative template could be properly manufactured, this would contribute even more to sustainability, as a large number of samples could all be tested on the same device. It would require more materials to manufacture such a mold, but this mold could also be reusable, allowing for many samples to be tested and saving materials in the long term.

Chapter 8: Conclusions and Recommendations

The major objective of this project was to create a microscale model of tissue contraction, which can be used to measure tissue function in response to chemical compounds. After extensive research, we determined that using a micropost array was the best method in not only obtaining a contractile force but also providing high throughput potential. Combining this system with a novel design of using cell-derived tissue constructs, we demonstrated the ability to fabricate stable tissue rings on agarose. Rat aortic smooth muscle cells (rASMCs) were carefully seeded onto each agarose well and formed viable tissue constructs after one week. The tissue constructs were then induced to contract around posts by KPSS within the same mold. The resulting contraction led to post deflection, which was simultaneously imaged by a Leica stereoscope positioned on top of the wells. The deflection of the posts were measured and analyzed using the Leica software, and thus the contractile force was determined in Excel and confirmed using the ANSYS software.

Future work on improving the PDMS molds may first include a better technique to determine the elastic modulus in order to verify that all manufactured posts have the same mechanical properties. Although our last set of Instron testing resulted in precise data collection, the modulus value obtained was less than results from literature. Additionally, the Instron machine resulted in inconsistent data as the some of the PDMS strips failed at the grips and not in the middle of the sample. Although our manual modulus calibration method resulted in accurate results, it was time consuming and is prone to some user error. Further advanced techniques of calibration, such as microindentation or force transducer testing, were not available. Additionally, testing should be done on the creep and hysteresis properties of the PDMS microposts, as over time they may not return to their original position after deflection. Although the deflections produced by SMC contraction are small, the posts may eventually lose some of their material integrity over time.

Future work on improving the negative template for making PDMS micropost arrays may include implementing more advanced fabrication technique, such as photolithography. Rapid prototyping our templates in ABS resulted in acceptable bench top testing, however, the overall quality of the template can be improved. The surface of the ABS was not entirely smooth, which probably contributed to the lack of tissue formation in the multifunctional molds. A new material, such as polycarbonate, would provide more strength and a much smoother surface, but could not be machined by the rapid prototype 3D printer. Additionally, the rapid prototyped ABS template eventually broke and was unusable after a few of the PDMS molds were made, and a new one

needed to be manufactured. In order to improve the overall quality and structural symmetry of the PDMS molds, the use of a more advanced fabrication method is desired. Photolithography allows for the PDMS posts to be made without the need for a negative template. Ultraviolet radiation is used to "carve" PDMS material into desired shapes and can create micro-scale features with great accuracy (Sniadecki, 2007). This will allow for more uniform posts, the addition of caps on the posts, and the potential to create a full micropost array consisting of at least 24 wells from one negative template. Most importantly, this will allow for more accurate deflection measurements contributed by more uniform tissue rings.

Future work on verifying the versatility of the device may include seeding and culturing of different cell types into the wells to form tissue rings. Future work on making the device more effective and user-friendly may include making an array that is high throughput. Ideally, an array of wells should vary with different sizes and diameters in order to grow an assortment of tissue rings. This would also require a means of imaging that would allow for proper data acquisition of all ring samples. The imaging would need to monitor contraction in all wells (occurring simultaneously) with adequate resolution to view minor post deflection. These future improvements could make this device extremely powerful and able to collect a multitude of data from different vascular ring constructs in response to various agonists simultaneously.

References

"Advancing Tissue Science and Engineering." National Science and Technology Council, United States Government. June 2007. retrieved 12 September 2011 at http://tissueengineering.gov/advancing_tissue_science_&_engineering.pdf

Akiyama, H., Ito, A., Sato, M., Kawabe, Y., & Kamihira, M. (2010). Construction of cardiac tissue rings using a magnetic tissue fabrication technique. International Journal of Molecular Sciences, 11(8), 2910-2920.

Auger, Francois, A. et al. (2004). "Recent optimization of a tissue engineered blood vessel: the LOEX experience." *International Congress Series,* 1262, 126-128.

Bevan, Christopher D. (2000). "A High-Throughput Screening Method for the Determination of Aqueous Drug Solubility Using Laser Nephelometry in Microtiter Plates". *Analytical chemistry*, 72 (8), 1781-1787.

Bhogal, N. et al. (2005). "Toxicity testing: creating a revolution based on new technologies". *Trends in biotechnology*, 23(6), p.299-307.

Birla, R. K., Borschel, G. H., & Dennis, R. G. (2005). "In vivo conditioning of tissue-engineered heart muscle improves contractile performance." *Artificial Organs*, 29(11), 866-875.

Bitar, K. N., Hecker, L., Baar, K., & Somara, S. (2006). In The Regents of The University of Michigan (Ed.), Three dimensional bioengineered smooth muscle tissue and sphincters and methods therefor (435/284.1 ed.). MI/US.

Brandon, Esther F.A et al. (2003). "An update on in vitro test methods in human hepatic drug biotransformation research: pros and cons." *Toxicology and Applied Pharmacology* 189: 233-246.

Bramley, AM, Roberts, CR, Schellenberg, RR. (1995). "Collagenase increases shortening of human bronchial smooth muscle in vitro." *Am J Respir Crit Care Med*, 152, 1513-1517.

Byrom, Michael J., P. Bannon, G. White, & M. Ng. (2010). "Animal models for the assessment of novel vascular conduits." *Journal of Vascular Surgery,* 52(1), 176-195.

Campbell, BH (2003). "A multi-station culture force monitor system to study cellular contractility". *Journal of Biomechanics*, 36(1), 137.

Cheng, Qi et al. (2010). "Micropost array for Force Mapping of Vascular Smooth Muscle Cells."

Sensors, 2010 IEEE Conference, 1583-1587.

Clark, Joseph F. and G. Pyne-Geithman. (2005). "Vascular smooth muscle function: The physiology and pathology of vasoconstriction." *Pathophysiology,* 12, 35-45.

Craige, Siobhan. Personal Interview. 3 October 2011.

Crandall, SH et al. (1999). *An Introduction to the Mechanics of Solids.* New York: Mcgraw-Hill; 1999.

Dahl, Shannon L.M et al. (2011). "Readily Available Tissue-Engineered Vascular Grafts." *Science Translational Medicine.* 3.68: 1-11.

Danish MyoTechnology. (2011). DMT. Retrieved September 25, 2011, from http://www.dmt.dk/

Danish MyoTechnology. (2008). Multi Wire Myograph System 610M: User manual 2.2. Atlanta, GA.

Desai, Ravi A. (2007). "Microfabricated Post-Array-Detectors (mPADs): an Approach to Isolate Mechanical Forces". *Journal of visualized experiments*, 7, 311-315.

Dow-Corning. (2012a). An Overview of Polydimethylsiloxane (PDMS) Fluids in the Environment. Retrieved February 24, 2012 from <http://www.dowcorning.com/content/publishedlit/01-1034A-01.pdf>.

Dow-Corning. (2012b). Sylgard 184 Silicone Elastomer Curing Agent: Materials Safety Data Sheet. Retrieved February 24, 2012 from http://www4.dowcorning.com/DataFiles/090007b281762143.pdf.

Furchgott, Robert F. et al. (1984). "The Role of Endothelium in the Responses of Vascular Smooth Muscle to Drugs." *Ann. Rev. Pharmacol. Toxicol.* 24: 175-197.

Gentile, Carmine et. al. (2008). "VEGF-Mediated Fusion in the Generation of Uniluminal Vascular Spheroids." *Developmental Dynamics.* 237, 2918-2925.

Gisela L., et al. (2001). "Miniature heart cell force transducer system implemented in MEMS technology". *IEEE transactions on biomedical engineering*, 48(9), 996-1006.

Gwyther, T. A. et al. (2011). Directed Cellular Self-Assembly to Fabricate Cell-Derived Tissue Rings for Biomechanical Analysis and Tissue Engineering. *J. Vis. Exp.* (57).

Gwyther, T. A. et al. (2011). "Engineered vascular tissue fabricated from aggregated smooth muscle cells". *Cells, tissues, organs*, 194 (1), p. 13-24.

Hansen, A., et al. (2010). "New Methods in Cardiovascular Biology." *Circulation Research.* 107:35-44.

Harris, Lisa J. et al. (2011). "Differentiation of Adult Stem Cells into Smooth Muscle Cells for Vascular Tissue Engineering." *Journal of Surgical Research,* 168, 306-314.

"Interstate Plastics-Black ABS Sheet-Extruded." Interstate Plastics, Inc., 2012. viewed 23 March 2012 at http://www.interstateplastics.com/Black-Abs-Extruded-Sheet-ABSBE.php?sku=ABSBE&vid=2012032011041p&dim2=12&dim3=12&thickness=0.250&qty=1&EMAIL=

Hecker, L., Khait, L., Welsh, M. J., & Birla, R. (2008). Bioengineering functional human aortic vascular smooth-muscle strips in vitro. *Biotechnology and Applied Biochemistry*, 50(3), 155-163.

"Introduction to Finite Element Analysis." (1997). Virginia Tech Material Science and Engineering. viewed 7 December 2011 at http://www.sv.vt.edu/classes/MSE2094_NoteBook/97ClassProj/num/widas/history.html.

Khetani, Salman R. (2008). "Microscale culture of human liver cells for drug development". *Nature Biotechnology*, 26 (1), 120-126.

Knight, A. (2008). "Non-Animal Methodologies within Biomedical Research and Toxicity Testing". *Altex*, 25(3), 213-231.

Kim, K. (2011). "Calibrated micropost arrays for biomechanical characterization of cardiomyocytes". *Micro & nano letters*, 6 (5), 317-322.

Knight, Andrew. (2008). "Non-animal methodologies within biomedical research and toxicity testing." *ALTEX,* 25(3), 213-231.

Konig, Gerhardt et al. (2009). "Mechanical properties of completely autologous human tissue engineered blood vessel." *Biomaterials,* 30, 1542-1550.

LabLife (2011). Leica EZ4D Stereo Zoom Microscope. Retrieved April 4, 2012, from http://www.lablife.org/p?a=products_show&id=223005

Leica (2012). Educational Stereo Microscope with Integrated LED llumination and Digital 3 MP Camera Leica EZ4 D. Retrieved February 22, 2012, from http://www.leica-microsystems.com/products/light-microscopes/education/life-science/details/product/leica-ez4-d/.

Legant W.R., Pathak A., Yang M.T., Deshpande V.S., McMeeking R.M., & Chen, C.S (2009). "Microfabricated tissue gauges to measure and manipulate forces from 3D microtissues," *Proc Nat Acad Sci*, 106, 10097-10102.

L'Heureux Nicolas et al. (1998). "A completely biological tissue-engineered human blood vessel." *The FASEB Journal.* 12: 47-56.

L'Heureux, N., Stoclet, J. C., Auger, F. A., Lagaud, G. J., Germain, L., & Andriantsitohaina, R. (2001). "A human tissue-engineered vascular media: A new model for pharmacological studies of contractile responses." *The FASEB Journal*, 15(2), 515-524.

Li, Bin et al. (2007). "Development of Micropost Force Sensor Array with Culture Experiments for Determination of Cell Traction Forces." *Cell Motility and Cytoskeleton*, 64, 509-518.

Lin, G. et al. (1995). "Micro-scale force-transducer system to quantify isolated heart cell contractile characteristics". *Sensors and Actuators*. A. Physical, 46(1-3), 233-236.

Liu, Jin et al. (2008). "Contractile smooth muscle cells derived from hair-follicle stem cells." *Cardiovascular Research*, 79, 24-33.

Liu M. et al. (2009). "Thickness dependent mechanical properties of PDMS membranes." *J. Micromech. Microeng*. 19, 1-4.

MakerBot Industries (2011). MakerBot Thing-O-Matic Kit. Retrieved December 7, 2011, from http://store.makerbot.com/thing-o-matic-kit-mk7.html.

McKim J., et al. (2005). ". A biochemical approach to in vitro toxicity testing." *Pharmaceutical Discovery,* 1-6.

Morgan, Jeffrey and Francois Berthiuame. (2010). *Methods in Bioengineering: 3D Tissue Engineering.*

Artech House Publishing, 31 May 2010.

Moss, Emma et al. (2010). "A novel system for the investigation of microvascular dysfunction including permeability and flow-mediated dilation in pressurized human arteries." *Journal of Pharmacological and Toxicological Methods.* 62, 40-46.

Moraes, Christopher. (2010). "Microfabricated Devices for Studying Cellular Biomechanics and Mechanobiology." *Cellular and Biomolecular Mechanics and Mechanobiology*, 4, 145-175.

Muntwyler, S. (2010). "Three-axis micro-force sensor with sub-micro-Newton measurement uncertainty and tunable force range". *Journal of micromechanics and microengineering*, 20(2), 1-8.

Murphy, R.A. et al. (1974). "Force generating capacity and protein content of arterial smooth muscle." *Journal of General Physiology,* 64, 691-705.

National Toxicology Program. (2010). "High throughput Screening Initiative." Retrieved September 12, 2011, from http://ntp.niehs.nih.gov/?objectid=05F80E15-F1F6-975E-77DDEDBDF3B941CD#2.

Neff, Lucas P. et al. (2011). "Vascular smooth muscle enhances functionality of tissue engineered blood vessels in vivo." *Journal of Vascular Surgery* 53: 426-434..

Perry, C., Spiers, A., Cleland, S., Lowe, G., Petrie, J., & Connell, J. (2003). Glucocorticoids and insulin sensitivity: Dissociation of insulin's metabolic and vascular actions. *Journal of Clinical Endocrinology & Metabolism*, 88(12), 6008-6014.

Piersma, A. (2004). "Validation of alternative methods for developmental toxicity testing". *Toxicology letters (0378-4274)*, 149 (1-3), p. 147-153.

Photomacrography (2005). Telecentric Optics. Retrieved February 5, 2012 from http://www.photomacrography.net/forum/viewtopic.php?t=1472.

"Physiological Saline Solution." Material Safety Data Sheet: #535. Scholar Chemistry, 2008. Updated 20 December 2011.

Prater, C. et al. (2002). U.S. Patent No. 2002/0092340-A1. Milwaukee, WI: U.S.

Purchase, I. (1999). "Ethical review of regulatory toxicology guidelines involving experiments on animals: the example of endocrine disrupters". *Toxicological Sciences*, 52 (2), p. 141-147.

"Removing Barriers to Responsible Scientific Research Involving Human Stem Cells." Whitehouse.gov. 9 March 2009. Executive Order. Retrieved 25 February 2012 at >http://www.whitehouse.gov/the_press_office/Removing-Barriers-to-Responsible-Scientific-Research-Involving-Human-Stem-Cells/>.

Rhim, Caroline and Laura E. Nikalson. (2006). "Tissue engineered vessels: cells to telomeres." *Progress in Pediatric Cardiology* 21: 185-191.

Rouwkema, Jeroen et al. (2008). "Vascularization in Tissue Engineering." *Trends in Biotechnology,* 26(8), 434-441.

Sanz, Laura et al. (2008). "Long term in vivo imaging of human angiogenesis: Critical role of bone marrow derived mesenchymal stem cells for the generation of durable blood vessels." *Microvascular Research* 75, 308-314.

Sasoglu, F.M. et al. (2007). "Design and microfabrication of a high-aspect-ratio PDMS microbeam array for parallel nanonewton force measurement and protein printing." *Journal of Micromechanics and Microengineering* 17, 223-232.

Sato, M., Ito, A., Kawabe, Y., Nagamori, E., & Kamihira, M. (2011). "Enhanced contractile force generation by artificial skeletal muscle tissues using IGF-I gene-engineered myoblast cells." *Journal of Bioscience and Bioengineering*, 112 (3), 273-278.

Science Learning Hub (2012). Which Microscope. Retrieved March 28, 2012 from http://www.sciencelearn.org.nz/Contexts/Exploring-with-Microscopes/Sci-Media/Interactives/Which-microscope

Sine Law Calculator and Solver (2011). Analyze Math. Retrieved December 10, 2011 from http://www.analyzemath.com/Geometry_calculators/sine_law_calculator.html

Sklarew, M (1993). "Toxicity tests in animals: alternative models." *Environmental health perspectives*, 101(4), 288-291.

Sniadecki, N. et al. (2008). "Magnetic microposts for mechanical stimulation of biological cells: Fabrication, characterization, and analysis". *Review of Scientific Instruments*, 79 (4), 44302-44310.

Sniadecki, S. & Chen, C. (2007). "Microfabricated Silicone Elastomeric Post Arrays for Measuring Traction Forces of Adherent Cells". *Methods in Cell Biology,* 83 (7), p. 313-328.

Spires, Angela and Neal Padmanabhan. (2005). "A Guide to Wire Myography." *Methods in Molecular Medicine Vol. 108: Hypertension Methods and Protocol.* 91-104.

Tan, John L. et al. (2003). "Cells lying on a bed of microneedles: An approach to isolate mechanical force." *PNAS,* 100(4), 1484-1489.

Tawkeer-Rashid, S et al. (2004). "The use of animal models in developing the discipline of cardiovascular tissue engineering: a review." *Biomaterials* 25: 1627-1637.

Thomas, Anita, G. Campbell, J. Campbell. (2003). Advances in vascular tissue engineering. *Cardiovascular Pathology,* 12, 271-276.

Truskey, George. (2010). "Endothelial Cell Vascular Smooth Muscle Cell Co-Culture Assay For High Throughput Screening Assays For Discovery of Anti- Angiogenesis Agents and Other Therapeutic Molecules." *Int J High Throughput Screen*, 2010(1), 171–181.

Vandenburgh, Herman et al. (2008)."Drug-screening platform based on the contractility of tissue-engineered muscle." *Muscle Nerve*, 37, 438-447.

Venkatraman, Subbu et al. (2003). *Collapse Pressures of Biodegradable Stents.* Biomaterials, 24, 2105-2111.

Visual Illusions (1996). Telecentric Lens System. Retrieved February 5, 2012 from http://www.lhup.edu/~dsimanek/3d/telecent.htm

Watanabe, M. (1997). "Telecentric optics for focus analysis". *Transactions on pattern analysis and machine intelligence*, 19 (12), 1360-1365.

Yagi, Shinobu et al. (1988). "Relationship between force and Ca^{2+} concentration in smooth muscle as revealed by measurements on single cells." *Physiological Sciences,* 85, 4109-4113.

Zheng, Tao et al.. (2000). “Effects of neutral sphingomyelinase on phenylephrine-induced vasoconstriction and Ca^{2+} mobilization in rat aortic smooth muscle.” *European Journal of Pharmacology.* 391: 127-135.

Zheng, Xiaoyu. (2010). "A Versatile Cell Contractility Mapping Transducer Utilizing Moiré-Based Technique". *Journal of microelectromechanical systems*, 19 (4), 764-773.

Ziegler, Thierry and Robert M. Nerem. (1994). “Tissue engineering a blood vessel: Regulation of vascular biology by mechanical stresses.” *Journal of Cellular Biochemistry,* 56(2), 204-209.

Appendix A: Interviews

Client Interview – Tissue Ring Contraction Project

Date: Thursday, September 01, 2011

Interviewee: Marsha Rolle, Ph.D

- **What is the ideal number of samples to be tested?**

  Highthroughput: 24 is the target amount, but may change.

- **Can we make co-culture rings?**

  *tissue engineered blood vessels, magnitude of 2 or lower to human blood vessel.
  Tissue ring model-application
  May be able to get rat blood vessels, will get contractile response
  *ideal thing we want to have? Alternatives for limitations

- **Is the video the set culture method? Do we need to develop a new method?**

  - **Video: are we making additions to the tensile test to enable it to also perform compression tests?**

    DMT Myograph system can suction out fluid. Contraction reading on force transducer can be pricey.
    Acetylcholine- contraction/relaxation from Sigma
    Really good human tissue models can reduce animal testing. Goal is to make a blood vessel as human as can be.

- **Is our project only designing a device to test for contractibility? Or will we be responsible for testing other factors such as protein interaction, cell signaling, etc.?**

  Focus on contraction!

- **Does the device have to work in a sterile environment?**

  Ideally, YES; however, it doesn't have to be.
  Create system where you can grow cells, and do the tests at the same time.
  Collagen- gel remodeling** idea to keep in mind
  1milliNewton, minimum amount of force the Keaney system can measure. We may need 10-20.

- **Are there specific chemicals to test for contractibility? Or do we determine those? What are the known and unknown chemicals?**

Potassium chloride- maximally contract cells
Phenalyepinephrine- vasoconstrictor
Acetylcholine- Magical. Stimulates contraction on SMC. Relaxation on endothelial cells.
Main outcome is device!

- **In the Blue Hill software, are we responsible to create a program for that for our device?**

  Come up with a design and show that it works.
  Methodology big accomplishment

- **What are the main problems of the current design?**

  Four different chambers for transferring ring from culture dish into system. Difficult to tell when force is at 0. Toss rings onto hooks, pull to certain length. Dial hard to read! Want gauge length to be close to same all the time or can screw up tissue. Low level contraction we can measure.

- **Are there other people we can interview to better understand the problems with the current design?**

  Lab technicians at UMASS who work with the DMT myograph

- **Can we go to UMass to look at the current device?**

  Mice- .5 mm in diameter. Endothelium on the inside
  Understanding vessel physiology, if we don't see much of a contractile response, what do we do?
  Toxicology tests for Liver. Livers on a chip, high throughput readouts, chemical compounds and how liver responds.
  *Good place to start, how to apply to our own system. Microtissue model best developed.
  Use of animal testing, develop assays to reduce animal tests.
  NIH released plans for a center for drug development

UMass Interview – DMT Wire Myograph

Date: Monday, October 03, 2011

Interviewee: Siobhan Craige, Ph.D

- **How long does the set-up of the myograph device take? How long does the entire procedure to measure the contractile force take?**

  The whole procedure takes about a full workday to obtain results for 4 rings using the DMT myograph.

- **What are some features of the myograph device/process of measuring force that you like/are easy?**

  It is convenient to have the four different testing platforms separate from one another. It removes the possibility of contamination from the application of different agonists to each platform.

- **What are some features of the device/set up procedure that are difficult or time consuming and why?**

  Recording and Equilibrating Time takes a total of 2 hours.

  Preconditioning of mice vessels take about an hour.

- **What are some common problems you experience when dealing with the device?**

  Some rings simply do not contract, possibly because the endothelium layer was damaged when extracted from the mice/rat.

  One platform had a loose piece, but it was eventually repaired.

  Other problems were due to wrong buffer solutions and other laboratory technician errors.

  Microsurgery techniques for placing the rings onto the pins require experience.

- **What are the typical values you get for contractile force of the rat arteries?**

  SMC without endothelium layer had a greater contractile force measurement.

  The values are recorded in milliNewtons, and values range depending on the size and type of ring.

- **Are the vessels tested at body temperature or in an organ bath?**

  The vessels are tested with human physiological conditions intact. A saline buffer solution (at 37°C) bubbled with oxygen is pumped into each platform.

- **Do you have a device protocol that we could take a look at?**

Yes, there is a device protocol for the DMT.

- **During the testing procedure, is there often damage to the endothelium? If so, do you think this affects your readings for contractile force?**

  No, the endothelium layer is not damaged. Placing the vessels around pins prevents the damage compared to the use of wire.

- **Any suggestions for improvements on a contractile force measurement device?**

  The preconditioning or "wake-up" time for the vessels of the mice takes about an hour. Finding a way to decrease this time or solve this problem could be beneficial to the user.

  Preventing salt accumulation in the tube that connects the saline bath and the platform can also be useful to the user.

Interview with Professor Granquist-Fraser Regarding the Thing-O-Matic and Imagining

WPI Gateway Park – January 26, 2012

Making molds using the Thing-O-Matic:

- Email Harry to start the process of creating a "PDMS mold" out of the Thing-O-Matic.
    - This will be the 1st project using the Thing-O-Matic so the mold may not come out the best
    - Cc: Professor Fraser
- Need to learn how to program the Thing-O-Matic
    - Work with Harry
- Professor Fraser wants us to write a report to him, explaining how we got the Thing-O-Matic to work

How can we use optics to image the deflection of the posts?

- Telecentric Optics
    - Most easiest and straightforward method
    - Telecentric lense to measure deflection
- Professor Fraser thinks that 2 posts deflection measurements will be more accurate than 4 posts
    - Adhesion properties will be altered with the 4 post design
- We may need to consider dyeing the PDMS to make more visible from background
    - Necessary to contrast post from background
    - It may also be possible to mask the base, if not a small laser can be used to illuminate the post instead of the base

Inquiry about Thing-o-Matic

WPI Gordon Library – February 3, 2012

Meeting with Harold Hovagimian

The team met with Harold to obtain information regarding the status of the Thing-O-Matic:

Harold is certain that the Thing-O-Matic will give us good tolerance and precision in machining our negative molds. However, nothing has been machined yet from this device. It should be available for our use once he receives the final replacement part.

The team sent Harold the CAD drawings of our most recent multifunctional design (4 parts) for machining. We also scaled up this design for precaution measures and sent it to him.

(However, later in the term, there was still some progress with the Thing-O-Matic- we met with Harold again to practice having our mold machined, but it was no use, as there were still some issues with the Thing-O-Matic. Our mold was able to be machined, but it was grainy and of lower quality than the molds machined by the rapid prototyping machine.)

Appendix B: Objective Tree

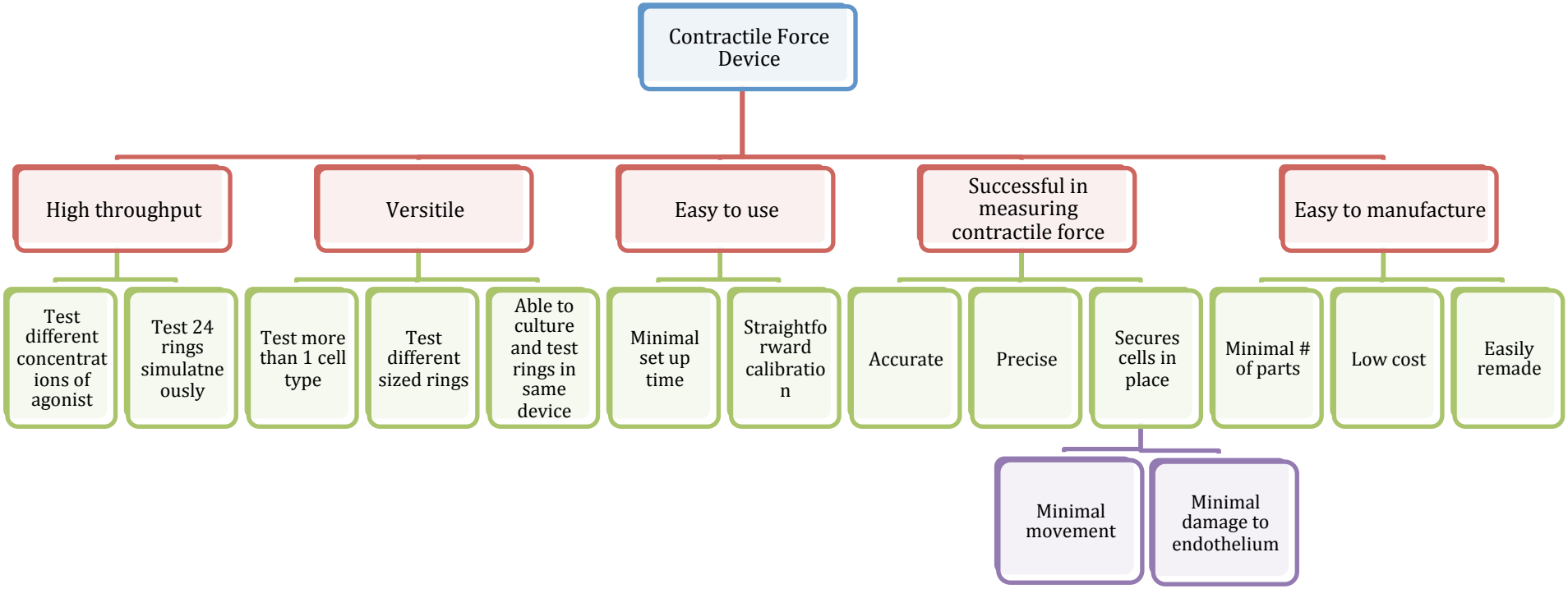

Appendix C: Pairwise Comparison Charts

Team's Pairwise Chart

Goals	Successful in Measuring Contractile Force	Versatile	Able to Mimic Native Environment	Easy to Manufacture	Easy to Use	High Throughput	Total
Successful in Measuring Contractile Force		1	1	1	1	1	5
Versatile	0		1	1	0	0.5	2.5
Able to Mimic Native Environment**	0	0		1	0	1	2
Easy to Manufacture	0	0	0		0	0	0
Easy to Use	0	1	1	1		1	4
High Throughput	0	0.5	0	1	0		1.5

** Note: After further discussion, we decided not to include "Able to Mimic Native Environment" as an objective, because the contraction testing does not need to be done at body temperature, or in an oxygenated organ bath

Advisor's Pairwise Chart

Goals	Successful in Measuring Contractile Force	Versatile	Able to Mimic Native Environment	Easy to Manufacture	Easy to Use	High Throughput	Total
Successful in Measuring Contractile Force		1	1	1	1	1	5
Versatile	0		1	1	1	0	3
Able to Mimic Native Environment**	0	0		1	0	0	1
Easy to Manufacture	0	0	0		0	0	0
Easy to Use	0	0	1	1		0	2
High Throughput	0	1	1	1	1		4

**** Note: After further discussion, we decided not to include "Able to Mimic Native Environment" as an objective, because the contraction testing does not need to be done at body temperature, or in an oxygenated organ bath**

Appendix D: Functions-Means Tree

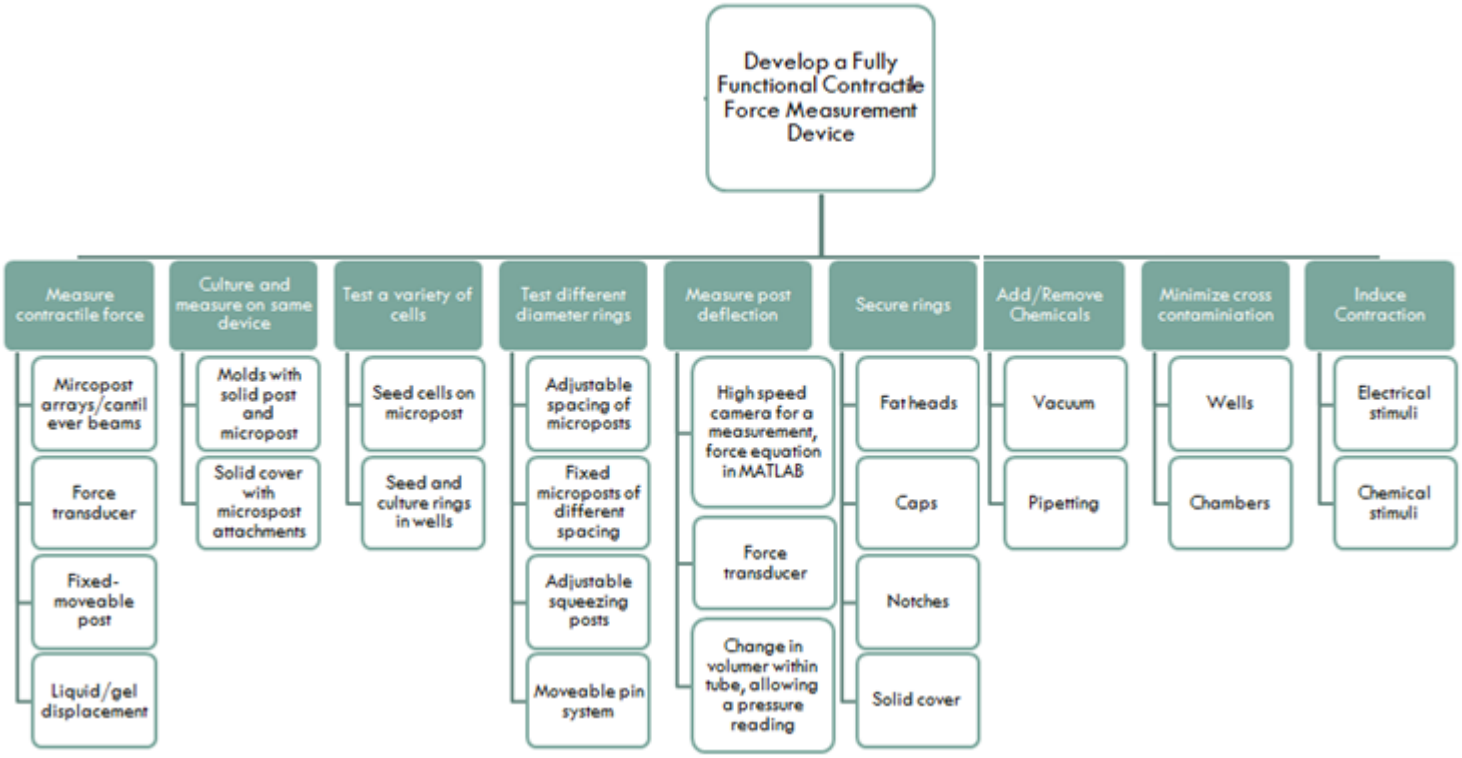

Appendix E: List of Materials Needed for Testing

- Terra cotta clay for posts
- Elastics for tissue rings (small circular bands)
- Agarose (negative mold)
- PDMS/other types of silicone elastomers (positive and negative mold)
- Polyacrylamide gel
- ABS negative molds
- Metal wire
- Digital Camera
- Polycarbonate
- Dulbecco's Modified Eagle Serum (DMEM) (Media)
- Trypsin
- Trypan Blue
- Hemocytometer
- Phosphate Buffered Saline (PBS)
- Bovine Serum Albumin (BSA)
- Potassium Chloride (KCL)
- Physiological Saline Solution (PSS)
- Potassium Physiological Saline Solution (KPSS)
- Deionized water
- Metal spring material
- Plastic casing for liquid
- Straws
- Deionized Water
- Forceps (45° and 90°)
- Pasteur pipettes
- Adjustable pipettes
- Serological pipettes
- Culture plates
- Weigh Boats
- Calipers
- LEICA Stereoscope
- LEICA Software
- Autoclave
- Incubator
- Rat Aortic Smooth Muscle Cells

Appendix F: Expected Deflection Calculations Based on Various Elastic Modulus Values

Force of expected ring contracton:		9-30 μN/1cm^2							
Elastic Modulus of PDMS:	400-800 kPa								
Length of post: (m)	0.005								
F (N/1cm^2)	F (N)	R (m) d=700	E (Pa)	Expected δ (m)		E (Pa)	Expected δ (m)	E (Pa)	Expected δ (m)
9.00E-06	0.09	3.50E-04	4.00E+05	0.795443953		6.00E+05	0.530295968	8.00E+05	0.397721976
1.00E-05	0.1	3.50E-04	4.00E+05	0.883826614		6.00E+05	0.589217743	8.00E+05	0.441913307
1.10E-05	0.11	3.50E-04	4.00E+05	0.972209275		6.00E+05	0.648139517	8.00E+05	0.486104638
1.20E-05	0.12	3.50E-04	4.00E+05	1.060591937		6.00E+05	0.707061291	8.00E+05	0.530295968
1.30E-05	0.13	3.50E-04	4.00E+05	1.148974598		6.00E+05	0.765983066	8.00E+05	0.574487299
1.40E-05	0.14	3.50E-04	4.00E+05	1.23735726		6.00E+05	0.82490484	8.00E+05	0.61867863
1.50E-05	0.15	3.50E-04	4.00E+05	1.325739921		6.00E+05	0.883826614	8.00E+05	0.662869961
1.60E-05	0.16	3.50E-04	4.00E+05	1.414122582		6.00E+05	0.942748388	8.00E+05	0.707061291
1.70E-05	0.17	3.50E-04	4.00E+05	1.502505244		6.00E+05	1.001670163	8.00E+05	0.751252622
1.80E-05	0.18	3.50E-04	4.00E+05	1.590887905		6.00E+05	1.060591937	8.00E+05	0.795443953
1.90E-05	0.19	3.50E-04	4.00E+05	1.679270567		6.00E+05	1.119513711	8.00E+05	0.839635283
2.00E-05	0.2	3.50E-04	4.00E+05	1.767653228		6.00E+05	1.178435485	8.00E+05	0.883826614
2.10E-05	0.21	3.50E-04	4.00E+05	1.856035889		6.00E+05	1.23735726	8.00E+05	0.928017945
2.20E-05	0.22	3.50E-04	4.00E+05	1.944418551		6.00E+05	1.296279034	8.00E+05	0.972209275
2.30E-05	0.23	3.50E-04	4.00E+05	2.032801212		6.00E+05	1.355200808	8.00E+05	1.016400606
2.40E-05	0.24	3.50E-04	4.00E+05	2.121183874		6.00E+05	1.414122582	8.00E+05	1.060591937
2.50E-05	0.25	3.50E-04	4.00E+05	2.209566535		6.00E+05	1.473044357	8.00E+05	1.104783268
2.60E-05	0.26	3.50E-04	4.00E+05	2.297949197		6.00E+05	1.531966131	8.00E+05	1.148974598
2.70E-05	0.27	3.50E-04	4.00E+05	2.386331858		6.00E+05	1.590887905	8.00E+05	1.193165929
2.80E-05	0.28	3.50E-04	4.00E+05	2.474714519		6.00E+05	1.64980968	8.00E+05	1.23735726
2.90E-05	0.29	3.50E-04	4.00E+05	2.563097181		6.00E+05	1.708731454	8.00E+05	1.28154859
3.00E-05	0.3	3.50E-04	4.00E+05	2.651479842		6.00E+05	1.767653228	8.00E+05	1.325739921

Appendix G: Procedure for Producing PDMS

1. Add 10 parts of silicone elastomer base to 1 part silicone elastomer curing agent in a disposable weigh boat.
2. Mix the base and curing agent together until uniformly mixed.
3. Place in degassing chamber.
4. Use vacuum pump to take air out of the chamber.
5. Once air is out, turn valve shut and pump off.
6. Let PDMS sit in chamber until no more bubbles are visible about 15 minutes.
7. Take PDMS out of chamber and pour into mold using a syringe to make sure PDMS falls in the hole.
8. Place mold in degasser chamber and repeat steps 4-6.
9. Take mold out of the chamber when no more bubbles are apparent and place in oven at 70°C for about an hour or until is no longer sticky to touch.

Appendix H: Calibration of Posts

Sniadecki & Chen (2007) measured the tractional forces of cells on an array of microfabricated posts. Each tip deflection represented the traction force and the relationship is proportional to the spring constant of a micropost. We investigated their experimentation in order to get a good idea of how they calibrated their various microposts. It was assumed that all the microposts had uniform material properties and dimensions. Calibration was required to obtain the spring constant of the posts against the deflection of a calibrated, pulled glass micro needle. In particular, our team was interested in understanding their method of calculating and calibrating the micropost stiffness. We will need to know the stiffness of the PDMS posts, as they are treated as cantilever beams, and the stiffness value is a vital portion of the force equation.

The posts' spring constant was calibrated against the known spring constant of a glass micropipette as shown in Figure 77 below (Sniadecki & Chen, 2007). The calibrated micropipette was positioned into contact with a micropost and the deflection was observed under a microscope. In image (A), the traction force (F) is linearly proportional to the tip deflection (X) as determined by the modulus of elasticity (E), the diameter (D), and height (L) of the micropost. In image (B), glass micropipettes with a calibrated tip has a known stiffness (K_p) are pressed against the post to a known distance (X_p). In image (C), the spring constant of the microposts can be calculated from the displacement of the micropost (X) against a translation of the micropipette (X_p) by the relationship for two springs in series. (K_p) is the spring constant of the glass micropipette.

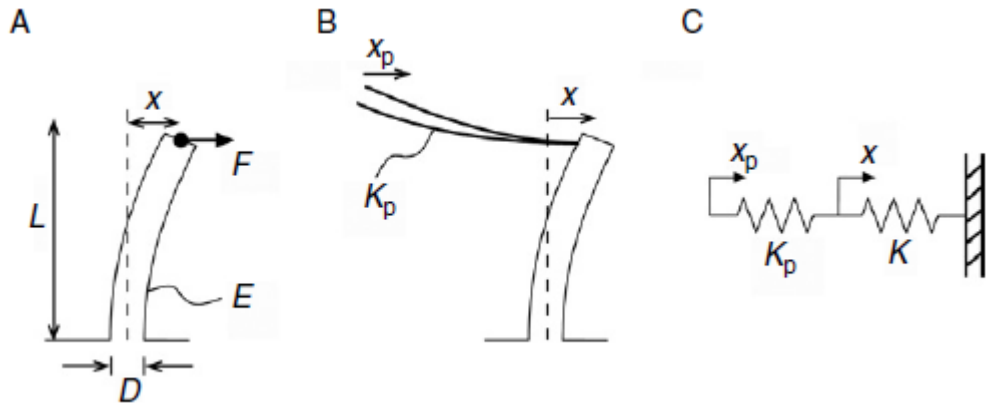

Figure 76: Calibration of micropost using a micropipette.

From this data, they ensured that the posts were all of equal stiffness. This is a method that can be implemented on the post calculations of our final design. The authors found generally the same values for the direct measurement and calculated spring constant values based on the properties and dimensions of the PDMS.

However, we have also found some interesting studies that have looked into the stiffness of PDMS posts based on the various thicknesses of the posts. Thus, we can use this material to get a good baseline value of what the thickness of our posts should be. Lui et. al (2009) looked into the stiffness of various thickness PDMS membranes. We know that we want our PDMS posts to be about 0.7 mm in diameter. According to their data, this should allow us to estimate that our posts will have a stiffness of around 800 kPa. Also, if we chose to make our posts any thicker, it appears that the curve levels off around 600 kPa, even as the posts get much thicker (Figure 78).

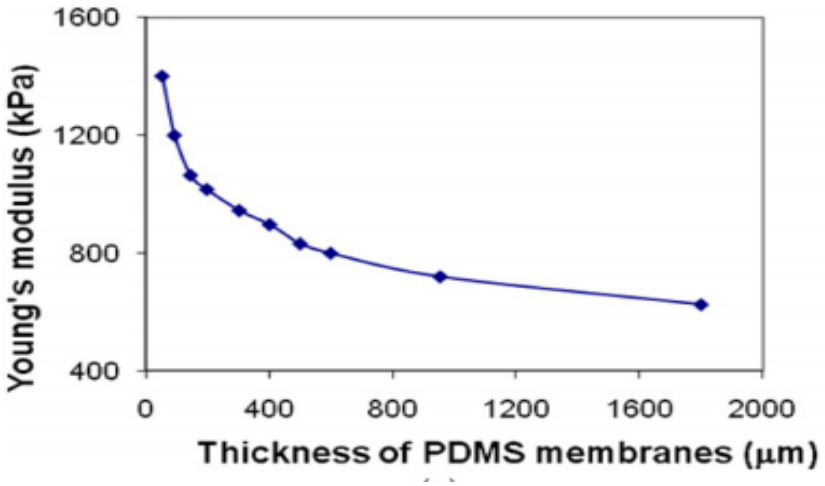

Figure 77: Stiffness of PDMS at various thicknesses (adapted from Liu et al., 2009).

Appendix I: Cell Culture Procedures

Since one of our objectives for this design is to be able to culture and test rings in the same device, we will have to conduct tests to seed and culture smooth muscle cells in our devices to see if they actually form rings. Another reason for constructing tissue rings is also for the team to be able to practice and develop good techniques in cell culture and creating and handling the tissue rings.

Making media:

1. Warm 500 mL bottle of Dulbecco's Modified Eagle Medium (DMEM), 50 mL vial of fetal bovine serum (FBS), a vial of 10X Glutmax, and a vial of 10X Penicillin/Streptomycin in an incubator
2. Once warm, add a 10% FBS (50 mL), 1% of Glutmax (1 mL), 1% and Pen/Strep (1 mL) to 500 mL DMEM
3. Mix thoroughly.

Thawing cells:

1. Keep cryopreserved vial of cells frozen until needed
2. Warm supplemented media
3. Add 10 mL of media into 150 mm plate (maxi plate)
4. Thaw cells in a 37°C incubator, plate cells immediately
5. Add another 10 mL of media into plate
6. Place in incubator

Making cell rings:

1. When cells are 70-80% confluent, aspirate media out of plate
2. Add 10 mL of trypsin, let plate of cells sit for 5 minutes
3. Pipette cells up and down to get rid of clumps
4. Add 10 mL of media to cells to stop reaction
5. Pipette cells into a 50 mL tube
6. Take 40 μL out and put it in Trypan Blue for counting
7. Centrifuge the rest of cells for 5 minutes at 1000 rpm
8. Count cells using a hemocytometer and calculate the concentration needed to acquire 5 million cells/mL (cell concentration subject to change)

9. Aspirate out trypsin and media mixture from centrifuged tube
10. Add amount of media needed for desired concentration
11. Mix cell suspension well
12. Seed rings (100 μL per ring)

Freezing cells

1. Follow Steps 1-8 in "Making cell rings" protocol
2. Prepare freezing medium (80% cell culture media, 10% FBS, and 10% serum)
3. Use the counted number of cells to calculate the media needed to acquire a concentration of 2-5 million cells/ml of freezing medium
4. Aspirate out trypsin and media mixture from centrifuged tube
5. Add amount of freezing medium for desired concentration
6. Aliquot cell suspension into cryovials. **Do not overfill cryovials!**
7. Place cryovials in -80°C freezer. Cells should be frozen slowly!

Blocking PDMS with Sterile 1% BSA

1. Make a solution of 1% BSA with PBS (1 g BSA per 100 ml of PBS)
2. Use a syringe and a sterile filter to filter the solution onto the PDMS surface to be blocked
3. Incubate the blocked PDMS at 37°C for 30-60 minutes or at 4°C overnight
4. Aspirate out BSA solution and seed cells immediately

Appendix J: Procedure for Making PSS and KPSS

16 February 2012

PSS: Physiological Saline Solution (1 Liter)

-consists of 99.1% water and 0.9% NaCl

- to make, we mixed 99.1 mL of water with 0.09 grams of NaCl

(1 liter of water=1 gram of water because Density =mass/volume, and mass=density*volume)

thus, 1 liter of water*1 g/L = 1 gram of water

KPSS: Potassium Physiological Saline Solution (1 Liter)

-consists of 99.1% water and 0.9 KCl instead of NaCl

-to make, we mixed 99.1 mL of water with 0.09 grams of KCl

***** as described in (Scholar Chemistry, 2008; Spires, 2005)

Appendix K: Work Breakdown Structure

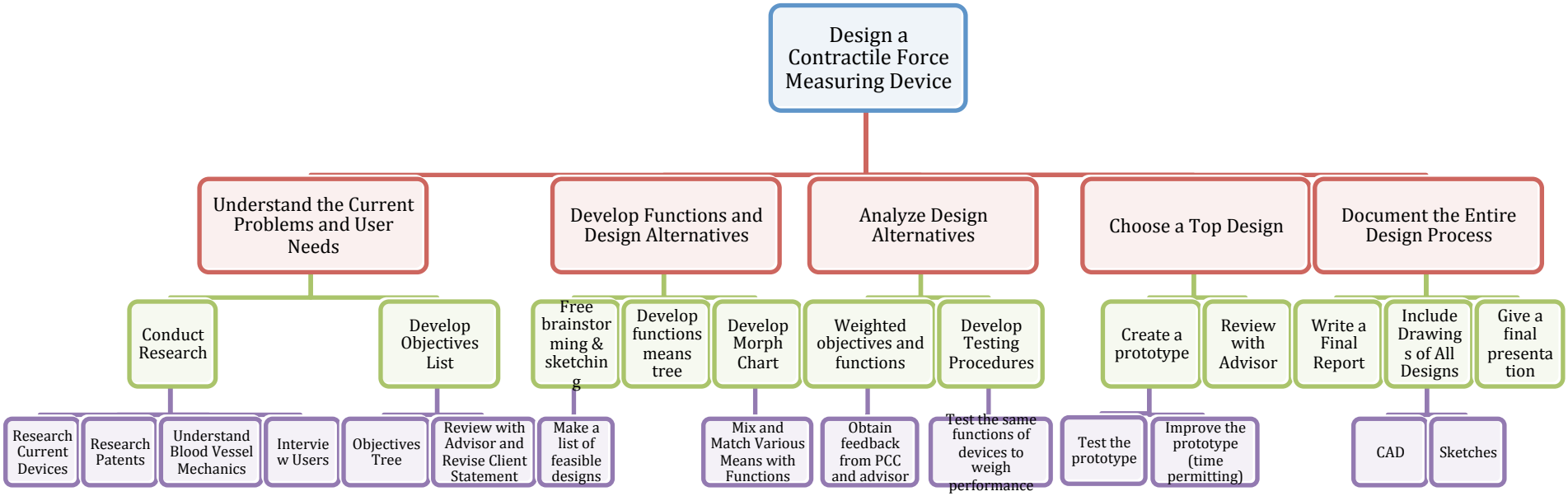

Appendix L: B-Term Gantt Chart

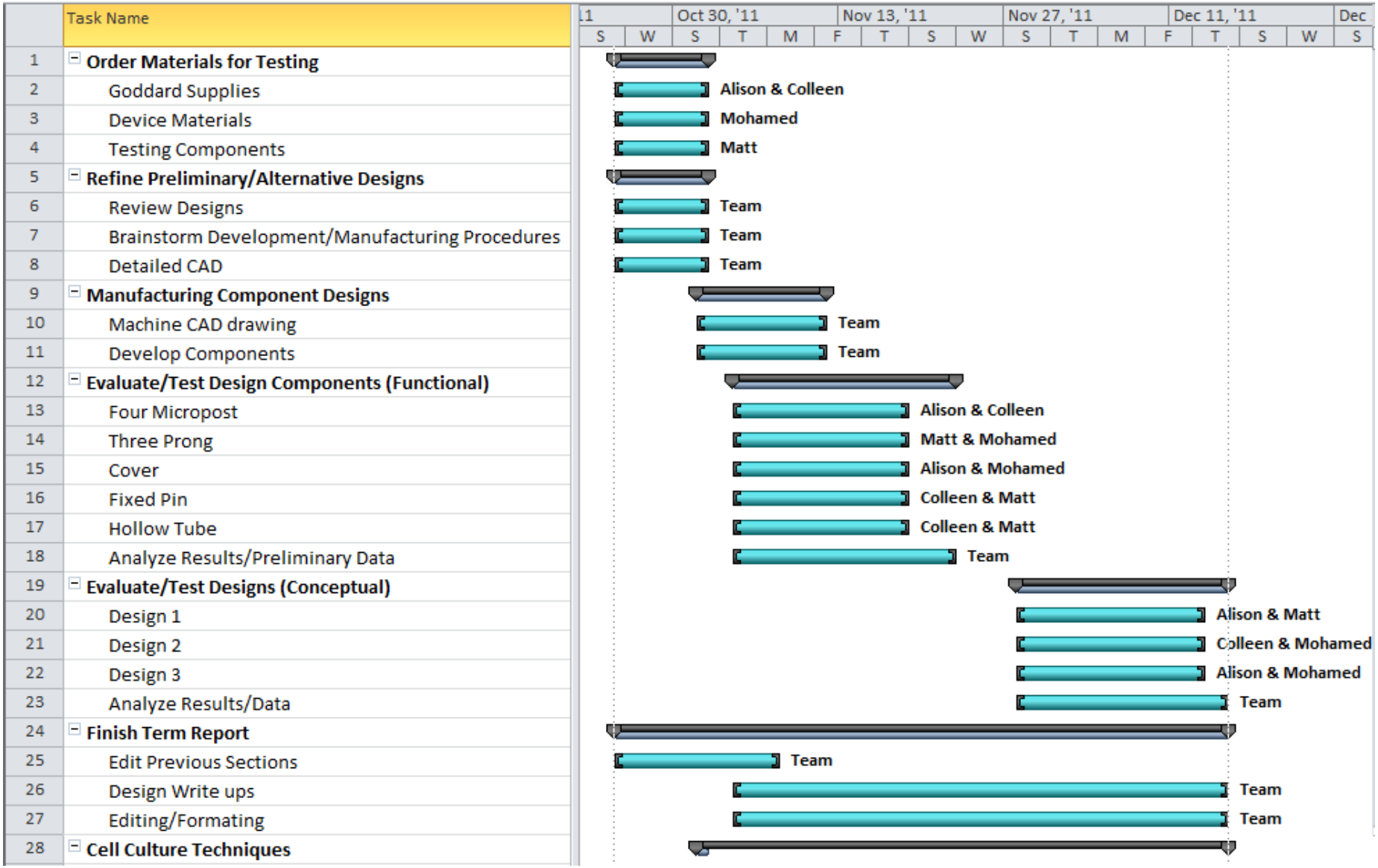

C-Term Gantt Chart

	Task Name	Duration	Start	Finish
1	**Select Final Design**	**7 days?**	**Thu 1/12/12**	**Fri 1/20/12**
2	Tensile Testing on Plastic Stirrers	2 days?	Thu 1/12/12	Fri 1/13/12
3	Final Force Testing on PDMS Posts	6 days?	Fri 1/13/12	Fri 1/20/12
4	Final Light Defraction Tests	4 days?	Tue 1/17/12	Fri 1/20/12
5	Force Calculations and Analysis	3 days?	Wed 1/18/12	Fri 1/20/12
6	**Optimize Design Components**	**5 days?**	**Mon 1/23/12**	**Fri 1/27/12**
7	Brainstorm Ways to Make Molds	3 days?	Mon 1/23/12	Wed 1/25/12
8	CAD New Molds	3 days?	Wed 1/25/12	Fri 1/27/12
9	**Manufacture CAD Designs**	**5 days?**	**Mon 1/30/12**	**Fri 2/3/12**
10	Send to Machine Shop or Thing-O-Matic	5 days?	Mon 1/30/12	Fri 2/3/12
11	**Preparation of Validation Tests**	**5 days?**	**Mon 1/30/12**	**Fri 2/3/12**
12	Brainstorm and Finalize Testing Procedures	5 days?	Mon 1/30/12	Fri 2/3/12
13	**Design Verification Tests**	**12 days?**	**Mon 2/6/12**	**Tue 2/21/12**
14	Multifuctionality	10 days?	Mon 2/6/12	Fri 2/17/12
15	Force Measurement	10 days?	Mon 2/6/12	Fri 2/17/12
16	Ring Damage Testing	10 days?	Mon 2/6/12	Fri 2/17/12
17	Calibration of Device	10 days?	Mon 2/6/12	Fri 2/17/12
18	High-Throughput	10 days?	Mon 2/6/12	Fri 2/17/12
19	Analysis of Results	10 days?	Wed 2/8/12	Tue 2/21/12
20	**Compile C-Term Deliverables**	**37 days?**	**Thu 1/12/12**	**Fri 3/2/12**
21	Write Methods and Results	25 days?	Mon 1/23/12	Fri 2/24/12
22	Discussion	5 days?	Mon 2/20/12	Fri 2/24/12
23	Conclusion	2 days?	Fri 2/24/12	Mon 2/27/12
24	Suggestions	2 days?	Fri 2/24/12	Mon 2/27/12
25	Revise B-Term Report	7 days?	Thu 1/12/12	Fri 1/20/12
26	Prepare Final Draft for Submission	5 days?	Mon 2/27/12	Fri 3/2/12
27	Prepare Final Presentation	37 days?	Thu 1/12/12	Fri 3/2/12

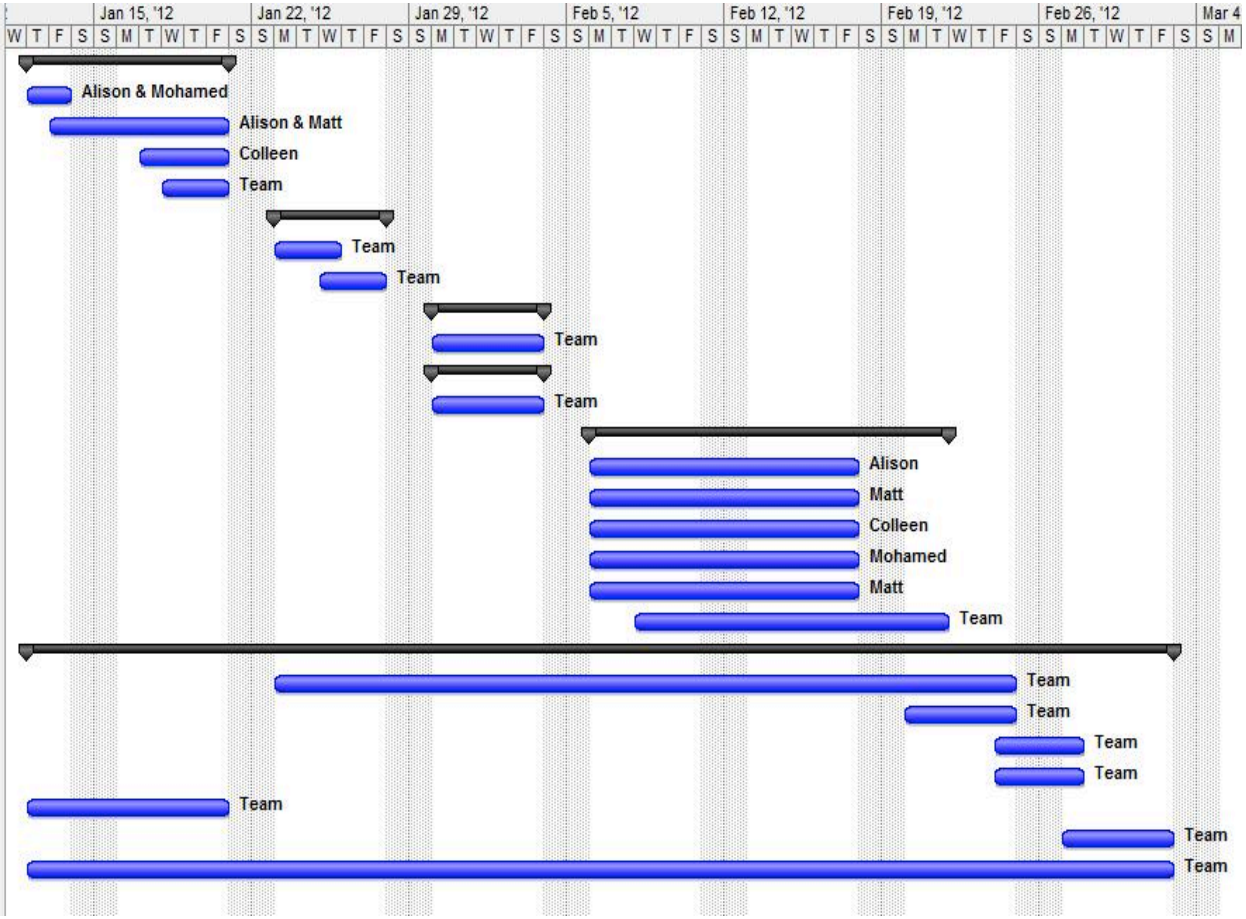

Appendix M: Common Abbreviations

TEBV – tissue engineered blood vessels

ECs – endothelial cells

SMCs – smooth muscle cells

hMSCs – human mesenchymal stem cells

HTS – high throughput screening

DMT – Danish MyoTechnology

PDMS – poly(dimethylsiloxane)

VSM – vascular smooth muscle

μN – microNewton

IAS – internal anal sphincter

FBS – fetal bovine serum

DMEM –Dulbecco's Modified Eagle Medium

ACh – acetylcholine

M – molar

mPADs – microfabricated post array detectors

mBAM – miniature bioartificial muscle

kPa- kilopascals

RAMSCs- rat aortic smooth muscle cells

BSA- Bovine Serum Albumin

PSS- Physiological Saline Solution

KPSS- Potassium Physiological Saline Solution

Appendix N: Summary of "3D Airway Model" Presentation

Speaker: Adrian West from Dalhousie University, Canada, who works in conjunction with Chen lab at the University of Pennsylvania

- Studying the mechanism of asthma, by which smooth muscle cells cause the airway tubules to constrict and limit breathing
- Problem with animal models: expensive and often have inappropriate mechanical features
- In vitro testing: easily manipulated, easy to focus on single cells
- First option: suspend bulk cells in 3D collagen gels, but this was not a tissue ring and the cells had very weak contractions
- Chris Chen's lab at UPENN- microfabricated tissue gauges (cantilever beams)
- The cells self assemble into a tube around the cantilever beams, KCl (80 mM) used to induce contraction, also used acetylcholine and histamine
- Cultured with 20% fibroblasts to help stabilization and so they would remain attached to the cantilevers (gives about a 50% success rate)
- Able to achieve repeated contraction and relaxation, calculated from the cantilever deflection
- Average contraction of in vivo SMCs (29.4 mN/mm^2) –Bramley et al. 1994)
- Need a baseline tension, still 10 fold less contraction than in vivo
- PROBLEM: Cantilevers are very difficult to make! Photolithography is expensive and difficult and requires skill to make good molds
- Chen's lab are the experts in photolithography, and they often still have trouble producing accurately made PDMS molds on such a small size scale

Appendix O: MakerBot Thing-O-Matic®

The Thing-O-Matic, as shown below, was created by MakerBot Industries and allows for rapid prototyping and low-cost 3D-printing (MakerBot Industries, 2011). It contains an extremely reliable extrusion system, is easy to use, and is relatively cheap to purchase. The drive system has been modified for higher quality in order to give the finest position accuracy. Theoretical XY positioning resolution of 20 microns and theoretical Z positioning resolution of 5 microns allows for high resolution prototyping. These dimensions will result for a much smoother template for PDMS molding compared to other rapid-prototyping methods. This device prints in acrylonitrile butadiene styrene (ABS), poly(lactic acid) (PLA), or high density polyethylene (HDPE) plastic using the Fused Deposition Modeling (FDM) process. The plastic can be made into any shape measuring up to 6×6×7 inches in dimension.

Figure 78: Thing-O-Matic printer (MakerBot Industries, 2011).

The machine on campus still needed some work to become fully functional, and after further research, we were confident that the rapid prototyping machine on campus allowed for better resolution negative molds to be made.